

**Interaction of structured RNAs with the N-terminal half of  
RNase E**

Jaskiran Singh Sabharwal

Submitted in accordance with the requirements for the degree of

Doctor of Philosophy

The University of Leeds

School of Molecular and Cellular Biology

September 2019

## **Statement of academic integrity**

The candidate confirms that the work submitted is his own, except where work which has formed part of jointly-authored publications has been included. The contribution of the candidate and the other authors to this work has been explicitly indicated below. The candidate confirms that appropriate credit has been given within the thesis where reference has been made to the work of others.

The work in Chapter 3 and 4 will appear in the following publication:

Clarke, J. E., Sabharwal, K., Kime, L. & McDowall., K. J. (in preparation) A major function of RNase E involves the recognition of structured elements by a conserved groove that is distinct from domains associated with catalysis.

This copy has been supplied on the understanding that it is copyright material and that no quotation from the thesis may be published without proper acknowledgement.

The right of Jaskiran Singh Sabharwal to be identified as Author of this work has been asserted by him in accordance with the Copyright, Designs and Patents Act 1988.

© 2019 The University of Leeds and Jaskiran Singh Sabharwal

## **Acknowledgements**

Firstly, I would like to thank my supervisor, Kenny McDowall for supporting me over the last four years and for having faith in me when I had lost hope. I did not think I would ever finish this thesis; thank you for getting me through my PhD.

Justin Clarke, your knowledge of RNase E and kinetics has always astounded me. I will be ever grateful that you took time out of your day to answer my constant questions.

To Mike, Sam and Rachel, thank you for kicking me off on this journey of science.

I want to thank past and present members of the O'Neill, Seipke and McDowall labs it has been a pleasure to work with you all. I also would like to thank various members of Garstang level 8 for help with equipment and helpful discussions. Thank you to the EM facility staff and Dave Nicholson for assistance with EM and data processing.

Great scientists. Better friends. The 'amigos'; thank you for being the source of questionable humour and good company. Maisie, Jamie & Em, my family in Leeds, thank you for being a constant source of support and friendship.

This thesis would not be possible without many of those listed above, but above all else, thank you, Mum, Dad and Jasmin.

## Abstract

RNase E, an endoribonuclease found in many bacteria, undertakes roles in the processing and degradation of RNA. Previous work on RNase E from *Escherichia coli*, has suggested that tRNA processing requires RNase E to interact with structured as well as single-stranded regions via a site on RNase E that had not yet been identified. Recently, X-ray crystallography by others revealed an interaction between a groove, distal to the site of catalysis, and a duplex region of an sRNA. Here the role of this RNA-binding groove in RNase E is explored using a combination of genetics, molecular and structural biology. It is shown that this groove is the site that contacts tRNA and is essential for efficient cleavage of tRNA precursors. However, contrary to current thinking, the groove appears not to be specific for double-stranded RNA. It may also be involved in allosteric regulation. The RNA-binding groove does not appear to be crucial for autoregulation of RNase E despite the cis-acting factor being a highly structured 5' untranslated region. This may suggest the existence of redundancy, a possibility open to functional analysis *in vivo*. However, any approach has to consider another key finding of this study, namely the RNA-binding groove is essential for *E. coli* viability. The RNA-binding groove is absent from a paralogue of RNase E called RNase G. This may be one reason why RNase G is unable to compensate for the loss of RNase E in *E. coli*. To provide a better platform for further functional analysis it is clear that further structural understanding of the interactions described here is required. To this end, study by electron microscopy was initiated. Discussed are the ramifications of insight gained here, direction of future structural studies, and the potential of new sequencing approaches to facilitate transcriptome-wide analyses.

## Contents

Statement of academic integrity .....	ii
Acknowledgements .....	iii
Abstract .....	iv
Contents .....	v
List of Tables .....	ix
List of Figures .....	x
List of Abbreviations .....	xiii
<b>Chapter 1 .....</b>	<b>1</b>
<b>General introduction .....</b>	<b>1</b>
1.1 Introduction to RNA decay .....	2
1.1.1 <i>Escherichia coli</i> as a model organism for explicating the role of RNA decay. ....	2
1.1.2 Antagonism of RNA synthesis, translation and decay .....	2
1.1.3 The organisation of the RNA decay machinery .....	5
1.1.4 RNA decay in other bacteria .....	8
1.2 Macromolecular components of the RNA decay machinery .....	10
1.2.1 Endonucleases .....	13
1.2.2 Exonucleases .....	16
1.2.3 Other components .....	19
1.3 RNase E .....	22
1.3.1 Structure .....	22
1.3.2 Substrate recognition .....	33
1.3.3 Regulation by secondary structure .....	36
1.4 Stable RNA processing .....	37
1.4.1 Maturation of transfer RNA (tRNA) .....	37
1.4.2 Maturation of ribosomal RNA (rRNA) .....	38
1.5 Concluding remarks .....	40
<b>Chapter 2 .....</b>	<b>42</b>
<b>Materials and methods .....</b>	<b>42</b>
2.1 Materials .....	43
2.1.1 Chemicals and Reagents .....	43
2.1.2 Growth and maintenance of bacteria .....	43
2.1.3 Buffers and solutions .....	48

2.2	RNA methods.....	49
2.2.1	Ribonuclease decontamination .....	49
2.2.2	Phenol extraction and Precipitation of nucleic acids.....	49
2.2.3	Spectrophotometric Quantitation of RNA .....	50
2.2.4	Synthesised RNA methods .....	50
2.2.5	Synthesis of RNA oligonucleotides .....	53
2.2.6	Electrophoretic mobility shift assays (EMSA).....	55
2.2.7	Discontinuous Cleavage Assays .....	56
2.3	DNA Methods.....	58
2.3.1	Deoxyribonuclease (DNase) decontamination .....	58
2.3.2	Quantification of DNA.....	58
2.3.3	Isolation of bacterial genomic DNA .....	58
2.3.4	Agarose gel electrophoresis.....	59
2.3.5	PCR methods.....	59
2.3.6	Plasmid DNA methods .....	63
2.4	Protein Methods .....	65
2.4.1	Overexpression of recombinant genes encoding histidine-tagged proteins in <i>E. coli</i> .....	65
2.4.2	Purification of histidine-tagged proteins.....	65
2.4.3	SDS-polyacrylamide gel electrophoresis.....	67
2.4.4	Quantitation of Protein .....	68
2.4.5	Mass Spectrometry .....	68
2.4.6	Small Angle X-ray Scattering .....	68
2.4.7	Circular Dichroism.....	69
2.4.8	Western blotting .....	69
2.5	Other Methods .....	71
2.5.1	Cell viability assays .....	71
2.5.2	$\beta$ -galactosidase assays.....	72
2.5.3	Glow Discharging EM grids.....	72
2.5.4	Grid preparation and Electron Microscopy (Negative-stain TEM) .....	73
2.5.5	Grid preparation (Cryo-EM).....	73
2.5.6	Electron Microscopy (Cryo-EM) .....	73
2.5.7	Processing of Micrographs.....	74
<b>Chapter 3</b>	<b>.....</b>	<b>75</b>

<b>Functional analysis of the alternative RNA-binding site within the N-terminal catalytic half of <i>E. coli</i> RNase E .....</b>	<b>75</b>
3.1 Introduction .....	76
3.2 Results .....	81
3.2.1 Site-directed mutagenesis and over-production of <i>E. coli</i> NTH RNase E.....	81
3.2.2 Purification of mutant RNase E proteins .....	89
3.2.3 Analysis of NTH RNase E binding to model RNA substrates.....	91
3.2.4 RNA-binding groove involvement in tRNA processing.....	97
3.2.5 Michalis-Menten analysis and dependency on ionic strength.....	103
Discussion.....	108
<b>Chapter 4.....</b>	<b>114</b>
4.1 Introduction .....	115
4.2 Results .....	119
4.2.1 Contribution of the RNA binding groove to RNase E essentiality .....	119
4.2.2 Contribution of the RNA-binding groove to autoregulation of RNase E .....	124
4.2.3 Sequence analysis and purification of RNase G .....	131
4.2.4 Biochemical analysis of RNase G .....	134
4.3 Discussion.....	143
<b>Chapter 5.....</b>	<b>150</b>
<b>Initial structural studies of RNase E by Electron Microscopy.....</b>	<b>150</b>
5.1 Introduction .....	151
5.1.1 Insight into NTH-RNase E function through structural studies .....	151
5.1.2 Electron Microscopy as a tool for structural biology ..	152
5.2 Results .....	156
5.2.1 Negative-stain Electron Microscopy of BR15 in complex with NTH-RNase E.....	156
5.2.2 Negative-stain Electron Microscopy of <i>glnW-metU</i> bicistronic tRNA precursor fragment in complex with D346N NTH-RNase E .....	159
5.2.3 Initial screening of RNase E by cryo-EM.....	169
5.3 Discussion.....	172
<b>Chapter 6.....</b>	<b>176</b>

<b>Discussion and future work .....</b>	<b>176</b>
6.1 Summary of work .....	177
6.2 Future work .....	179
<b>Chapter 7.....</b>	<b>183</b>
<b>References.....</b>	<b>183</b>



## List of Tables

Table 1.1 Ribonuclease distribution across the kingdom of bacteria.....	9
Table 1.2 Ribonucleases in <i>E. coli</i> . .....	11
Table 2.1 Antibiotics used for selection of bacteria. ....	44
Table 1.2 Bacterial strains used during this thesis. ....	45
Table 1.3 Plasmids used as part of this thesis. ....	46
Table 1.4 Synthetic oligonucleotides.....	54
Table 1.5 Primers for Site Directed Mutagenesis PCR.....	60
Table 1.6 cDNA amplicons.....	61
Table 3.1 List of NTH-RNase E Mutants. ....	85
Table 3.2 Rationale of amino acid substitutions made in RNase E .....	86
Table 3.3 Apparent Binding constant values for BR15 and the <i>rpsO</i> terminator RNA. (Data represents a single measurement) .....	96
Table 4.1 Doubling times of <i>E. coli</i> CJ1832 strains .....	124
Table 4.2 Summary of $\beta$ -Galactosidase-Autoregulation assay.....	129

## List of Figures

Figure 1.1 Spatio-temporal separation of degradosome from the transcription/translation apparatus. ....	7
Figure 1.2 Degradation of <i>rpsO-pnp</i> in <i>E. coli</i> Shown is a schematic of the degradation of the <i>rpsO-pnp</i> transcript.....	12
Figure 1.3 The Structure of RNase E. ....	24
Figure 1.4 Domain movement in NTH-RNase E during substrate binding. ....	34
Figure 1.5 Maturation of transfer RNA. Panel A shows a schematic representing a polycistronic transcript.....	38
Figure 1.6 Maturation of ribosomal RNA. ....	39
Figure 3.1 Crystal Structure of NTH-RNase E and the sRNA RprA. ....	78
Figure 3.2 Polypeptide Sequence alignment of members of the RNase E family from $\gamma$ -proteobacteria.....	83
Figure 3.3 SDS-PAGE analysis of <i>E. coli</i> BL21 (DE3) cellular extracts that have been induced to produce mutants of N-terminally tagged NTH-RNase E. ....	88
Figure 3.4 SDS-PAGE analysis of samples obtained during the purification of His-tagged NTH-RNase E by IMAC. ....	90
Figure 3.5 Electrophoretic mobility shift assay of BR15 by NTH-RNase E mutants.....	93
Figure 3.6 Electrophoretic mobility shift assay of the <i>rpsO</i> terminator by wild-type and 8x NTH-RNase E. ....	95
Figure 3.7 Electrophoretic mobility shift assay of radiolabelled <i>glnW</i> RNA subunits by wild-type and 8x NTH-RNase E.....	99
Figure 3.8 Electrophoretic mobility shift assay of FAM-labelled <i>glnW</i> RNA by wild-type and 8x NTH-RNase E. ....	100
Figure 3.9 Competition binding assay of <i>glnW</i> -RNase E with RprA. ....	101
Figure 3.10 Discontinuous Cleavage assay of a fragment of ArgX tRNA precursor by wild-type and 8x NTH-RNase E. ....	102
Figure 3.11 Michelis-Menten and Salt analysis of wild-type vs 8x mutant RNase E with LU13.....	105
Figure 3.12 Competition binding assay of <i>glnW</i> -RNase E with LU13.....	107
Figure 3.13 Hypothetical model of interactions of <i>glnW</i> and RNase E. Shown is the different possible explanations of the complex seen in the EMSA of 8x NTH-RNase E and <i>glnW</i> . ....	113
Figure 4.1 Structure of 5'UTR of <i>rne</i> mRNA. Shown is a diagram indicating the secondary structure of the <i>rne</i> 5'UTR. ....	116

Figure 4.2 Schematic representation of <i>E. coli</i> strain CJ1832.....	122
Figure 4.3 Assaying IPTG dependence and colony-forming ability of <i>E. coli</i> CJ1832 .....	122
Figure 4.4 RNase E complementation assay. ....	123
Figure 4.5 <i>E. coli</i> CJ1827 and CJ1828 temperature sensitivity. ....	126
Figure 4.6 Western Blot of c-Myc tagged RNase E from CJ1828 strains..	128
Figure 4.7 Electrophoretic mobility shift assay of 5'UTR of the <i>rne</i> transcript. ....	131
Figure 4.8 Sequence alignment of RNase G from select members of the $\gamma$ -proteobacteria with RNase E from <i>E. coli</i> .....	133
Figure 4.9 Analysis of samples taken during purification of RNase G by SDS-PAGE. ....	134
Figure 4.10 Confirmation of RNase G activity by discontinuous cleavage of LU13. ....	135
Figure 4.11 Electrophoretic mobility shift assay of BR15 and OH-LU13 by RNase G.....	137
Figure 4.12 Electrophoretic mobility shift assay of <i>glnW</i> and <i>rpsO</i> by RNase G. ....	138
Figure 4.13 Discontinuous cleavage of <i>argX-leuT-hisR-proM</i> tRNA precursor by RNase E and RNase G. ....	139
Figure 4.14 Congruence of RNase E and RNase G cleavage. ....	141
Figure 4.15 Conservation of RNase E and G cleavage site motif. ....	142
Figure 5.1 Single-particle EM workflow. ....	153
Figure 5.2 Negative-stain electron microscopy of BR15 in complex with NTH-RNase E. ....	157
Figure 5.3 Small-angle X-ray Scattering of NTH-RNase E apoprotein and BR15 RNP.....	158
Figure 5.4 Purification of D346N NTH-RNase E for structural studies. ....	161
Figure 5.5 Circular Dichroism of D346N NTH-RNase E. D346N.....	162
Figure 5.6 Analysis of the purification of <i>glnW-metU</i> RNA. ....	163
Figure 5.7 Small-angle X-ray Scattering of D346N NTH-RNase E apoprotein. ....	164
Figure 5.8 Negative-stain electron microscopy of <i>glnW-metU</i> RNA in complex with NTH-RNase E. ....	167
Figure 5.9 3D classification of NTH-RNase E in complex with <i>glnW-metU</i> . ....	168
Figure 5.10 3D auto-refinement of NTH-RNase E in complex with <i>glnW-metU</i> . ....	168
Figure 5.11 Size comparison of tRNA and RNase E.....	169
Figure 5.12 Initial screening by Cryo-EM. ....	171

Figure 6.1 Length and Sequence bias of Illumina vs Oxford Nanopore sequencing technologies..... 180

## List of Abbreviations

°C	Degrees Celsius
μ (unit)	Micro-
A	Adenosine
Å	Angstroms
APS	Ammonium persulphate
bp	Base pair
BSA	Bovine serum albumin
C	Cytosine
C (unit)	Centi-
CaCl <sub>2</sub>	Calcium chloride
Cryo-EM	Cryogenic Electron microscopy
CTH	C-terminal half
Da	Daltons
DEPC	Diethyl pyrocarbonate
D <sub>max</sub>	Maximum dimension
DMSO	Dimethyl sulphoxide
DNA	Deoxyribonucleic acid
DNase	Deoxyribonuclease
DTT	Dithiothreitol
<i>E. coli</i>	<i>Escherichia coli</i>
EDTA	Ethylenediaminetetraacetic acid
EM	Electron microscopy
EMSA	Electrophoretic mobility shift assay
g	Grams
<i>g</i>	Gravity
G	Guanosine
h	Hours
HCl	Hydrochloric acid
IMAC	Immobilised metal affinity chromatography
IPTG	Isopropyl-β-D-1-thiogalactopyranoside
K (unit)	Kilo-
KCl	Potassium chloride
l	Litre
LBA	Ligand binding assay
M	Molar
m (unit)	Milli-
MgCl <sub>2</sub>	Magnesium chloride
min	Minute
mol	Moles
mRNA	Messenger RNA
n (unit)	Nano-
NaCl	Sodium chloride
nt	Nucleotide
NTH	N-terminal half

NTP	Nucleotide triphosphate
OD <sub>x</sub>	Optical density at x nm
ORF	Open reading frame
PCR	Polymerase chain reaction
psi	Pounds per square inch
R <sub>g</sub>	Radius of gyration
RNA	Ribonucleic acid
RNase	Ribonuclease
RPM	revolutions per minute
rRNA	Ribosomal RNA
s	Second
S	Svedberg unit
SAXS	Small-angle X-ray Scattering
SDS	Sodium dodecyl sulphate
SEC	Size exclusion chromatography
sRNA	Small RNA
T	Thymine
TBE	Tris-borate-EDTA
TEMED	Tetramethylethylenediamine
T <sub>m</sub>	Melting temperature
Tris	Tris(hydroxymethyl)aminomethane
tRNA	Transfer RNA
U	Uracil
UV	Ultraviolet
V	Volts
v/v	Volume to volume
W	Watts
w/v	Weight to volume

# **Chapter 1**

## General introduction

## **1.1 Introduction to RNA decay**

### **1.1.1 *Escherichia coli* as a model organism for explicating the role of RNA decay.**

The genetically-tractable, model organism *Escherichia coli* has been studied extensively allowing the description and study of processes critical to life. Understanding the mechanisms that govern RNA decay, an essential process in gene regulation, will enable the improvement of systems that currently employ *E. coli* to produce macromolecules of academic, industrial and pharmaceutical interest. Whilst the focus of RNA decay appears to be trending to less tractable and more clinically- and industrially-relevant bacteria (Jones, 2010; Heo et al., 2016; Chao et al., 2017; Waters et al., 2017; Mardle et al., 2019), it is important to stress that the overall picture that governs mRNA stability remains incomplete even in *Escherichia coli*. Therefore, there is merit in continuing to elucidate the mechanisms that govern post-transcriptional gene regulation in model organisms.

### **1.1.2 Antagonism of RNA synthesis, translation and decay**

Each major step in the expression of proteins is catalysed and regulated by large macromolecular complexes and can be described in three largely contiguous stages; transcription, translation and decay. Transcription generates RNA that can be messenger RNA (mRNA), small regulatory RNA (sRNA) or precursors of the more stable transfer RNA (tRNA) and ribosomal RNA (rRNA). The synthesis and decay of RNA are antagonistic processes that determine mRNA levels. The transcription-degradation flux consequently establishes a steady state that can be altered by varying the rates of these two processes; increasing the rate of transcription increases



the input of RNA, while increased degradation reduces the size of the RNA pool. As the translation of proteins is dependent on the encoding RNA, the abundance of mRNA will affect protein levels in the cell. Global RNA stability is inversely correlated with abundance; thus, when transcription is repressed, the rate of degradation is reduced over time as the RNA pool is reduced (Bernstein et al., 2002). Therefore, the stability of a transcript may be described by a half-life. The half-lives of different bacterial RNAs show considerable variation, as a consequence of sequence and structural features. The half-life of an individual RNA can also vary, and this can be both dependent and independent of cell physiology (Bernstein et al., 2002). Mammalian mRNAs have half-lives ranging from minutes to many hours, which represents a much more stable RNA population compared to that of bacteria, with half-lives in the orders of seconds to minutes (Tourrière et al., 2002). The relative instability of bacterial mRNA results in close coupling of the transcriptome and proteome. Once transcription of a gene ceases, the mRNA tends not to linger and is degraded rapidly, halting protein production (Rauhut and Klug, 1999). Thus, RNA decay in bacteria facilitates transient changes in gene expression, allowing dynamic adaptation of the genetic programme to both internal and external stimuli. Importantly, RNA decay also results in the recycling of nucleotides, replenishing the pool that can then be utilised for further rounds of transcription.

RNA degradation and translation have been shown to be in direct competition. Previous work has demonstrated that increased translation of a transcript also results in increased stability (Deana and Belasco, 2005), most likely due to ribosomal coverage protecting the transcript from initial cleavages by endonucleases, such as RNase E. Confirming this, stalling of

ribosomes on transcripts has also led to increased stability. Interestingly, it was also found that 30S ribosome subunits could reduce cleavage in the 5' UTR of *rne* when bound, suggesting ribosomes provide steric protection and hinder the entry of RNase E even outside of the ORF (Richards et al., 2012). Also confirming these findings, Impairment of translation has been shown to result in unstable transcripts (Leroy et al., 2002). Furthermore, it has also been shown that transcripts produced by T7 RNA polymerase are less stable than normal transcripts. It has been proposed that T7 RNA polymerase advances much faster than the host polymerase, advancing far ahead of the translating ribosomes and thereby leaving free stretches of RNA that are exposed for endonucleolytic attack (Iost and Dreyfus, 1995). In addition to tight coupling of protein production and transcription, the competition between translation and degradation could occur for two other reasons: 1) Provides a form of RNA quality control, in that poorly translated mRNAs are rapidly degraded, this could serve as a buffer for genetic variation and aberrant transcription such that these mRNAs don't result in the production of potentially deleterious polypeptides and 2) Ensures that cleavages occur behind translating ribosomes, so that aberrant proteins and stalled ribosomes would not be accumulate and the last ribosomes can finish translation.

RNA decay in *E. coli* is primarily mediated by the multiprotein, membrane-bound, complex known as the degradosome, which is responsible for the processing and degradation of RNA (Vanzo et al., 1998; Mackie, 2013; Bandyra et al., 2013). The *E. coli* degradosome is primarily composed of RNase E, which forms the scaffold and initiates degradation by endonucleolytic cleavage, the 3'-5' exonuclease polynucleotide

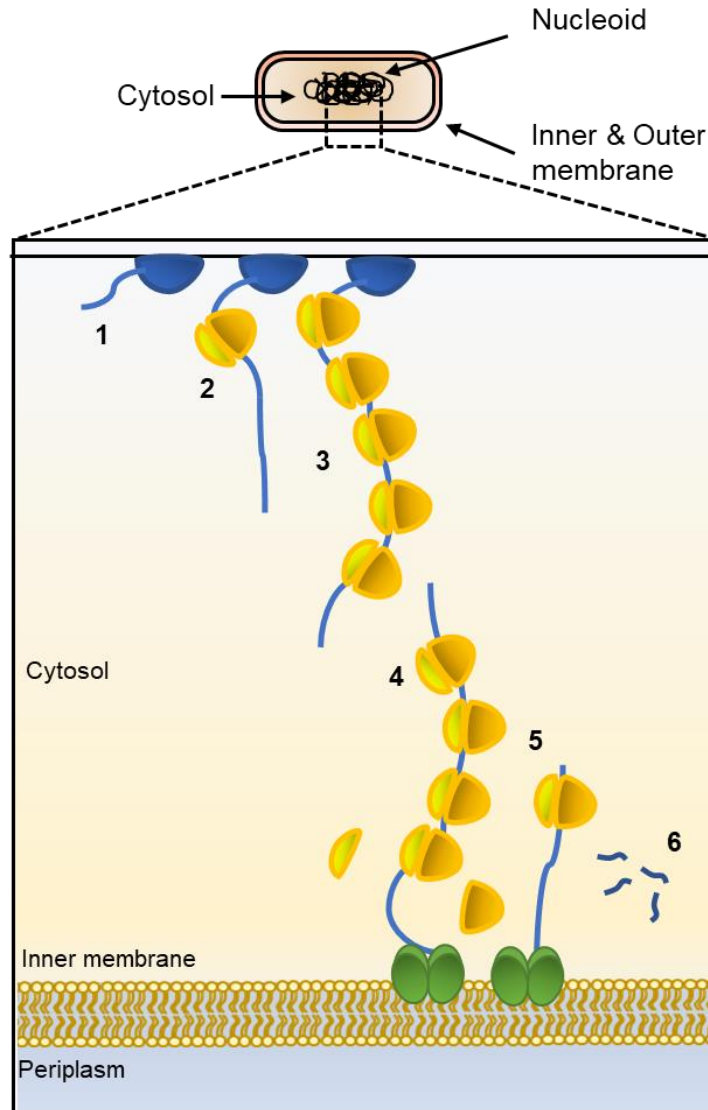
phosphorylase (PNPase), RNase helicase B (RhIB) and the glycolytic enzyme enolase (Bandyra et al., 2013). However, the degradosome is not fully capable of handling RNA processing and decay on its own and is assisted with the action of many other ribonucleases and additional factors. The *E. coli* degradosome was the first to be discovered, and analogues have since been seen in other bacteria, such as those based on RNase J1-J2 and the RNase Y in *Bacillus subtilis* (Vanzo et al., 1998; Lehnik-Habrink et al., 2012).

### **1.1.3 The organisation of the RNA decay machinery**

The degradosome is a membrane-bound complex that is spatially separated from the sites of transcription and translation (Khemici et al., 2008). Strains harbouring an RNase E variant that does not associate with the membrane have a slow-growth phenotype and show global stabilisation of mRNA (Hadjeras et al., 2019). Therefore, the positioning of the degradosome is vital for its function, and being the furthest intracellular location from the site of transcription, could suggest directionality to the RNA cycle.

*E. coli* possess an overall architecture that segments transcription/translation and RNA decay (Figure 1.1). Bacterial DNA is condensed into a nucleoid that remains in the centre of the cell and does not extend to the periphery (Robinow and Kellenberger, 1994; Bakshi et al., 2012). A ribosome-rich compartment encompasses it termed the 'ribosphere', which nascent mRNAs will laterally diffuse into shortly after initiation of transcription. Translation has been shown to start as soon as the 5' UTR of mRNA enters the 'ribosphere', resulting in polysomes that are effectively tethered to DNA via the RNA polymerases that are still transcribing the template DNA (Miller

et al., 1970; Stracy and Kapanidis, 2017). RNA polymerase can be present right at the edge of the 'nucleoid-ribosphere' boundary; however, ribosomes are largely excluded from the densest part of the nucleoid. Thus transcription and translation are less likely to be coupled in this region (Bakshi et al., 2012). Surrounding the 'ribosphere' is a 'degradosphere' – proximal to the membrane and is host to the RNA decay machinery (Taghbalout and Rothfield, 2008; Clarke, 2015).



**Figure 1.1 Spatio-temporal separation of degradosome from the transcription/translation apparatus.** The nucleoid (top) is the site of transcription initiation (1), mRNA (blue line) is synthesised by RNA polymerase (blue). The nascent 5' end of the RNA becomes accessible to ribosomes (orange), which allows for the initiation of translation. Transcription proceeds coupled to translation (3), once transcription ceases the RNA can then diffuse away from the nucleoid. Diffusion of RNA towards the periphery allows for capture by RNase E (green), which will then prevent further association by ribosomes (4). The passage of the last ribosomes is allowed to occur (5). Subsequently, cleavage is facilitated by the action of other members of the degradosome. Short oligonucleotides remain, which can then be degraded by oligoribonuclease (6).

#### 1.1.4 RNA decay in other bacteria

The N-terminal half of RNase E and RNase G have a high sequence and structural similarity and may have diverged from a common ancestor via a gene duplication event (Condon and Putzer, 2002). Therefore, homologues are often referred to as RNase E/G family members. The C-terminal half of RNase E is poorly conserved (Kaberdin et al., 1998; Ait-Bara et al., 2015), presumably due to a lesser sequence constraint as large regions of the protein in this region are intrinsically disordered (Callaghan et al., 2004; Bruce et al., 2018). Small islands of conservation within the C-terminal half can be seen in regions of functional relevance, with motifs <25 amino acids such as the arginine-rich regions and the motifs that interact with the other degradosome members (Ait-Bara et al., 2015).

Degradation and processing of RNA in bacteria that lack RNase E- proceeds similarly to *E. coli*, albeit by different ribonucleases. *Bacillus subtilis*, which is a Gram-positive member of the firmicutes, possesses RNase Y, an enzyme that has functional, but not structural, homology to RNase E (Lehnik-Habrink et al., 2011). Much like RNase E, RNase Y is stimulated by the presence of a 5' monophosphate (Shahbadian et al., 2009), which can be generated on nascent transcripts by an RppH homologue (Hsieh et al., 2013). Further parallels can be drawn between RNase E and RNase Y, despite sequence dissimilarity, both possess a catalytic N-terminal half and a disordered C-terminal half which may be responsible for degradosome formation (Lehnik-Habrink et al., 2012). Interestingly, membrane-tethering of the *B. subtilis* degradosome is required (Lehnik-Habrink et al., 2011) in contrast to *E. coli* where disruption only reduces the rate of growth (Hadjeras et al., 2019). One

of the other differences in *E. coli* and *B. subtilis* is the fact that the processing of 9S in *E. coli* is carried out by RNase E whereas in *B. subtilis* it is carried out by RNase M5. Besides the processing of 9S RNA which is performed by RNase M5 in *B. subtilis* (Condon et al., 2001), many of the other functions of *E. coli* RNase E are carried out by either RNase Y or RNase J in *B. subtilis* (Yao and Bechhofer, 2010; Lehnik-Habrink et al., 2011; Durand et al., 2012; Lehnik-Habrink et al., 2012). RNases E, G, J and Y are widely distributed amongst bacteria (Condon and Putzer, 2002) (Table 1.1). Just like RNase Y, there is no *E. coli* homologue of RNases J1 and J2. RNase J1 is essential in *B. subtilis*, whilst RNase J2 is dispensable for cell viability and only has a minor role in RNA decay. Whilst both RNase J1 and J2 are endoribonucleases, RNase J1 also possesses 5'-3' exonuclease activity (Mathy et al., 2007).

**Table 1.1 Ribonuclease distribution across the kingdom of bacteria**  
(reproduced from (Ait-Bara and Carpousis, 2015))

	RNase E	RNase G	RNase J	RNase Y
Acidobacteria	+	-	+	+
Actinobacteria	+	-	+	+
Bacteroidetes	-	+	-	+
Chlamydiae	-	+	-	+
Cyanobacteria	+	-	+	-
Proteobacteria				
• $\alpha$	+	-	+	-
• $\beta$	+	+	-	-
• $\gamma$	+	+	+	-
• $\delta$	+	+	+	+
• $\epsilon$	-	-	+	+
Firmicutes				
• Bacillales	+	+	+	+
• Clostridia	-	+	+	+
• Lactobacillales	-	-	+	+
Mollicutes	-	-	+	+
Spirochaetes	-	-	+	+

## **1.2 Macromolecular components of the RNA decay machinery**

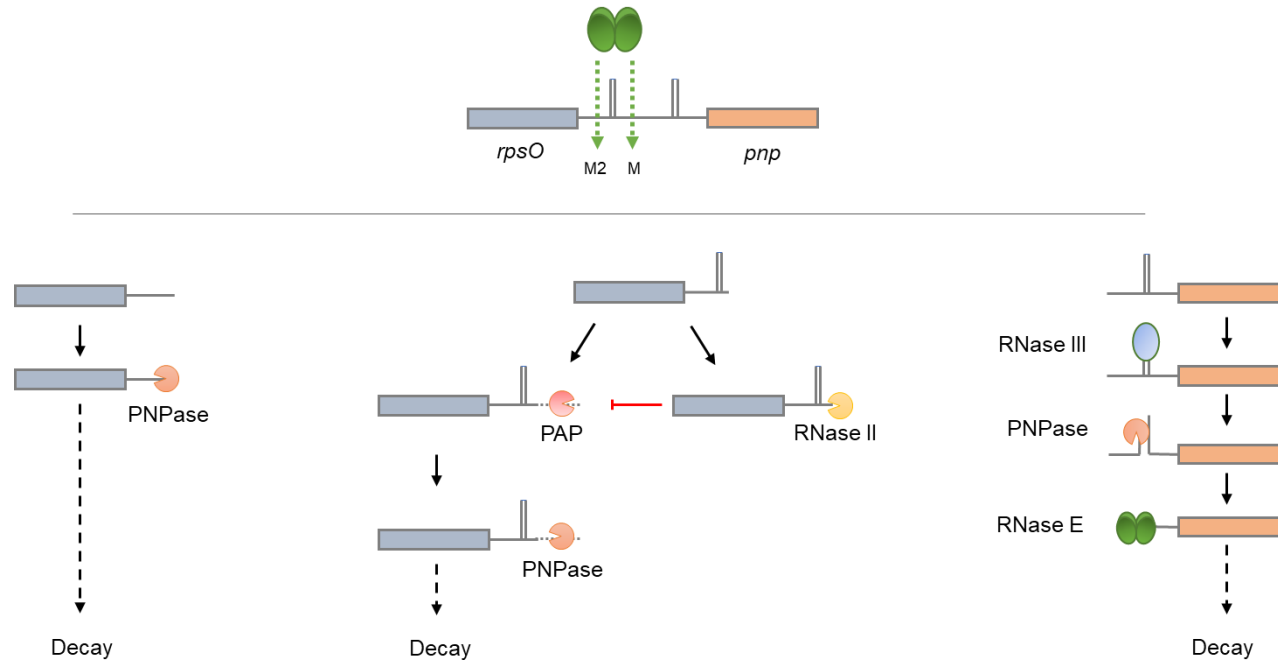
RNases catalyse the breakdown of the phosphodiester backbone of an RNA. The action of RNases can be categorised as either exonucleolytic or endonucleolytic. Exonucleases digest RNA by removing one ribonucleotide either from either the 5' or 3' terminus at a time, whilst endonucleases digest RNA internally to generate shorter fragments. Although, only three ribonucleases are essential in *E. coli* (Apirion and Lassar, 1978; Stark et al., 1978; Ghosh and Deutscher, 1999; Ow and Kushner, 2002; Hammarlöf et al., 2015). However, more than 15 ribonucleases (Table 1.2) contribute to maintaining proper regulation of gene expression along with several other auxiliary proteins. The interplay of multiple ribonucleases is required for the degradation of many RNAs as illustrated by the well-studied example of the *rpsO-pnp* transcript, encoding the S15 ribosomal protein and the RNase PNPase (Figure 1.2).



**Table 1.2 Ribonucleases in E. coli.**

Ribonuclease	Gene	Mechanism	Substrate preference	Class of RNA cleaved	Essentiality?
RNase E	<i>rne</i>	Endoribonuclease	ssRNA	mRNA, rRNA, tRNA, sRNA	Yes
RNase G	<i>rng</i>	Endoribonuclease	ssRNA	mRNA, rRNA, sRNA	
RNase HI/HII	<i>rnhA/rnhB</i>	Endoribonuclease	DNA:RNA	mRNA	
RNase P	<i>rnpA/rnpB</i>	Endoribonuclease	ssRNA	mRNA, rRNA, tRNA	Yes
RNase BN	<i>rnb</i>	Endoribonuclease	ssRNA	mRNA, tRNA	
RNase I	<i>rna</i>	Endoribonuclease	ssRNA	rRNA	
RNase III	<i>rnc</i>	Endoribonuclease	dsRNA	mRNA, rRNA, sRNA	
RNase D	<i>rnd</i>	Exoribonuclease (3'-5')	ssRNA	tRNA	
RNase PH	<i>rph</i>	Exoribonuclease (3'-5')	ssRNA	tRNA	
RNase R	<i>rnr</i>	Exoribonuclease (3'-5')	ssRNA	rRNA, sRNA	
RNase T	<i>rnt</i>	Exoribonuclease (3'-5')	ssRNA	rRNA, tRNA	
oligoribonuclease	<i>orn</i>	Exoribonuclease (3'-5')	ssRNA	short oligoribonucleotides	Yes
PNPase	<i>pnp</i>	Exoribonuclease (3'-5')	ssRNA	mRNA, tRNA, sRNA	
RNase II	<i>rnb</i>	Exoribonuclease (3'-5')	ssRNA	mRNA, tRNA	

Data from (Mackie, 2013)



**Figure 1.2 Degradation of *rpsO-pnp* in *E. coli*.** Shown is a schematic of the degradation of the *rpsO-pnp* transcript. RNase E makes the initiating cleavage which generates two products either by cleavage at M or M2. Cleavage at M2 removes the stabilising 3' stem-loop that allows entry and degradation of *rpsO* by PNPase. Cleavage at M generates a product consisting of *rpsO* possessing a stabilising 3' stem-loop which must be extended from by PolyA-polymerase (PAP) in order to provide a single-stranded entry point for PNPase which can slowly process through the stem-loop and degrade the RNA, this can also be performed by RNase R. RNase II antagonises degradation of *rpsO* by removing the poly-A tail generated by PAP, stabilising the transcript. Initial cleavage by RNase E of the *rpsO-pnp* transcript generates a 3' product consisting of *pnp*. Initial cleavage by RNase III within the 5' UTR of *pnp* generates a single-stranded region which allows access by PNPase allowing degradation to occur, the rest of *pnp* can be fragmented further by RNase E facilitating degradation of *pnp*. Image adapted from (Clarke, 2015).

### 1.2.1 Endonucleases

The majority of transcripts are stabilised by structured regions that inhibit entry by exonucleases, which includes rho-independent transcriptional terminators (Farnham and Platt, 1981; Mott et al., 1985; Newbury et al., 1987). Endonucleases cleave substrates internally by removing such regions, allowing exonucleases to enter. The action of endonucleases generates multiple products allowing for distributive degradation by exonucleases. In addition, one of the vital transition steps between translation and RNA decay could theoretically be cleavage within the 5' UTR to remove translation initiation regions. This step would be particularly important in ensuring that there is no steric clash between the 5'-3' action of ribosomes and the 3'-5' action of exonucleases.

#### 1.2.1.1 RNase E

RNase E is able to engage with its substrates in two ways (see section 1.3.2) One pathway involves the presence of 5' monophosphate either generated by the action of RppH (section 1.2.3.1) or by cleavage of RNA (Mackie, 1998). RNase E was identified as the enzyme responsible for the processing of 9S rRNA (Ghora and Apirion, 1978; Misra and Apirion, 1979), a role that is exclusive to RNase E and thus thought to be the source of its essentiality (Apirion and Lassar, 1978). The mutation *ams-1* was discovered around the same time and results in the accumulation of the majority of RNAs at a non-permissive temperature (Ono and Kuwano, 1979). The *ams-1* mutation was later found to be in the same gene, *rne*, as another temperature-sensitive mutation *rne-3071* (Mudd et al., 1990; Babitzke and Kushner, 1991; Melefors and von Gabain, 1991; Taraseviciene et al., 1991)

therefore showing that RNase E is the major endonuclease involved in RNA decay as well. RNase E has multiple essential functions that extend to its role in rRNA (Ghora and Apirion, 1978; Misra and Apirion, 1979) and tRNA processing (Ow and Kushner, 2002) as well as mRNA degradation (Anupama et al., 2011; Hammarlöf et al., 2015; Himabindu and Anupama, 2017).

#### 1.2.1.2 RNase G

CafA was originally implicated in the regulation of structuration of the cytoplasm (Okada et al., 1994). It was shown to be responsible for 16S rRNA processing (Li et al., 1999b; Wachi et al., 1999). Not only does RNase G possess high sequence similarity to RNase E, but disruption of *mng* exacerbates the *ams-1* temperature sensitivity, in that it lowers the permissive temperature (McDowall et al., 1993; Wachi et al., 1997). RNase G has a preference for substrates possessing a 5' monophosphate that improves substrate occupancy (Jourdan and McDowall, 2007). It has critical involvement in the regulation of several genes such as the transcript encoding alcohol dehydrogenase, *adhE*, (Umitsuki et al., 2001). Indeed, *mng* disruption leads to a significant overproduction of encoded AdhE (Umitsuki et al., 2001). RNase G cleaves within the 5' UTR of *adhE*, and fusion of this region onto other transcripts direct them to RNase G mediated regulation (Umitsuki et al., 2001). Alcohol dehydrogenase is not the only glycolytic enzyme whose production is regulated by RNase G, as the production of Enolase, a component of the degradosome, is regulated by RNase G. The *eno* transcript has an increased half-life (3-fold) when *mng* is disrupted (Kaga

et al., 2002). Further work has shown that RNase G is involved in the regulation of multiple genes involved in metabolic pathways (Ito et al., 2013). Although inactivation of RNase E is lethal, it has been shown that rescue can occur by 1000 fold overexpression of its paralogue RNase G. However, growth in this strain is impaired (Lee et al., 2002). It is important to note that RNase G is normally present at a concentration of 3% compared with RNase E (Lee et al., 2002). More recent work has shown that complementation of RNase E inactivation can be achieved by expressing RNase G with mutations in the RNase H domain (Chung et al., 2010).

#### 1.2.1.3 RNase III

RNase III cleaves double-stranded RNA and is important in making initiating cleavages during rRNA processing (see section 1.4.2). Disruption of the encoding, *rnc* gene is not lethal (Apirion et al., 1976). However, disruption reduces the rate of *E. coli* growth which has been linked to decreased rate of protein synthesis due to improper rRNA processing (Apirion et al., 1976; Talkad et al., 1978; Babitzke et al., 1993).

The *rpsO-pnp* transcript is stabilised by *rnc* disruption (Takata et al., 1987). RNase III makes a cleavage within a stem-loop within the 5' UTR of *pnp* (Régnier and Portier, 1986; Portier et al., 1987) generating a product in which PNPase can act upon (Jarrige et al., 2001).

The *adhE* transcript, introduced earlier as a substrate for RNase G is also a substrate for RNase III. However, unlike with *rng*, disruption of *rnc* results in a decrease in the abundance of the AdhE protein (Aristarkhov et al., 1996), suggesting that RNase III, in this case, stimulates, rather than antagonises, protein production. It has been found that a stem-loop encapsulates the RBS

within the 5' UTR of *adhE* and therefore inhibits ribosomal interaction. Cleavage by RNase III acts as a positive regulator of translation in this case, by disrupting this stem-loop and exposing the RBS to ribosomes. Additionally, the resultant 5' monophosphate is inaccessible to endonucleases, such as RNase G, as the last the nucleotides at the 5' end of the RNA form a stem-loop (Aristarkhov et al., 1996; Ito et al., 2013). Globally, only 12% of transcripts seemed to have differential stability when *rnc* was disrupted (Stead et al., 2011), suggesting other ribonucleases can compensate in the absence of RNase III activity.

### 1.2.2 Exonucleases

All identified exonucleases in *E. coli* possess 3'-5' exonucleolytic activity

#### 1.2.2.1 PNPase

Polynucleotide phosphorylase (PNPase) is a phosphorolytic exonuclease, which consumes phosphates to hydrolyse the phosphodiester backbone (Zuo and Deutscher, 2001). PNPase associates with the degradosome in *E. coli* and shares structural similarity to a component of the exosome (Januszyk, 2012). PNPase requires a decanucleotide overhang in order to load onto substrates, but once attached can process through stem-loops, albeit at a reduced rate (McLaren et al., 1991; Coburn and Mackie, 1998).

Inactivation of PNPase, although tolerated results in accumulation of the *rpsO-pnp* transcript (Jarrige et al., 2002). However, deletion of the *rpsO* region from the transcript abolishes accumulation, indicating PNPase activity is only necessary for exonucleolytic cleavage within the 5' UTR after cleavage by RNase III (Jarrige et al., 2001). Whilst disruption of *pnp*, the gene encoding PNPase is not lethal; a synthetic lethal effect is seen if both

*pnp* and *rnb* (encoding RNase II) is disrupted. If only one of the above is disrupted, it results in upregulation of the other (Donovan and Kushner, 1986; Zilhão et al., 1996). Interestingly, at low temperatures, functional PNPase is vital for cell viability (Zangrossi et al., 2002).

PNPase displays some polymerase-like activity, in which the 3' end of an RNA can be elongated under high nucleotide diphosphate concentration. Under these conditions, CDP is preferably used as a substrate (Ost and Deutscher, 1990), and similar activity has been seen in PNPase from chloroplasts (Yehudai-Resheff et al., 2001).

PNPase has been shown to be regulated by citrate, a product of the citric acid cycle. PNPase degradation activity is inhibited by chelation of citrate by magnesium within the active site, whereas polymerase activity by PNPase is increased in the presence of citrate (Nurmohamed et al., 2010).

#### 1.2.2.2 RNase II

RNase II is a hydrolytic exonuclease that only cleaves single-stranded RNA. RNase II requires an overhang of at least a decanucleotide (Frazão et al., 2006). Once the RNA is shorter than this, RNase II is still able to cleave it but in a distributive manner until the substrate becomes a tetranucleotide (Zuo and Deutscher, 2001; Frazão et al., 2006).

RNase II contributes to the processing of the bicistronic *rpsO-pnp* transcript (Figure 1.2). However, it has a stabilising effect on the transcript by removing the single-stranded overhang required for exonucleolytic degradation by PNPase (Hajnsdorf et al., 1994; Marujo et al., 2000). In fact, RNase II contributes to the stabilisation of multiple transcripts, shown by decreases in the half-life of 31% of mRNAs upon RNase II inactivation.

However, RNase II is not exclusively involved in stabilisation, as 7% of transcripts are stabilised upon inactivation (Mohanty and Kushner, 2003).

#### 1.2.2.3 RNase R

RNase R has a similar domain organisation to RNase II (Matos et al., 2011) but also possesses another domain that displays helicase activity. This region is dependent on an initial interaction with a single-stranded region of seven nucleotides and can process through strong secondary structure where PNPase cannot (Cheng and Deutscher, 2002; Vincent and Deutscher, 2006). RNase R is also involved in processing and degradation of the *rpsO-pnp* transcript (Figure 1.2), and like PNPase, its activity is antagonised by the action of RNase II (Andrade et al., 2009). RNase R associates with a complex that is responsible for ribosome rescue. The complex is constituted of SmpB and the non-coding RNA tmRNA/SsrA (which is similar to both mRNA and tRNA) (Karzai and Sauer, 2001). The complex is responsible for the rescue of ribosomes that are stalled on mRNAs that do not possess a stop codon (Sauer et al., 2000). The complex directs the polypeptide associated with a stalled ribosome for proteolysis, and RNase R degrades the RNA preventing both the generation of more stalled ribosomes and mitigating the risk of release of potentially deleterious polypeptides (Richards et al., 2006).

#### 1.2.2.4 Oligoribonuclease

Oligoribonuclease (*orn*) is a 'nanoRNase' (Danchin, 2009) which is responsible for the exonucleolytic digestion of the fragments generated as by-products of the action of other RNases. The production of short oligonucleotides can have potentially deleterious consequences, replication



and transcription bubbles can be affected severely by the presence of short oligonucleotides (Milne et al., 2001) In addition, action by orn is vital to prevent the accumulation of products of RNA decay and restore the ribonucleotide pool. This is confirmed by the fact that orn is essential and generates mononucleotides from these short oligonucleotides (Ghosh and Deutscher, 1999).

### **1.2.3 Other components**

Several other proteins contribute to RNA degradation in *E. coli* without possessing ribonuclease activity themselves.

#### **1.2.3.1 RppH**

RNA pyrophosphohydrolase (RppH) is a non-essential protein that is responsible for the removal of pyrophosphates from the 5' end of mRNA, which as a consequence of the directionality of transcription, are triphosphorylated (Deana et al., 2008). Knockout of *rppH* results in stabilisation of a quarter of transcripts (Belasco, 2010; Richards et al., 2012). Decapping in *E. coli* is thought to be a two-stage process possibly involving an unknown enzyme that removes the  $\gamma$ -phosphate followed  $\beta$ -phosphate removal by RppH. However, RppH can remove both  $\gamma$ - and  $\beta$ -phosphates but at a reduced rate compared with removing the  $\beta$ -phosphate alone (Luciano et al., 2017). The generated 5' monophosphorylated RNA can engage with RNase E via the 5' monophosphate dependent pathway (Mackie, 1998).

#### **1.2.3.2 RhIB**

RNase helicase B (RhIB) is a non-essential helicase that features the 'DEXD/H' motif found in many helicases (Morita et al., 2004; Cordin et al.,

2006). RhlB unwinds stretches of RNA of less than twenty-two base pairs in an ATP dependent manner (Py et al., 1996). This assists PNPase-mediated degradation by unwinding short stem-loops of RNA that would otherwise prevent further degradation (Lin and Lin-Chao, 2005; Carpousis, 2007). Whilst RhlB associates with the degradosome (Bruce et al., 2018) it is also able to directly interact with PNPase (Liou et al., 2002). Random mutagenesis has revealed that direct interaction with PNPase is necessary for its function even if it is still able to associate with RNase E (Tseng et al., 2015). During cold shock RhlB is replaced with another RNA helicase, CsdA (Prud'homme-Généreux et al., 2004).

#### 1.2.3.3 Poly(A) polymerase

Polyadenylation serves a different role in prokaryotes compared with eukaryotes. Whilst the poly(A) tail can have a protective role in eukaryotes (Wu and Brewer, 2012), it promotes degradation in prokaryotes by assisting exonuclease entry (Xu et al., 1993). Poly(A) polymerase I (PAP) is a polymerase that elongates the 3' end of RNA by polyadenylation, typically adding around ten nucleotides (Cao and Sarkar, 1992). Although elongation at the 3' end of RNA mainly occurs by through PAP-mediated polyadenylation, generation of 3' tails occur through polymerase activity of PNPase as mentioned above (Ost and Deutscher, 1990). Pulse labelling experiments have revealed that poly-adenylation occurs only on the minority of transcripts; only 2% of total RNA contains poly-A tails (Nakazato et al., 1975). Therefore, it is unsurprising that PAP is dispensable for cell viability (Masters et al., 1993). The proportion of individual transcripts that are poly-adenylated also varies for example 40% of *trpA* mRNAs are poly-adenylated

whereas polyadenylation on *rpsO* is only present on 10% of transcripts (Karnik et al., 1987; Le Derout et al., 2003).

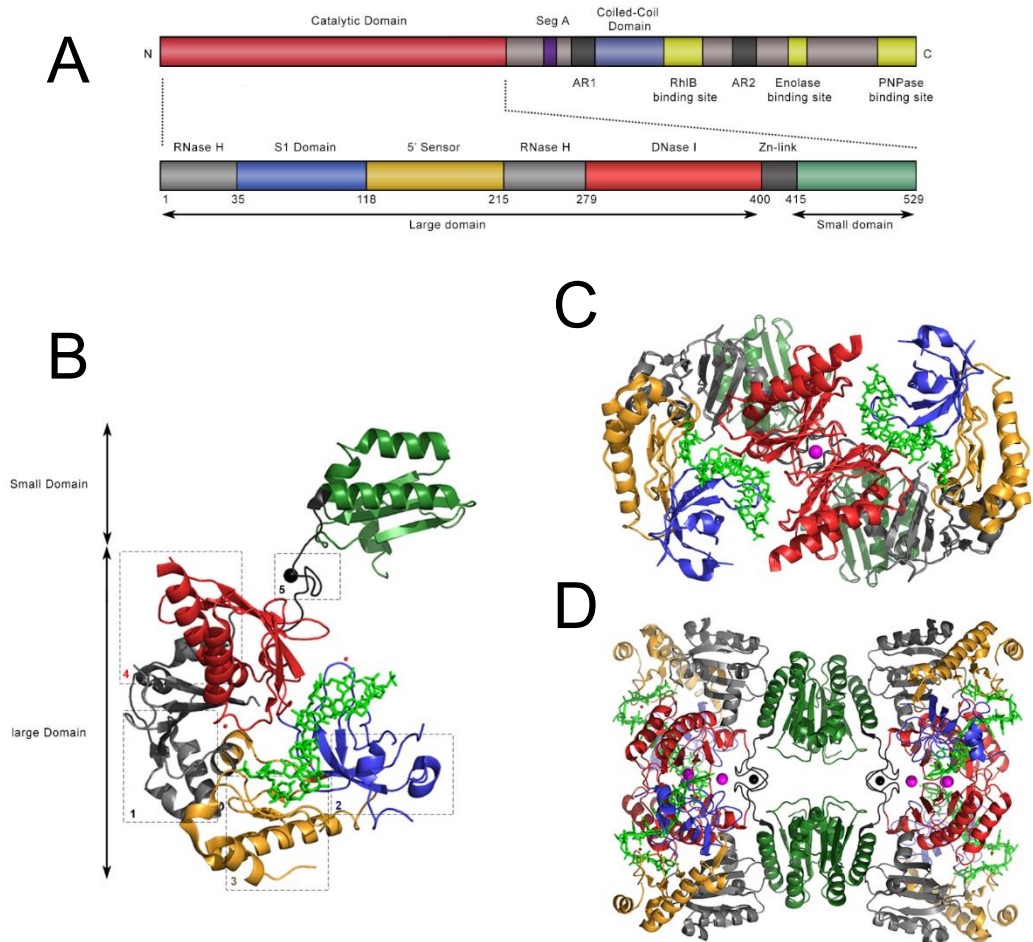
### **1.3 RNase E**

Introduced above (section 1.2.1.1), RNase E is an essential endonuclease, although its role extends beyond this. RNase E acts as an organising centre, anchoring the degradosome to the inner membrane of *E. coli* (Lopez et al., 1999; Callaghan et al., 2004; Khemici et al., 2008). Messenger RNAs must first become vulnerable to initiate decay; this may occur through weak interactions with ribosomes or translational repression to reduce ribosomal coverage and expose regions of the transcript to RNase E (Braun et al., 1998; Tsai et al., 2012). Exposed mRNA is cleaved by RNase E, and in the majority of cases this represents the initiating step for cleavage, Subsequent cleavages are also catalysed by RNase E, with each cleavage event creating smaller RNA fragments that are then acted upon by other RNases that scavenge the cleaved products. In this way, RNase E digests up large fragments effectively creating multiple smaller substrates, allowing the ‘workload’ to be spread amongst multiple enzymes, reducing the time for digestion as well as increasing the area for which exonucleases can act.

#### **1.3.1 Structure**

RNase E is functionally active as a homotetramer. RNase E monomers are 118 kDa constituted of 1061 amino acids (Figure 1.3). Monomers are composed of a globular, catalytic amino-terminal half (NTH) (1-529) and a largely disordered carboxy-terminal half (CTH) (530-1061) which contains regions that may undergo disordered-to-ordered transitions to facilitate binding to other components of the degradosome (Bruce et al., 2018). RNase E monomers associate via two different surfaces to form a dimer of dimers that are stabilised through coordination between cysteines and a

Zn<sup>2+</sup> ion (Callaghan et al., 2003; Callaghan, Redko, et al., 2005). Whilst the structure of the NTH has been solved, the exact organisation of the CTH tails relative to the catalytic core remains unknown (Callaghan, Marcaida, et al., 2005). The purified NTH (amino acids 1-529) of RNase E is active *in vitro*, but *in vivo*, its activity is concordant with the activities of the rest of the degradosome (Carpousis, 2007), and it is believed that native RNase E is almost exclusively active in its membrane-bound form (Taghbalout and Rothfield, 2008) Although release of RNase E into the cytosol is tolerated, its spatial positioning is vital for function (Hadjeras et al., 2019).



**Figure 1.3 The Structure of RNase E.** Panel A shows the primary structure of the RNase E polypeptide (1-1061). The monomer can be divided into two halves, a catalytically active N-terminal half (NTH) and a C-terminal half (CTH) that has domains that are necessary for the interaction with other members of the degradosome. NTH (1-529) can be divided into two globular domains, the large domain (1-400) and the small domain (415-529). The domains within the CTH are as follows (numbers indicate the amino acids of which the domains span) segment (seg) A (565-585), coiled-coil domain (533-712), RhlB binding site (698-762), enolase binding site (823-847) and the PNPase binding site (1021-1061). Panel B shows a cartoon representation of the crystal structure (PDB: 2C0B) showing the RNase E monomer interacting with an RNA substrate, labelled as follows; 1. RNase H like fold shown in grey, 2. S1 Domain shown in blue, 3. 5'-monophosphate sensor domain shown in orange, 4. DNase I Domain is shown in red, 5. Zinc Link is shown in black. Panel C shows a cartoon representation of the crystal structure showing the principal dimer formed by RNase E. The second dimer would lie below the plane of the cartoon. Panel D shows a cartoon representation of the crystal structure showing the RNase E homotetramer. Figure generated in PyMOL based on (Callaghan, Marcaida, et al., 2005).

#### 1.3.1.1 The RNase H domain (1-35, 215-279)

The RNase H domains (also called RNase H-like fold, referred simply in this work as the RNase H domain) have been of interest recently as mutations in this domain have had surprising effects on RNase E activity. A Q36R mutation was found to increase the ability of RNase E to bind RNA at its active site. It has been suggested that RNA may bind this region as a form of uncompetitive regulation (Go et al., 2011). A proximal tyrosine residue at position 25 was mutated to an alanine, which resulted in decreased activity but increased binding to a potential allosteric site (Kim et al., 2014). Recently, crystallographic data has provided more concrete evidence for the interaction of RNA at this site. Indeed, RNA was found to interact with both of the RNase H domains and also make contacts within the small domain (Bandyra et al., 2018) (also see Figure 3.1). As mentioned above, RNase G is unable to compensate for RNase E, but mutations made within the RNase H domain of RNase G allow it to compensate RNase E deficiency when *mng* was placed under the control of the *mne* promoter (Chung et al., 2010).

#### 1.3.1.2 The S1 domain (35-118)

The S1 domain (also referred to as S1-like domain) is highly conserved within RNase E; it is also present in many RNA-binding proteins for example in the degradosome-associated exonuclease PNPase as well as RNase II, RNase R and RNase G (Bycroft et al., 1997; Schubert et al., 2004; Matos et al., 2011; Qu et al., 2012). Together with the DNase I domain, the S1-like domain forms the catalytic surface which is able to accommodate RNA (Callaghan, Marcaida, et al., 2005). The S1 domain displays some flexibility which may allow it to vary to accommodate RNAs of varying structure

(Callaghan, Marcaida, et al., 2005; Koslover et al., 2008; Bandyra et al., 2018). Two phenylalanine residues at positions 57 and 67, known as the hydrophobic pocket, are thought to make contacts with RNA through  $\pi$ -stacking interactions, aligning the scissile phosphodiester bond for cleavage (Callaghan, Marcaida, et al., 2005). It is thought that stacking of one of the bases between the phenylalanine residues and bases within the RNA results in distortion of phosphodiester RNA backbone phosphodiester RNA backbone, predisposing it for cleavage (Diwa et al., 2003). Substitution of these residues with alanine resulted in a 50-fold reduction in enzyme activity but no change in RNA affinity (Callaghan, Marcaida, et al., 2005).

The  $\beta$ -amino group of lysine at position 112 makes contacts with the scissile phosphate, potentially contributing to cleavage by lowering the activation energy (Callaghan, Marcaida, et al., 2005). It is also thought that interaction occurs between the oxygen on the base two nucleotides upstream of the scissile bond and the amine group of the lysine at position 106 on the protein, and this may explain the substrate preference for purines at this site (McDowall et al., 1995; Kaberdin, 2003; Callaghan, Marcaida, et al., 2005).

Double-stranded RNA could possibly enter the RNA binding channel, but it would not be able to interact with F57 and F67. Previous work has shown that the pucker of the ribose ring confers susceptibility of RNA to cleavage, and therefore dsRNA may not adopt the same confirmation that is required for cleavage (Redko et al., 2003). However, a monophosphate can be provided *in trans*, by base pairing to the RNA to be cleaved provided that the region around the scissile bond is unpaired (Bandyra et al., 2012; Mardle et al., 2019).



The essentiality of RNase E has been demonstrated using two mutations that are located within the S1 domain. G66S and L67F, located beneath residues 57 and 67 conferred temperature sensitivity (Apirion, 1978).

#### 1.3.1.3 The 5' monophosphate sensor domain (118-215)

The 5' monophosphate sensor contributes to substrate recognition and binding. The hydroxyl group of the tyrosine at 170 can hydrogen bond with oxygen in the 5' monophosphate of bound RNA. This is further strengthened by additional interactions with arginine at position 169 which makes ionic interactions with one of the anionic oxygens. Valine at position 128 contributes through hydrophobic interactions with the 5' terminal base which helps to stabilise the accommodation of the 5' monophosphate into the sensing pocket (Callaghan, Marcaida, et al., 2005). The T170V mutation does not affect the cleavage of hydroxylated RNA but reduces the rate of cleavage of monophosphorylated RNA (Callaghan, Marcaida, et al., 2005; Clarke, 2015). V128A mutation has a modest effect on cleavage (approximately 10%) suggesting that has a minor contribution to interaction with monophosphorylated RNA (Stead and McDowall, unpublished data).

As the 5' monophosphate sensor is too small to accommodate larger chemical groups such as tri- or diphosphate, it explains observations of inefficient cleavage of 5' triphosphorylated RNAs (Garrey et al., 2009; Kime et al., 2010). 5' hydroxylated RNAs would not be able to make the necessary contacts with R169 and T170 (Callaghan, Marcaida, et al., 2005). Presumably, secondary structure within the 5' end of RNAs would also reduce cleavage, by interfering with the V128 interaction with the first base (Emory and Belasco, 1990; Chen et al., 1991).

Structural information has revealed that RNase E is not rigid, with 'open' and 'closed' conformations shown through X-ray crystallography (Callaghan, Marcaida, et al., 2005; Koslover et al., 2008; Bandyra et al., 2018). Interpolation between the 'open' and 'closed' forms shows very obvious movement of the S1-like domain and 5' sensor, which move together with a 55° movement, which has been termed the mousetrap model (Koslover et al., 2008). The mousetrap model hypothesises that interaction with the 5' sensor causes a conformational change that results in the S1 domain moving down onto the DNase I domain to promote cleavage (Koslover et al., 2008). However, biochemical data suggests that a monophosphate only contributes to improving substrate occupancy and does not affect the catalytic step (Kime et al., 2014). This may indicate that the S1-like domain samples many conformations between the defined 'open' and 'closed' states seen by X-ray crystallography.

#### 1.3.1.4 The DNase I domain (279-400)

The DNase I domain coordinates a  $Mg^{2+}$  ion required for cleavage by two aspartate residues at positions 303 and 346. A  $Mn^{2+}$  ion can also be used in place of the magnesium (Thompson et al., 2015). D346N and D303N mutants bind RNA with comparable affinity but cleave with a 25-fold decrease in efficiency (Callaghan, Marcaida, et al., 2005). The D303 residue is maintained in a specific orientation by hydrogen bonding with N305. N305D mutation disrupts this interaction and also results in decreased catalytic activity (Callaghan, Marcaida, et al., 2005). Crosslinking experiments have revealed RNA interaction with an asparagine at 323 within this domain. N323 is beyond the RNA-binding channel, and RNA interaction

at this site has not been shown by any published crystallographic studies (Callaghan, Marcaida, et al., 2005; Bandyra et al., 2018). Mutation N323A decreases the ability of RNase E to regulate its own production and thus may reflect a specialised interaction (Schuck et al., 2009).

The DNase I domain also contains a hydrophobic stretch of residues that strengthens interaction with the adjacent protomer within the principle dimer (Callaghan, Marcaida, et al., 2005). As two surfaces are responsible for the hydrolysis of RNA each protomer contributing one of the two surfaces, resulting in a dimer with two active sites (Callaghan, Marcaida, et al., 2005).

RNase E possesses some sequence specificity, the stringency of which is contended. However, broadly, it prefers to cleave in AU-rich regions, with a preference for a purine two nucleotides upstream from the scissile bond (McDowall et al., 1994; Kaberdin, 2003; Clarke, 2015; Del Campo et al., 2015; Chao et al., 2017), with a prefer although RNase E has been shown to cleave poly-A RNA *in vitro* (Walsh et al., 2001; Kaberdin, 2003). A cleavage site would typically look like: 5'-AN↓AU-3' or 5'-GN↓AU-3' (↓ represents scissile bond) (Kaberdin, 2003). Occlusion of RNase E by secondary structure can prevent cleavage; it is possible that this could also occur through steric hindrance by RNA binding proteins (Coburn and Mackie, 1998).

#### 1.3.1.5 The Zn-link and small domain (400-415, 415-529)

The Zn-link is necessary for tetramer formation; co-ordination of a Zn<sup>2+</sup> ion by C401 and C411 (Callaghan, Redko, et al., 2005). Mutation of either cysteine results in the inability to form the full tetramer, resulting in a decrease in catalytic activity, suggesting that complete tetramer formation is

required for optimal activity. Conformational changes within the small domains have been observed which may indicate cooperation between the two dimers possibly explaining the dramatic decrease in activity in the absence of the full tetramer (Koslover et al., 2008). Furthermore, reorganisation is seen in the small domain upon RNA interaction, showing the 'closed state' of RNase E can be achieved even in no RNA is within the active site (Bandyra et al., 2018).

#### 1.3.1.6 Segment A (565-582)

Segment A (sometimes referred to as MTS) is an amphipathic  $\alpha$ -helix that is present within the C-terminal half. It is made up of 20 amino acids between positions 565-585. The helix features a unique pattern of residues that consist of hydrophobic residues down one half of the helix that can be buried into the phospholipid bilayer and hydrophilic residues down the other half that can be exposed to the cytosol. The helix also possesses a boundary between the two halves consisting of cationic residues that can interact with the anionic phosphate groups on the phospholipids (Khemici et al., 2008), membrane tethering is not necessarily restricted to this region of RNase E as it has been shown that the N-terminal half also can interact with liposomes (Murashko et al., 2012). Furthermore, membrane tethering is not absolutely essential for function *in E. coli*. However, there are consequences on both RNase E stability, autoregulation, RNA turnover and cell physiology by abolishing it (Hadjeras et al., 2019). RNase E in species other than *E. coli* such as *Caulobacter crescentus*, a member of the  $\alpha$ -proteobacteria does not possess segment A and thus is not membrane-bound (Ait-Bara et al., 2015; Bayas et al., 2018).

#### 1.3.1.7 Arginine rich domains 1 and 2 (AR1 & AR2; 604-644, 796-814)

The roles of the AR1 and AR2 in RNA decay have not been well characterised. However, it has been shown that the rate of 9S cleavage *in vitro* is improved by utilising a construct that extends 1-844 when compared with an RNase E construct constituting residues 1-488 (Kaberdin et al., 2000). Whilst no catalytic activity is detectable for the C-terminal half alone, it is possible that interactions at this site promote many cleavages that RNase E makes by improving substrate occupancy (Callaghan et al., 2004). As the arginine rich regions occupy either side between the RhIB binding site, it is plausible that RNA binding in these regions assist in function of RhIB, possibly by facilitating substrate engagement with the helicase.

#### 1.3.1.8 RhIB binding site (719-731)

RhIB binds with a 1:1 stoichiometry to its binding site on RNase E (Chandran et al., 2007). Which is where the majority of RhIB resides (Khemicci et al., 2005). Disruption of interaction with the C-terminal half of RNase E results in an inability for RhIB to function (Worrall et al., 2008). ATP binding and hydrolysis stimulates unwinding of RNA by the helicase, the action of which could simultaneously present the 5' end of the RNA to RNase E and the 3' end to PNPase (Bandyra et al., 2013). A synthetic lethal effect is seen in RNase E mutants that possess a CTH deletion in addition to R169Q mutation (Garrey and Mackie, 2011), constructs that include the RhIB binding site result in restoration in viability, suggesting a role for RhIB in mechanisms of RNA decay not involving the 5' monophosphate dependent pathway (Garrey and Mackie, 2011; Anupama et al., 2011).

#### 1.3.1.9 Enolase Binding site (734-850)

RNase E-bound enolase does not represent its primary cellular locale; bound species represent only 10% of the total population (Py et al., 1994). Enolase interacts with a small  $\alpha$ -helix that is present on the CTH of RNase E (Chandran and Luisi, 2006; Nurmohamed et al., 2010). No difference in activity of enolase has been found following binding to RNase E (Callaghan et al., 2004). It has been hypothesised that localisation of enolase to the membrane could facilitate its role within glycolysis as it is the penultimate step in pathway, the next step is performed by pyruvate kinase which is also membrane-bound. Localisation of glycolysis to the membrane could aid RNA decay by providing a source of ATP for helicase activity by RhlB and polymerase activity by PAP I (Bandyra et al., 2013). The presence of enolase within the degradosome has been shown to allow rapid degradation of *pstG* RNA, encoding a glucose transporter, during phosphosugar stress. Under normal conditions there is no apparent difference in *pstG* degradation with or without enolase, this may point to a direct role of enolase being associated with the degradosome rather than a moonlighting function of RNase E (Morita et al., 2004).

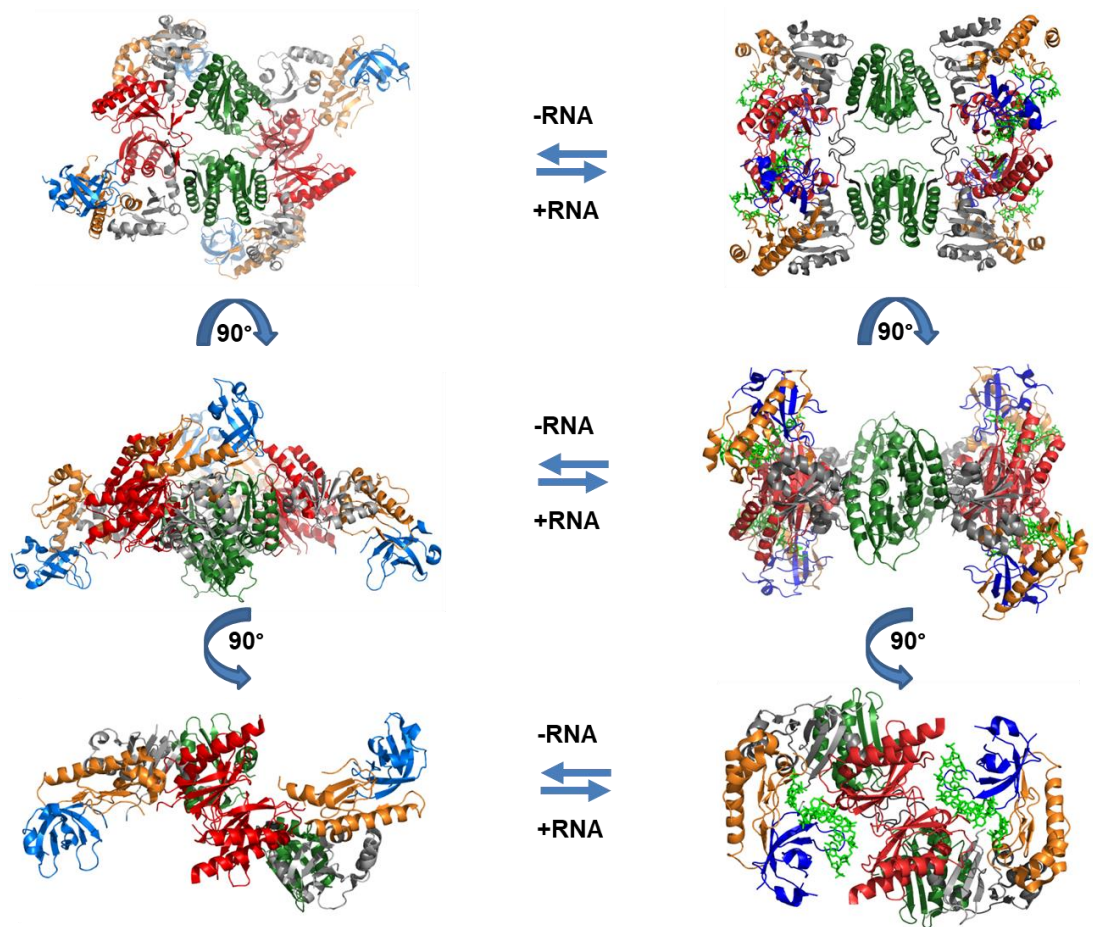
#### 1.3.1.10 PNPase-binding site (1021-1061)

PNPase interacts with RNase E at positions 1021-1061, a domain that is folded into a  $\beta$  sheet that is able to form a docking surface for PNPase through a series of hydrogen bonds (Nurmohamed et al., 2009). PNPase can form up to three contacts with RNase E as it is a trimer, but as RNase E is a tetramer, the stoichiometry of the interaction is not fully understood (Nurmohamed et al., 2009). Only a small proportion of PNPase is associated

with the RNase E (Liou et al., 2001) but its presence is required along with RhlB for efficient degradation of polycistronic RNAs that contain stabilising elements between cistrons (Khemici and Carpousis, 2003).

### **1.3.2 Substrate recognition**

RNase E is able to make large conformational changes which may be brought about by interaction with RNA. A 'closed' conformation results the DNase I and S1 domains being brought together to clamp down onto RNA (Figure 1.4). Currently, RNase E is thought to interact with RNA via two different modes that is dependent or independent on the presence of a 5' monophosphate.



**Figure 1.4 Domain movement in NTH-RNase E during substrate binding.** Shown are three different views of the catalytic N-terminal half of RNase E with and without RNA. Structural rearrangement into the 'closed' form can be seen, through movement of the 5' sensor and S1 domain. Colouring is as follows, RNase H like fold is shown in grey, S1 domain is shown in blue, 5'-monophosphate sensor domain is shown in orange, DNase I domain is shown in red, Zinc Link is shown in black. Figure generated in PyMOL using published structures 2C0B (Callaghan, Marcaida, et al., 2005) and 2VMK (Koslover et al., 2008) based on (Bandyra et al., 2013).



### 1.3.2.1 5' monophosphate dependent pathway

Described in section 1.3.1.3, the interactions made by the 5' monophosphate sensing pocket with a 5' monophosphate group provide a 'foothold' for RNase E onto RNA. Previous studies have suggested that this promotes conformational change and have suggested a role for the 5' monophosphate group acting allosterically with the enzyme to promote catalysis (Mackie, 1998; Jiang and Belasco, 2004). Later work suggested that the 5' monophosphate group may enhance both cleavage and binding (Garrey et al., 2009). This was refuted by recent evidence indicating that the 5' monophosphate group improves affinity and thus increases substrate occupancy and does not affect catalysis (Kime et al., 2014). As cleaved substrates possess a 5' monophosphate, downstream products can then be cleaved again by this pathway.

RppH (see section 1.2.3.1) can initiate the 5' end dependent cleavage on nascent transcripts by removing a pyrophosphate to generate a 5' monophosphorylated end (Celesnik et al., 2007; Deana et al., 2008).

### 1.3.2.2 Direct Entry

Although the 5' monophosphate dependent pathway provides a simple mechanism for the initiation of mRNA decay, mutations in the 5' sensor have shown to be viable (Garrey and Mackie, 2011). In addition, inactivation of RppH does not result in cell death and results in only a portion of transcripts being stabilised (see section 1.2.3.1) (Deana et al., 2008). The existence of a 5' monophosphate independent mechanism was confirmed when RNase E was shown to cleave a 5' triphosphorylated transcript rapidly (Kime et al., 2010). Indeed, further work has shown that cleavages within tRNA

precursors occur via direct entry. The pathway involves the interaction of multiple single-stranded engaging with RNase E simultaneously (Kime et al., 2014). It was found that the site selection can be alternated based on the order of cleavage events, engagement of multiple single-stranded regions allows one of two sites to be cleaved. However, the product of the first cleavage is no longer a direct entry substrate and thus prevents cleavage of the other site. The prevalence of direct entry has been investigated on a transcriptome-wide scale, with direct entry being designated as a major pathway of interaction (Clarke et al., 2014).

As the products of direct entry cleavages possess a 5' monophosphate they are then able to engage with RNase E via the 5' monophosphate dependent pathway. Whilst the two pathways are described separately, there is no evidence to preclude mixed modes of interaction with substrates.

### **1.3.3 Regulation by secondary structure**

Expectedly, the activity of RNase E is subject to several regulatory mechanisms, interactions with the substrate can be modified by secondary structure, RNA binding proteins and by translation efficiency of the transcript. Autoregulation of RNase E can be considered as a master regulator for RNase E levels (addressed in Chapter 4) (Mudd and Higgins, 1993; Jain and Belasco, 1995; Diwa et al., 2000; Sousa et al., 2008; Schuck et al., 2009). RNase E interacts directly with hp2 within the 5' UTR of its own transcript, *rne*. Thus allowing for autoregulation through a feedback loop (Schuck et al., 2009). The mechanism of autoregulation is not the only instance of secondary structure regulating the activity of RNase E. It has been shown that tRNA engagement with RNase E can allosterically activate the enzyme

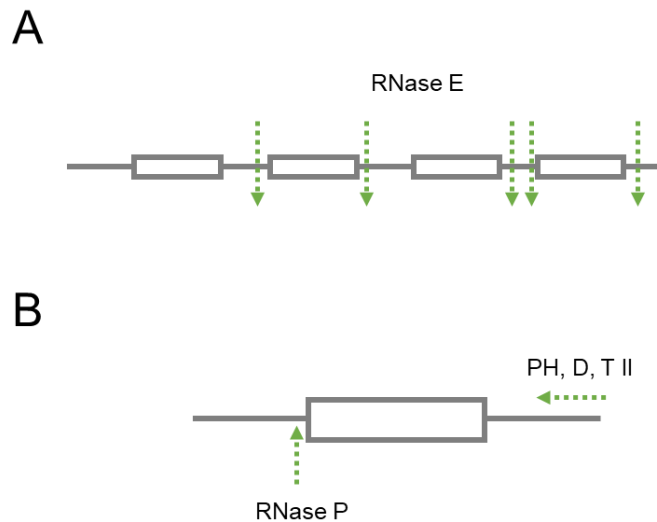
(Clarke, 2015) this builds on work that suggests that multiple single-stranded regions of RNA are required to direct tRNA processing (Kime et al., 2014). Furthermore, evidence obtained through X-ray crystallography indicates that structured RNAs directly bind RNase E, making contacts with the RNase H and small domains (Bandyra et al., 2018). This site is distal to the RNA-binding channel that constituting the surface between the S1 and DNase I domains.

## **1.4 Stable RNA processing**

The instability of RNA is a property that is fundamental to the control of gene expression, change in the genetic programme requires RNA to be unstable to prevent translation of proteins that are no longer required. Stable RNAs are present within bacteria such as transfer and ribosomal RNAs. Stability of these RNAs is not absolute but relative as they are degraded as part of a stress response. The action of the ribonucleases is surprisingly paramount to their function as the decay machinery must process them as part of maturation into the functional form (Deutscher, 2003; Deutscher, 2006).

### **1.4.1 Maturation of transfer RNA (tRNA)**

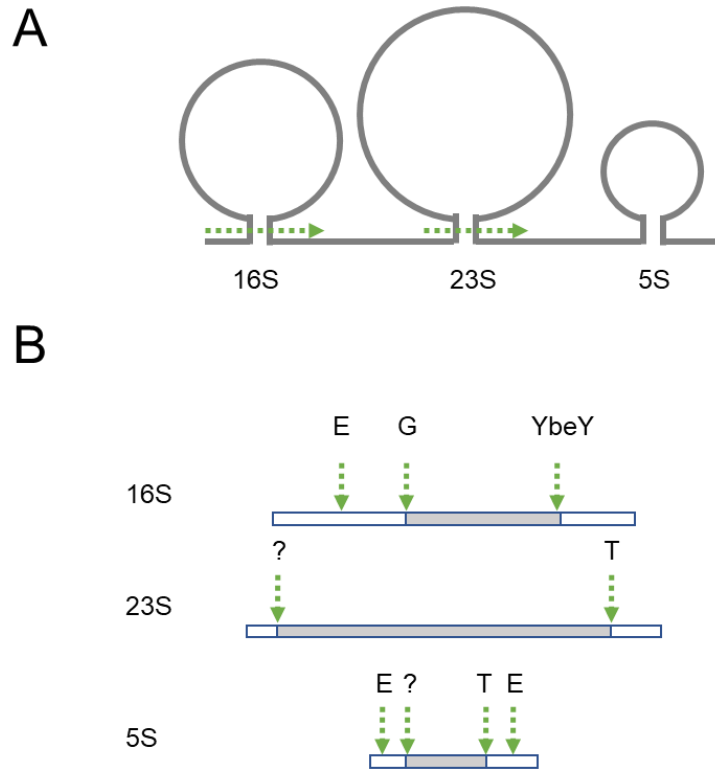
Prokaryotic tRNAs are produced as a polycistronic transcript, connected by flanking sequences that require processing to yield functional tRNAs. RNase E makes cleavages within the trailer sequences of tRNA precursors that generate products that are then processed further by other enzymes (Li and Deutscher, 2002; Ow and Kushner, 2002). RNase P performs maturation of the 5' end of the tRNA and 3' end is then trimmed by an exonuclease (Shepherd and Ibba, 2015) (Figure 1.5).



**Figure 1.5 Maturation of transfer RNA.** Panel A shows a schematic representing a polycistronic transcript. Initial cleavages are made by RNase E (green arrows) to separate the sequences into pre-tRNAs. Panel B shows a schematic of the product of RNase E cleavage that is further processed by RNase P to yield a mature 5' end. The 3' end is trimmed by exonucleases PH, D, T or II.

#### 1.4.2 Maturation of ribosomal RNA (rRNA)

Prokaryotic ribosomes are composed of a large (50S) and small (30S) subunit. The large, 50S subunit is a ribonucleoprotein (RNP) that consists of 33 ribosomal proteins and the 23S and 5S rRNA. The small, 30S subunit is also an RNP that consists of 21 ribosomal proteins and the 16S rRNA (Deutscher, 2009). rRNA is matured (Figure 1.6) as part of an immature pre-rRNA-ribosomal complex (Mackie, 2013). RNase III is responsible for making an initiating cleavage excising the pre-rRNA from the transcribed operon (Young and Steitz, 1978; Nicholson, 1999). In the excised pre-16S RNA, RNase E cleavage at the 5' end is followed by RNase G. The 3' end is then matured by cleavage by YbeY (Davies et al., 2010). Excised pre-23S has the 5' end matured by an unknown enzyme, whilst the 3' end is matured by the 3'-5' exonuclease RNase T (Li et al., 1999a). RNase E excises pre-5S RNA, and an unknown enzyme performs further 5' maturation whilst 3' maturation is performed by RNase T (Li et al., 1999a).



**Figure 1.6 Maturation of ribosomal RNA.** Panel A shows a schematic of a transcribed ribosomal RNA operon (*rrn*) which features sequences of the pre-16S, pre-23S and pre-5S which are cleaved (as indicated by the green arrow) by RNase III, which makes staggered cleavages. Panel B shows the resultant RNAs that are then cleaved after associating with ribosomal proteins by the indicated enzymes, E denotes RNase E, G denotes RNase G, T denotes RNase T, and YbeY is as indicated (Deutscher, 2009).

## 1.5 Concluding remarks

As an enzyme that is central to degradation, RNase E holds many potentially exciting applications for synthetic biology. Rationalised design of ground-up synthetic biological systems requires a complete understanding of the mechanisms that control expression. Understanding how RNase E orchestrates RNA turnover and what controls the switch to RNA decay will ultimately allow more informed design choices when producing synthetic systems through precise control of the functional life times of RNAs.

Previously, BL21 (DE3) star, a protein expression strain has been developed to contain a mutation in the gene encoding RNase E, to enhance expression of the desired product (Lopez et al., 1999). Following from this, decoy mRNAs may also be used to saturate RNase E preventing it from cleaving other targets (Makeyev et al., 2002; Marzi and Romby, 2012) or conversely, protection of a single target through design of sRNAs that remove vulnerable single-stranded character or structural features that promote entry of RNase E. Interesting future applications could also include the stochastic control of genes that are expressed as a polycistronic transcript through the design of intergenic secondary structures (Smolke and Keasling, 2002; Pflieger et al., 2006). Given that RNase E is essential for cell viability in *E. coli*, it also has the potential to be a target for structure-based drug design given that it is pervasive through Gram-negative bacteria and is not present within humans. RNase E has already been used in computational high throughput screening to find small molecules that result in inhibition (Kime et al., 2015).

As mentioned above, the overall picture of RNA decay in *E. coli* remains incomplete. A poignant challenge in the RNA decay field is to uncover the mechanisms that determine the functional life-time of mRNA given recent work that suggests that RNase E may make contacts with RNA, beyond those with single-stranded regions. The broad objective of this thesis is to describe for the first time the contribution of stem-loop recognition to the capture and cleavage of RNA by RNase E. The specific aims are to **(i)** mutagenize the residues associated with a newly identified RNA-binding site and characterise the effects on cleavage **(ii)** determine if alteration of the site has effects *in vivo* **(iii)** Initiate structural analysis of RNase E by Electron Microscopy.

## **Chapter 2**

### Materials and methods



## **2.1 Materials**

### **2.1.1 Chemicals and Reagents**

Unless otherwise stated; chemicals and reagents for general-purpose were purchased from Sigma-Aldrich or ThermoFisher Scientific and were of analytical grade or higher; modifying enzymes were purchased from New England Biolabs, Promega or Invitrogen; radiochemicals were purchased from Perkin Elmer; for electrophoresis premixed acrylamide solutions were purchased from Severn Biotech Ltd. and Agarose Powder from ThermoFisher Scientific.

### **2.1.2 Growth and maintenance of bacteria**

#### 2.1.2.1 Media

LB broth (Lennox) solid and liquid media were purchased in tablet form from Sigma Aldrich.

#### 2.1.2.2 Sterilisation

Sterilisation was achieved by autoclaving all media at 121°C for 20 min. Antibiotics and IPTG were sterilised by filtration either through 0.2 µm filters (Sarstedt) or vacuum-filtration through Durapore 0.22 µm filters (Merck).

#### 2.1.2.3 Antibiotic selection

To ensure the maintenance of plasmids and to prevent contamination, solid and liquid culture media was supplemented when necessary with the antibiotic as indicated below (Table 2.1). All antibiotics were stored at -20 °C as a 1000x stock.

**Table 2.1 Antibiotics used for selection of bacteria.**

<b>Antibiotic</b>	<b>Solvent</b>	<b>Working Concentration</b>	<b>Source</b>
Carbenicillin	50% (v/v) ethanol	100 µg/mL	Formedium
Tetracycline	H <sub>2</sub> O	10 µg/mL	Sigma Aldrich
Kanamycin	H <sub>2</sub> O	50 µg/mL	Sigma Aldrich

## 2.1.2.4 Bacterial strains

**Table 1.2 Bacterial strains used during this thesis.**

<i>E. coli</i> strain	Genotype	Source
BL21(DE3)	<i>E. coli</i> str. B F <sup>-</sup> <i>ompT gal dcm lon hsdS<sub>B</sub>(r<sub>B</sub><sup>-</sup>m<sub>B</sub><sup>-</sup>)</i> λ(DE3 [ <i>lacI lacUV5 T7p07 ind1 sam7 nin5</i> ]) [ <i>malB</i> <sup>+</sup> ] <sub>K-12</sub> (λ <sup>S</sup> )	Purchased from Agilent Technologies
DH5α	F <sup>-</sup> <i>endA1 glnV44 thi-1 recA1 relA1 gyrA96 deoR nupG purB20 φ80dlacZΔM15 Δ(lacZYA-argF)U169, hsdR17(r<sub>K</sub><sup>-</sup>m<sub>K</sub><sup>+</sup>), λ<sup>-</sup></i>	Purchased from Invitrogen
XL10-Gold	Tet <sup>r</sup> Δ ( <i>mcrA</i> )183 Δ( <i>mcrCB-hsdSMR-mrr</i> )173 <i>endA1 supE44 thi-1 recA1 gyrA96 relA1 lac Hte [F' proAB lacIqZDM15 Tn10 (Tet<sup>r</sup>) Amy Cam<sup>r</sup>]</i>	Purchased from Agilent Technologies
CJ1827	<i>araD39Δ(ara,leu)7697ΔlacX74 galU<sup>-</sup>galK<sup>-</sup>hsr<sup>-</sup>hsm<sup>+</sup>strA zce::Tn10 (λez1)</i>	Obtained as a gift from Joel Belasco (Jiang et al., 2000)
CJ1828	<i>araD39Δ(ara,leu)7697ΔlacX74 galU<sup>-</sup>galK<sup>-</sup>hsr<sup>-</sup>hsm<sup>+</sup>strA Tn10 ams-1 (λez1)</i>	Obtained as a gift from Joel Belasco (Jiang et al., 2000)
CJ1832	<i>araD39Δ(ara,leu)7697ΔlacX74 galU<sup>-</sup>galK<sup>-</sup>hsr<sup>-</sup>hsm<sup>+</sup>strA P<sub>lac</sub>::rneΔ337 (λez1) recA1 srl::Tn10 F':cat lac<sup>q</sup></i>	Obtained as a gift from Joel Belasco (Jiang et al., 2000)

### 2.1.2.5 Plasmids

**Table 1.3 Plasmids used as part of this thesis.**

Plasmid	Description	Source
pRNE529N	a pET16b-based vector containing the T7-lac promoter controlling the expression of a truncated <i>rne</i> gene (encoding amino acids 1-529) fused to an N-terminal decahistidine tag. Confers ampicillin resistance.	Redko et al., 2003
pRNED346N	As pRNE529N but with D346N mutation.	Callaghan et al., 2005
pRNEM4	As pRNE529N but with R3Q mutation.	This study
pRNEM5	As pRNE529N but with Q22N mutation.	This study
pRNEM6	As pRNE529N but with H268S mutation.	This study
pRNEM7	As pRNE529N but with Q270N mutation.	This study
pRNEM8	As pRNE529N but with K433N mutation.	This study
pRNEM9	As pRNE529N but with R488Q mutation.	This study
pRNEM10	As pRNE529N but with R490Q mutation.	This study
pRNEM3	As pRNE529N but with H268S, Y269F and Q270N mutations.	This study
pRNEM11	As pRNE529N but with H268S, Y269F, Q270N and R490Q mutations.	This study
pRNE8X	As pRNE529N but with R3Q, Q22N, H268S, Y269F, Q270N, K433N, R488Q and R490Q mutations.	This study
pCafA	pET16b-based vector containing the T7-lac promoter controlling expression	Tock et al. 2000

---

	of <i>rng</i> fused to an N-terminal decahistidine tag. Confers ampicillin resistance.	
pMPM-K1	pBluescript related plasmid, confers kanamycin resistance.	Obtained as a gift from Joel Belasco (see Mayer et al., 1995)
pRNE1000	Derivative of pMPM-K1 containing the RNase E gene fused to an N-terminal hexahistidine tag and c-Myc epitope tag under the control of an IS10 promoter.	Obtained as a gift from Joel Belasco (see Jiang et al., 2000)
pNRNE1000	As pRNE1000 but with amino acid 530 of RNase E replaced with a stop codon.  This differs from (Jiang et al., 2000) as the position of the stop codon was introduced at position 530 rather than 499	This study
pRNE1008	As pRNE1000 but with R3Q, Q22N, H268S, Y269F, Q270N, K433N, R488Q and R490Q mutations	This study
pNRNE1008	As pRNE1008 but with amino acid 530 of RNase E replaced with a stop codon	This study

---

### 2.1.3 Buffers and solutions

Unless otherwise stated, buffers were either purchased from Sigma-Aldrich or prepared as described previously.

**Acrylamide stock solutions** of 30% (w/v; 29:1 acrylamide: *bis*-acrylamide) and 40% (w/v; 19:1 acrylamide: *bis*-acrylamide) were purchased from Severn Biotech Ltd (UK). All acrylamide solutions were stored at 4°C.

**10x SDS running buffer** was purchased from Bio-Rad and consisted of 250 mM Tris-HCl (pH 8.3), 1.9 M glycine, 1% (w/v) SDS. Stored at room temperature.

**10x Tris-Borate-EDTA (TBE)** running buffer was purchased from Severn Biotech Ltd (UK), consisting of 890 mM Tris (pH 8.3), 890 mM boric acid and 0.2 mM EDTA. Stored at room temperature.

**6x DNA loading dye** was purchased from Thermo Fischer Scientific and consisted of 10 mM Tris-HCl (pH 7.6), 0.03% (w/v) Bromophenol Blue, 0.03% (w/v) Xylene cyanol, 60% (v/v) glycerol and 60 mM EDTA. 6x DNA loading dye was stored at 4°C

**2x RNA loading dye** was purchased from Ambion (listed as Gel Loading Buffer II) and consisted of 95% (v/v) formamide, 18 mM EDTA, 0.025% (w/v) BPB, 0.025% (w/v) XyCy and 0.025% (w/v) SDS. 2x RNA loading dye was stored at -20°C

**2x SDS loading dye** consisted of 100 mM Tris-HCl (pH 6.8), 4% (w/v) SDS, 0.2% (w/v) bromophenol blue, 20% (v/v) glycerol and 200 mM  $\beta$ -mercaptoethanol. 2x SDS loading dye was stored at -20°C.

## **2.2 RNA methods**

### **2.2.1 Ribonuclease decontamination**

Ribonuclease contaminants were inactivated by addition of diethylpyrocarbonate (DEPC; Sigma Aldrich, UK) to solutions to a final concentration of 0.1% (v/v), followed by incubation overnight at 37°C. The solutions were then autoclaved at 121°C for 20 min to inactivate residual DEPC. Solutions that were not amenable to decontamination by DEPC, due to reactivity to DEPC or heat-sensitivity, were purchased from Sigma Aldrich, which were guaranteed as nuclease-free. Equipment and surfaces were decontaminated with RNaseZAP® solution (Ambion, USA). RNA samples were stored at -20°C for short term storage or -80°C for long term storage.

### **2.2.2 Phenol extraction and Precipitation of nucleic acids**

The volume of nucleic acid solution was made up to at least 200 µl with ultrapure water then mixed with an equal volume of acidic phenol:chloroform:isoamyl alcohol (25:24:1). Phase separation was accelerated by centrifugation at 16,100 x *g* for 3 min. The aqueous phase was removed using a micropipette and mixed with an equal volume of chloroform in a 2.0 ml microcentrifuge tube. The mixture was once again centrifuged, and the aqueous phase was transferred to a new microcentrifuge tube. Precipitation of nucleic acid was then achieved by the addition of 0.1 volumes of 3 M NaOAc pH 5.2 and 2.5 volumes of ethanol followed by incubation at -20 °C for at least 1 hour. Precipitated nucleic acid was then pelleted by centrifugation at 16,100 x *g*, 4°C for 30 min. The pellet was washed twice using 70% (v/v) ethanol and resuspended

in ultrapure water, with brief centrifugation at 16,100 x g between washes to prevent loss of the pellet.

### **2.2.3 Spectrophotometric Quantitation of RNA**

RNA concentration was determined using the RNA quantitation programme on a NanoPhotometer P300 spectrophotometer (Implen). Samples were diluted to ensure measurement was conducted within the linear range of absorbance. Purity was also assessed by measuring the  $A_{260} : A_{280}$  ratio which was expected to be around 2.0 for RNA and  $A_{260} : A_{230}$  which was also expected to be around 2.0

### **2.2.4 Synthesised RNA methods**

#### **2.2.4.1 *in vitro* transcription of unlabelled RNA by T7 RNA polymerase**

RNA was transcribed *in vitro* using the HiScribe Kit from New England Biolabs following the manufacturer's recommendations for standard transcripts. RNA was subsequently phenol extracted and precipitated as described above (Section 2.2.2).

#### **2.2.4.2 *in vitro* transcription of $\alpha$ - $^{32}\text{P}$ labelled RNA by T7 RNA polymerase**

RNA was transcribed *in vitro* using the HiScribe Kit from New England Biolabs following the manufacturer's recommendations for High Specific Activity radiolabeled RNA Probe Synthesis. Reactions contained 0.17  $\mu\text{M}$  UTP [ $\alpha$ - $^{32}\text{P}$ ]- 3000Ci/mmol. Radiolabelled transcripts were extracted using the Zymo RNA clean and concentrate kit (Zymo research) according to the manufacturer's recommendations. Briefly, the *in vitro* transcribed RNA was mixed with binding buffer and passed through a silica column by centrifugation. The silica was then washed with provided wash buffers and then eluted into nuclease-free water. The efficiency of incorporation of  $\alpha$ - $^{32}\text{P}$



was estimated by comparing the unincorporated radioactivity emitted from the silica column containing the flow-through and washes to the final eluant. This was performed using a Geiger-Muller detector placed 30 cm from the source. High specific activity RNA generation was deemed successful if >50% incorporation was achieved. Typically, reactions described yielded incorporation  $\geq 70\%$ . The RNA was then subjected to PAGE purification (section 2.2.4.4).

#### 2.2.4.3 Denaturing polyacrylamide gel electrophoresis (PAGE)

Polyacrylamide gels were made to desired concentration by diluting 20% (w/v; 19:1 acrylamide: *bis*-acrylamide) acrylamide, 7 M urea, 1x TBE stock solution with 7M urea, 1x TBE stock solution. Polymerisation was catalysed by adding 10% (w/v) APS 1:100 and TEMED 1:1000 followed by inversion. Vertical PAGE gels were cast using either Mini-PROTEAN for mini gels or PROTEAN casting apparatus for larger gels. Gels were allowed to polymerise for at least an hour. Samples to be loaded were diluted with equal volumes of 2x RNA loading dye and heat-denatured at 95°C for 3 min, followed by storage on ice until ready to be loaded. Gels were pre-run at 12 W (6 W for mini gels) for at least 20 minutes prior to use. Wells were flushed twice with 1x TBE using a needle and syringe prior to loading of samples. Samples were separated by applying an electric field which was set to 12 W (6 W for mini gels). When necessary, the gel was stained by incubation for 5 min in 1x TBE containing either ethidium bromide (1  $\mu\text{g/ml}$ ), SYBR™ Safe (Thermofisher Scientific) or SYBR® Gold Nucleic Acid Gel Stain (Thermofisher Scientific). (see Figure legends for details). Ethidium bromide stained gels were imaged under UV light. SYBR™ Safe stained gels were

visualised by blue light or scanning at 473 nm, see (Section 2.2.6.3). SYBR® Gold stained gels were visualised by UV light or scanning at 473 nm (Section 2.2.6.3).

#### 2.2.4.4 PAGE purification of transcripts

Contaminant nucleic acid (incomplete transcripts and cDNA template) was removed (when deemed necessary) by PAGE purification. RNA obtained by T7 *in vitro* transcription was separated by denaturing page and stained as described above (Section 2.2.4.3). RNA bands corresponding to the expected size were visualised on a UV box and excised with a clean razor. Radiolabelled RNAs were visualised using autoradiography. Gel slices were placed in a 2.5 ml syringe and forced through into a 2.0 ml microcentrifuge tube to break up the gel into smaller pieces. Gel pieces were covered with an equal volume of acidic phenol:chloroform:isoamyl alcohol (25:24:1) and pH 7.0 Tris buffer supplemented with 300 mM NaCl and incubated at 37°C overnight. Phase separation was achieved by centrifugation at 16,100 x *g* for 3 min. The aqueous phase was removed using a micropipette and mixed with an equal volume of chloroform in a 2.0 ml microcentrifuge tube. The mixture was once again centrifuged, and the aqueous phase was transferred to a new microcentrifuge tube. Precipitation of nucleic acid was then achieved by the addition of 2.5 volumes of ethanol followed by incubation at -20 °C for at least 1 hour. Confirmation of successful purification was then assessed by denaturing PAGE, and the concentration was determined by nanodrop spectrophotometry (described above in Sections 2.2.4.3 and 2.2.3 respectively).

### **2.2.5 Synthesis of RNA oligonucleotides**

Synthetic oligonucleotides that were used during this thesis were purchased as indicated below (Table 1.4).

**Table 1.4 Synthetic oligonucleotides**

Name	Sequence (5' -3') <sup>A</sup>	Modification	Source
BR15-FI	GGGGG <b>ACAGU</b> UUUG	3'- Fluorescein	Eurogentec
rpsO term	GAAAAGGGGGCCUGAGUGGCCCCUUUUUCAA	3'- Cy5	Eurogentec
5'P-LU13-FI	GAGACAGU <b>UUUG</b>	5'-Phosphate, 3'- Fluorescein	Eurogentec
5'OH-LU13-FI	GAGACAGU <b>UUUG</b>	3'- Fluorescein	Eurogentec
glnW-FI	UGGGGU <b>AUCG</b> CCAAGCGGUAAGGCACCGUUUUUGAUACCGCAU <b>UCCCU</b> GGUUCGAAUCCAGGUACC CCAGCCA	3'- Fluorescein	IDT

**A** - Bold text denotes 2'-O-Methylated RNA.

RNA was stored at -80°C in RNase-free water. BR15 oligonucleotides were stored in 100 mM KCl.

## 2.2.6 Electrophoretic mobility shift assays (EMSA)

### 2.2.6.1 Ligand-binding assay with NTH-RNase E to estimate apparent $K_d$

Final substrate concentration to be used in EMSAs was first empirically determined by establishing the minimum concentration that could be detected on an agarose gel. NTH-RNase E samples were dialysed against 10 ml of binding buffer containing 25 mM *bis*-Tris-propane (pH 8.3), 100 mM KCl, 15 mM CaCl<sub>2</sub>, 0.1% (v/v) Triton X-100, 20% (v/v) glycerol, and 1 mM DTT for 30 min at room temperature using a MF-Millipore 0.025 µm membrane filter (Merck, USA). Serial 2-fold NTH-RNase E dilutions were prepared in binding buffer followed by addition of substrate. Reactions were then incubated at 37°C for 20 min. Samples were collected at the bottom of the tube by centrifugation at 16,100 x *g* for 1 min and subsequently separated on a 1% (w/v) agarose gel. Gels containing unlabelled RNA were stained for 20 min in 1x TBE containing 0.01% (v/v) SYBR® Gold Nucleic Acid Gel Stain (Thermofisher Scientific). Gels containing radiolabelled RNA were first fixed for half an hour in a fixative solution of 25% (v/v) Isopropanol and 10% (v/v) Glacial acetic acid prior to drying onto Whatman filter paper in a Bio-Rad gel drier for 2 hours at 80°C. Dried gels were then placed against a phosphor screen overnight which was subsequently imaged as described below in place of the gel. Images of gels were captured using a Fujifilm FLA-5000 scanner (Section 2.2.6.3). Band intensity was quantified via 2D densitometry using the gel analyser function in ImageJ software. The proportion of bound RNA was calculated in each lane and plotted as a function of protein concentration and fitted with a sigmoidal fit with non-linear

regression using OriginPro 8.6. From this graph, the  $K_d$  value was calculated as the concentration of protein at which 50% of the substrate was bound.

#### 2.2.6.2 Competition binding assays to estimate apparent $IC_{50}$

Dilutions of competitor RNAs were performed in the same buffer as above (Section 2.2.6.1). To each of these volumes, reporter substrate and NTH-RNase E were added. Samples were set up and analysed as described above. The proportion of bound to unbound reporter was plotted as a function of competitor RNA concentration and fitted with using OriginPro 8.6. From this graph,  $IC_{50}$  values were calculated as the concentration of competitor RNA required to dissociate 50% of reporter RNA from NTH-RNase E.

#### 2.2.6.3 Fujifilm FLA-5000 imaging of gels

A Fujifilm FLA-5000 scanner was used to image gels. Gels containing fluorescein-labelled RNA or stained with SYBR® Gold or SYBR™ Safe were imaged by using a 473 nm excitation laser and choosing the FITC emission filter. Cy5-labelled RNA was imaged using a 635 nm excitation laser and using the LPR emission filter. Phosphor screens were imaged by using the IP setting.

### 2.2.7 Discontinuous Cleavage Assays

RNase E or RNase G, and RNA substrate (see Figure legends for further details) to be cleaved, were preincubated separately in reaction buffer (25 mM *bis*-Tris-propane-HCl pH 8.3, 100 mM NaCl, 15 mM MgCl<sub>2</sub>, 0.1% (v/v) Triton X-100, 1 mM DTT and RNaseOUT™ 0.32 U/μl ) at 37°C for 10 min. Enzyme and substrate were then combined, and a 0 s time point was taken and quenched in 2x RNA loading dye. Further time points were

subsequently taken and quenched in 2x RNA loading dye (see Figure legends for details). Samples were separated by denaturing PAGE (see Section 2.2.4.3).

## **2.3 DNA Methods**

### **2.3.1 Deoxyribonuclease (DNase) decontamination**

Inactivation of potential DNase contaminants was achieved by autoclaving all solutions for at 121°C for 20 min. Solutions that were not amenable to decontamination by autoclaving were purchased from Sigma Aldrich, which were guaranteed as nuclease-free.

### **2.3.2 Quantification of DNA**

The concentration of DNA in samples was calculated by nanodrop spectrophotometry (as in section 2.2.3, except using the DNA quantitation programme) or separated by gel electrophoresis and band intensity was compared to a quantitative 1 kb DNA ladder. Purity was assessed by the  $A_{260} : A_{280}$  ratio, which was expected to be around 1.8 for pure DNA. All DNA samples were stored at -20°C.

### **2.3.3 Isolation of bacterial genomic DNA**

*E. coli* MG1655 was streaked onto an LB agar plate and incubated overnight at 37°C. A single colony was then used to inoculate 10 ml of LB in a 50 ml centrifuge tube and grown at 37°C with shaking (200 rpm) until the culture reached an  $OD_{600}$  of 0.6. Cells were harvested by centrifugation at 3000 x g, 4°C for 15 min. The supernatant was discarded, and the pellet was resuspended in 5 ml TE (10 mM Tris pH 8.0, 1 mM EDTA). An equal volume of cell lysis buffer (20 mM Tris-Cl pH 8, 40 mM EDTA, 0.3 M NaCl, 0.5% w/v SDS) was added, and the centrifuge tube was immersed in boiling water for 30 s. 10 ml of phenol saturated with 10 mM Tris-HCL, pH 8.0 was added and the contents of the centrifuge was mixed by inversion. Phase separation was



accelerated by centrifugation at 3000 x g, 4°C for 10 min. The aqueous phase was then transferred to a new 50 ml centrifuge tube. 2.5 volumes of ethanol was added and precipitated nucleic acid was pelleted by centrifugation at 4000 x g, 4°C for 15 min. The supernatant was discarded, and the pellet was allowed to air dry for 15 min. The pellet was resuspended in 0.4 ml of Tris pH 8.0, 300 mM NaCl. The genomic DNA was reprecipitated by addition of 1 ml of ethanol, and the precipitated nucleic acid was pelleted and air-dried as above. This was then resuspended in H<sub>2</sub>O and stored at -20°C.

#### **2.3.4 Agarose gel electrophoresis**

Nucleic acids were separated by size using horizontal agarose gel electrophoresis. Agarose gels, at a final agarose concentration of 0.8-3% (w/v), were immersed in 1x TBE. 6x DNA loading dye was added to samples at a ratio of 1:6, followed by separation on agarose gels at 60-110 V. Gels were stained and visualised as described above (Section 2.2.4.3).

#### **2.3.5 PCR methods**

##### 2.3.5.1 Primer Design

DNA PCR primers were synthesised either by Eurofins or IDT. Primers used for QuikChange mutagenesis (Table 1.5) were designed using the QuikChange Primer Design Program. (Available at: <http://www.genomics.agilent.com/primerDesignProgram.jsp>). Primers used for *in vitro* transcription are shown below (Table 1.6).

**Table 1.5 Primers for Site Directed Mutagenesis PCR**

<b>Primer Name</b>	<b>Sequence (5'-3')</b>
R3QF	CTGCTGAGTTGCGTTGATTAACATCTGTTTCATATGACGACCTTCGATATGG
R3QR	CCATATCGAAGGTCGTCATATGAAACAGATGTTAATCAACGCAACTCAGCAG
Q22NF	ATCCAGGTCATACAGACGATTCCCATCTACAAGGGCAAC
Q22NR	GTTGCCCTTGAGATGGGAATCGTCTGTATGACCTGGAT
H268SF	GTGACTCGATCTGGTAGCTGCTGAACAGCGGGATCT
H268SR	AGATCCCGCTGTTCCAGCAGCTACCAGATCGAGTCAC
Q270NF	CTCGATCTGTGACTCGATATTGTAGTGGCTGAACAGCGG
Q270NR	CCGCTGTTCCAGCCACTACAATATCGAGTCACAGATCGAG
K433NF	CGAAGAAGAAGCGCTGAATGAGAACACCCAGG
K433NR	CCTGGGTGTTCTCATTGAGCGCTTCTTCTTCG
R488QF	CTTCCCCTTTACGCACCTGCAGCACGTGGTAGTG
R488QR	CACTACCACGTGCTGCAGGTGCGTAAAGGGGAAG
R490QF	GTTTCTTCCCCTTTCCGCACGCGCAGCAC
R490QR	GTGCTGCGCGTGCGGAAAGGGGAAGAAAC
HYQ268269270SFNF	GGACTCGATCTGTGACTCGATATTGAAGCTGCTGAACAGCGGGATCTCGCC
HYQ268269270SFNR	GGCGAGATCCCCTGTTCCAGCAGCTTCAATATCGAGTCACAGATCGAGTCC
R3Q_pRNE1000F	GTTGCCCTTGAGATGGGAATCGTCTGTATGACCTGGAT
R3Q_pRNE1000R	ATCCAGGTCATACAGACGATTCCCATCTACAAGGGCAAC
Q22N_pRNE1000F	GATCTGAATGGGGCCGCAAGATCTAAACAGATGTTAATCAACGCAACTCAG
Q22N_pRNE1000R	CTGAGTTGCGTTGATTAACATCTGTTTAGATCTTGCGGCCCCATTGAGATC
529STOP_pRNE1000F	TCCGGCATGGCAAAGGTCTACAGCGCAGGTTGTTCCG
529STOP_pRNE1000R	CGGAACAACCTGCGCTGTAGACCTTTGCCATGCCGGA
R488490QF	GGGTTTTCTTCCCCTTTCTGCACCTGCAGCACGTGGTAGTGC
R488490QR	GCACTACCACGTGCTGCAGGTGCAGAAAGGGGAAGAAACCCC

**Table 1.6 cDNA amplicons**

cDNA Name	Size (bp)	Primer Sequences (5'-3') <sup>A</sup>	T <sub>m</sub> (°C)
<i>argX-leuT-hisR-proM</i>	502	Forward: ATCCTAATACGACTCACTATAGGGAACGGCGCTAAGCGCCCG Reverse: AAAAAACCCCGCCGAAGCGG	60
<i>glnW-metU</i>	238	Forward: ATCCTAATACGACTCACTATAGGGTGGGGTATCGCCAAGC Reverse: ACAAATTGGTTTTGAATTTGCC	55
<i>glnW</i>	99	Forward: ATCCTAATACGACTCACTATAGGGTGGGGTATCGCCAAGC Reverse: TGGCTGGGGTACCTGGAT	57
<i>-metU</i>	163	Forward: ATCCTAATACGACTCACTATAGGGTCGAAGAAACAATCTGGCTAC Reverse: ACAAATTGGTTTTGAATTTGCC	55
<i>cspA</i>	420	Forward: ATCCTAATACGACTCACTATAGGGTTTGACGTACAGACC Reverse: AAAATCCCCGCCAAATGGCAGGG	55
<i>rne</i> 5' UTR	519	Forward: ATCCTAATACGACTCACTATAGGGGTTTCCGTGTCCATCCTTGT Reverse: CTCGTGCCCTGGACTTG	55

Forward primers contained the sequence TAATACGACTCACTATA which is the T7 promoter sequence

#### 2.3.5.2 Polymerase chain reaction

PCR reactions consisted of up to 100 ng of genomic DNA incubated with 2 U of GoTaq® DNA polymerase, 4.5 mM MgCl<sub>2</sub>, 0.8 mM dNTPs, 0.5 μM forward primer, 0.5 μM reverse primer, and 5% (v/v) DMSO in 1x Gotaq Flexi colourless buffer. All reagents were obtained from Promega, UK except for DMSO and dNTPs, which were purchased from Sigma Aldrich and Invitrogen, respectively. A Bio-Rad T100 Thermal Cycler was employed for PCR, and the following thermal cycling parameters were used: Initial denaturation at 95°C for 3 min followed by 30 cycles of 95°C for 30 s, 57-63°C for 30 s and 72°C for 60 s. Afterwards, a final extension was performed at 72°C for 7 min. Successful amplicon generation was confirmed by agarose gel electrophoresis.

#### 2.3.5.3 Amplicon purification

Amplicons that had contaminating products were purified using a Monarch® DNA Gel Extraction kit (New England Biolabs) according to the manufacturer's instruction. If no other bands were seen after confirmation by agarose gel electrophoresis samples were purified using Monarch® PCR & DNA Cleanup Kit (New England Biolabs).

#### 2.3.5.4 Site-directed Mutagenesis

Site-directed mutagenesis was performed using a QuikChange Multi Site-Directed Mutagenesis Kit according to the manufacturer's instructions (Agilent). QuikChange PCR was performed, followed by transformation into XL10-Gold cells (see Section 2.3.6.2). The success of mutagenesis was subsequently confirmed by Sanger sequencing, performed as a service by GeneWiz (formerly Beckman Coulter Genomics).

## 2.3.6 Plasmid DNA methods

### 2.3.6.1 Generation of chemically-competent cells

*E. coli* colonies were used to inoculate 10 ml of LB in a 50 ml centrifuge tube which was subsequently grown at 30°C with shaking (180 rpm) until cultures reached an OD<sub>600</sub> of 0.4. Cultures were cooled in an ice bath for 10 min, and cells were harvested by centrifugation at 3000 x *g* for 15 min at 4°C. The supernatant was discarded, and the pellet was gently resuspended in 10 ml of ice-cold 0.1 M CaCl<sub>2</sub> and incubated on ice for 20 min. Cells were harvested again, and the pellet was resuspended in 5 ml ice-cold 0.1 M CaCl<sub>2</sub>, 15% (v/v) glycerol. The cell suspension was aliquoted into 100 µl aliquots and flash-frozen in a dry ice-ethanol bath before storage at -80°C.

### 2.3.6.2 Introduction of plasmid by transformation

Competent *E. coli* cells either bought or prepared (Section 2.3.6.1) were allowed to thaw on ice for 5 minutes. 10 ng of purified plasmid DNA or 2 µl from a QuikChange reaction to be transformed was added to the cell suspension, which was then mixed gently and left on ice for a further 30 min. Cells were then heat shocked in a 42°C water bath for 30 s, followed by incubation on ice for 2 min. 475 µl of LB broth was added to the cells, which were then recovered in a shaking incubator at 37°C for 45 min. Cells were plated onto LB agar plates supplemented with appropriate antibiotic and incubated overnight at 37°C.

### 2.3.6.3 Purification of plasmid DNA from bacteria

*E. coli* strains harbouring plasmids were streaked onto LB agar plates supplemented with appropriate antibiotics and incubated overnight at 37°C. Colonies were picked and used to inoculate 1-10 ml of LB broth

supplemented with an antibiotic in 50 ml centrifuge tubes (StarLab, Germany). Cultures were incubated at 37°C with shaking (200 rpm) for 12-16 hours. Cells were harvested by centrifugation at 3,300 x g, 4°C for 20 min and the supernatant was discarded. Plasmid DNA was subsequently purified using a Monarch® Plasmid Miniprep Kit (New England Biolabs) as per the manufacturer's instructions. Sanger sequencing (as in Section 2.3.5.4) of coding regions was then performed to confirm plasmid integrity and successful isolation.

## **2.4 Protein Methods**

### **2.4.1 Overexpression of recombinant genes encoding histidine-tagged proteins in *E. coli***

BL21 (DE3) strains harbouring the intended plasmid containing a T7-lac cassette were generated as described above (Section 2.3.6.2). Colonies were then used to inoculate liquid culture, which was grown overnight (as in Section 2.3.3). The overnight culture was then used to inoculate a large batch of LB broth with a dilution factor of 1:100. Expression of the chromosomal T7 RNA polymerase gene was induced by adding IPTG to a final concentration of 1 mM when cultures reached mid-log phase ( $OD_{600}$  0.4-0.6). Induced cultures were incubated under the same conditions for 3 hours. Cells were pelleted by centrifugation at 3,300 x *g*, 4°C for 15 min using an SLA-3000 fixed-angle rotor (Sorvall, Germany). Pellets were washed by resuspension in 20 ml of ice-cold lysis buffer (20 mM Tris-HCl pH 7.6, 0.5 M NaCl, 10 mM MgCl<sub>2</sub>, 50 mM imidazole) and re-pelleted as before and stored at -80°C.

### **2.4.2 Purification of histidine-tagged proteins**

#### **2.4.2.1 Preparation of cleared extract from cell lysate**

Cell pellets were resuspended in 5-10 ml of lysis buffer with a pre-dissolved cComplete Mini EDTA-free protease inhibitor cocktail tablet (Roche, Germany). Cells were then lysed at 15 kpsi in a Z-plus 1.1 kW Constant systems cell disruptor with a one-shot head (Constant systems Ltd, UK). Cell lysate was diluted in lysis buffer to a final volume of around 30 ml and cleared by ultracentrifugation at 122,000 x *g*, 4°C for 30 min using a

Beckman Optima™ XPN ultracentrifuge (SW32Ti rotor). The supernatant was then filtered through a 0.45 µm (Sartorius, Germany) to remove particulate matter.

#### 2.4.2.2 FPLC chromatography

Protein was purified using an ÄKTA Pure FPLC system (GE Healthcare, USA). All buffers used during this process were filtered through 0.2 µm vacuum-driven Stericups (Millipore, USA) and degassed with agitation by using a magnetic stirrer for at least 45 min. Both pumps were washed with deionised water, followed by elution buffer (20 mM pH 7.6 Tris-HCl, 0.5 M NaCl, 10 mM MgCl<sub>2</sub>, 1 M imidazole) through inlet B1 and then lysis buffer (see above) through inlet A1. A 1-ml HiTrap Nickel-chelating HP column (GE Healthcare, USA) was attached to the ÄKTA and equilibrated with lysis buffer. The lysate was loaded onto the column at a flow rate of 0.7 ml/min using a sample pump. The column was washed with 5 column volumes (CVs) of lysis buffer followed by 20 CVs of high salt buffer (20 mM Tris-HCl pH 7.6, 1 M NaCl, 10 mM MgCl<sub>2</sub>, 50 mM imidazole) followed by a further 5 CVs of lysis buffer. The protein was eluted by an imidazole gradient set up as 10 column volumes B1 gradient 0-10%, 10 column volumes B1 gradient 10-100% and 10 column volumes 100% B1. Samples were collected in 2.0-ml volumes at a flow rate of 1 ml/min. Peak fractions were pooled and desalted at 4°C using a PD-10 Sephadex G25 10 ml desalting column (GE Healthcare, UK) equilibrated with 20 mM Tris-HCl (pH 7.6), 0.5 M NaCl, 10 mM MgCl<sub>2</sub>, 1 mM DTT, 0.5 mM EDTA, 5% (v/v) glycerol. If required, protein samples were then concentrated in a Corning Spin-X UF 20 ml concentrator 30 kDa MWCO (Corning International, Japan) by centrifugation at 3,300 x g,



4°C in 10-minute intervals. When deemed necessary, further purification was achieved using Size Exclusion chromatography as described previously (Redko et al., 2003).

#### 2.4.2.3 Batch Protein Purification

Cleared extract from cell lysate (Section 2.4.2.1) was applied to a Bio-Rad Econo-Pac® Chromatography Column containing 500 µl of HisPur™ Ni-NTA resin (Thermo Scientific™) that had been equilibrated by flushing the column with 10 ml of lysis buffer. The column was washed with 10 ml of lysis buffer, followed by 10 ml of high salt buffer followed by 10 ml of low imidazole wash buffer (20 mM Tris-HCl pH 7.6, 1 M NaCl, 10 mM MgCl<sub>2</sub>, 300 mM imidazole). Protein was eluted using 2.5 ml of elution buffer, and the eluant was subsequently desalted as above (Section 2.4.2.2).

#### 2.4.3 SDS-polyacrylamide gel electrophoresis

SDS-Polyacrylamide resolving gels were made to either 8% or 15% (v/v) acrylamide by mixing 4 ml (for 8%) or 7.5 ml (for 15%) of 30% (w/v; 29:1 acrylamide: *bis*-acrylamide) acrylamide, 3.8 ml of 1.5 M Tris-HCl (pH 8.8), 75 µl of 20% (w/v) SDS together to a final volume of 15 ml, for mini gels these volumes were halved. Polymerisation was catalysed by adding 10% (v/v) APS to 1:100 and TEMED 1:1000 (v/v) followed by gentle mixing. Stacking gel solutions were produced at a concentration of 5% by mixing 0.8 ml of 30% (w/v; 29:1 acrylamide: *bis*-acrylamide) acrylamide, 0.63 ml of 1 M Tris-HCl (pH 6.8), 25 µl of 20% (w/v) SDS together to a final volume of 5 ml (volumes halved for mini gels). Polymerisation was catalysed as above. Vertical PAGE gels were cast using either Mini-PROTEAN for mini gels or PROTEAN casting apparatus for larger gels (Both from Bio-Rad). The top

and bottom buffer chambers were then filled with 1x SDS Running buffer. Samples to be loaded were diluted with equal volumes of 2x SDS loading dye and heated to 99°C for 5 min, followed by storage on ice until ready to be loaded. Samples were separated based on polypeptide length by differential migration through the matrix of the gel by applying an electric field which was set to 160-180 V. After electrophoresis, the apparatus was dismantled, and the gel was transferred to a plastic container. Stacking gels were removed using a clean razor and discarded. Resolving gels were stained in a plastic container using InstantBlue™ (expedon) and left to stain for at least an hour.

#### **2.4.4 Quantitation of Protein**

Protein was quantitated using the Bio-Rad protein assay according to the manufacturer's instructions using bovine serum albumin (Bio-Rad) as a protein standard.

#### **2.4.5 Mass Spectrometry**

Molecular mass measurement was performed by Rachel George at the University of Leeds as a service to confirm the identity of purified proteins.

#### **2.4.6 Small Angle X-ray Scattering**

Data for D346N NTH-RNase E was collected at beamline B21 at the Diamond Light Source (Didcot, UK) by SEC-SAXS. D346N RNase E at 5 mg/ml was applied to a Superdex 200 Increase 3.2/300 column attached to an Agilent HPLC system which was run at 0.06 ml/min equilibrated with Tris pH 8.0, 100 mM KCl, 15 mM CaCl<sub>2</sub>, 1 mM DTT, 12.5% (v/v) glycerol. Data were processed using ATSAS 2.8.3 (Franke et al., 2017) which was used to calculate the  $R_g$  and  $D_{max}$  values. Data for wild-type NTH-RNase E and wild-

type NTH-RNase E in complex with BR15 was collected by batch-mode alongside binding buffer (see section 2.2.6.1). Buffer subtraction and averaging of data for samples at 0.6 and 0.3 mg/ml was processed in ATSAS 2.8.3, which was used to calculate the  $R_g$  and  $D_{max}$  values.

#### **2.4.7 Circular Dichroism**

D346N NTH-RNase E was desalted into CD buffer (5 mM Tris-acetate pH 8.0, 100 mM NaSO<sub>4</sub>, 10 mM MgSO<sub>4</sub> and 1 mM DTT) and subsequently diluted using the same buffer to 0.25 mg/ml. Protein solutions were placed in a quartz cuvette with a path length of 1 mm. The cuvette was placed into a Chirascan™- Circular Dichroism Spectrometer (Applied Photophysics) and allowed to equilibrate at 20°C for 10 min. A spectrum of buffer alone was subtracted from an averaged spectrum of RNase E. High tension values remained below 600 between 190 and 260 nm indicating high signal to noise ratio. Subsequently, a temperature ramp was performed where the same sample was first cooled to 18 and then heated to 87 °C at an interval of 1°C min<sup>-1</sup>. Spectra were recorded at each temperature interval.

#### **2.4.8 Western blotting**

Western blotting was performed to calculate the relative intracellular concentration of RNase E. *E. coli* cells grown to an OD<sub>600</sub> of approximately 0.4-0.6 were pelleted by centrifugation at 4000 x g, 4°C for 15 min and resuspended in 1x SDS loading buffer to an equivalent OD<sub>600</sub> of 4. Samples were then heated to 95°C for 10 min and separated by SDS-PAGE on an 8% acrylamide gel (section 2.4.3). Protein was transferred onto polyvinylidene difluoride (PVDF; Millipore) membranes using a Bio-Rad Trans-blot Turbo. The successful transfer was confirmed by staining the

acrylamide gel with InstantBlue™, and the membrane with Ponceau S. Membranes were incubated in 10% milk, TBS-tween for 1 hour. Proteins were immunoblotted with a primary, anti-c-Myc antibody (Mouse mAb #2276, Cell Signalling Technology) in 5% milk, TBS-tween for 1 hour at room temperature, then with an HRP-conjugated secondary antibody (Anti-Mouse IgG A4416, Sigma Aldrich) in 5% milk, TBS-tween. Protein bands were visualised by enhanced chemiluminescence (ECL; Promega), and the film was developed using a Xograph processor. Subsequent analysis was then performed in ImageJ.

## **2.5 Other Methods**

### **2.5.1 Cell viability assays**

#### 2.5.1.1 Confirmation of CJ1827 and CJ1828

The identity of CJ1827 and CJ1828 cells were confirmed by demonstrating temperature-tolerance of CJ1827 and -sensitivity of CJ1828. Strains were received blotted onto cardboard, which was wiped onto LB agar plates supplemented with tetracycline and grown overnight at 30°C. Subsequently, colonies were picked and used to inoculate LB broth supplemented with tetracycline and grown overnight at 30°C. The cultures were then serially diluted and spotted onto a pair of LB agar plates, one of which was grown at 30°C and the other at 42°C.

#### 2.5.1.2 Confirmation of CJ1832

The identity of CJ1832 cells were confirmed by demonstrating IPTG-dependent growth. Strains were isolated and grown (as in Section 2.5.1.1) and spotted onto LB agar plates both supplemented with carbenicillin and only one supplemented with IPTG.

#### 2.5.1.3 CJ1832 complementation assays

Competent CJ1832 cells (Section 2.3.6.1) were transformed (Section 2.3.6.2) with pRNE1000, pNRNE1000, pRNE1008, pNRNE1008 or pMPM-K1 and plated onto LB agar plates supplemented with kanamycin and IPTG. LB agar plates were incubated overnight at 37°C. To assess colony-forming ability, three separate colonies of each strain were resuspended in 50 µl of LB broth and were streaked on LB agar plates supplemented with kanamycin and LB agar plates supplemented with kanamycin and IPTG,

which were then incubated at 37°C overnight. To assess growth in liquid media, three separate colonies of each strain were each resuspended in 500 µl of LB broth and 2 µl of that was used to inoculate 200 µl LB broth supplemented with kanamycin or kanamycin and IPTG. Growth was monitored in a clear 96-well microtiter plate (Greiner Bio-One) by measuring the OD<sub>600</sub> of the culture using a FLUOstar Omega plate reader (BMG Labtech) with orbital shaking (200 rpm) between readings.

### **2.5.2 β-galactosidase assays**

Competent CJ1828 cells (Section 2.3.6.1) were transformed (Section 2.3.6.2) with pRNE1000, pNRNE1000, pRNE1008, pNRNE1008 or pMPM-K1 and plated onto LB agar plates supplemented with kanamycin. LB agar plates were incubated overnight at 30°C. Competent CJ1827 cells were plated onto LB agar plates supplemented with kanamycin and incubated overnight at 30°C. Colonies were used to inoculate LB broth supplemented with kanamycin (CJ1828) or tetracycline (CJ1827) and grown at 30°C until cultures reached an OD<sub>600</sub> of 0.4-0.6. Cells were normalised to an OD<sub>600</sub> of 0.4 by dilution in LB broth, and then they were subsequently diluted 1/50 in PBS. 25 µl of cell suspension was added to 25 µl of prepared Beta-Glo® Assay Reagent (Promega) in a white 384-well microtiter plate (Greiner Bio-One) and allowed to equilibrate for 30 min. Luminescence was measured using a FLUOstar Omega plate reader (BMG Labtech).

### **2.5.3 Glow Discharging EM grids**

Carbon-coated EM grids were placed on a glass slide coated in parafilm and made hydrophilic by glow-discharging using a PELCO easiGlow™ in air.

#### **2.5.4 Grid preparation and Electron Microscopy (Negative-stain TEM)**

3  $\mu$ l of the sample (as indicated in figure legends) was applied to a glow-discharged carbon-coated grid and allowed to stand for 30 s. The sample was blotted away using Whatman No. 1 filter paper. The grid was washed with a droplet of aqueous 1% (w/v) uranyl acetate and excess was immediately blotted off, the stain was reapplied and allowed to stain for 20 s. Excess stain was then wicked off using Whatman No. 1 filter paper, and the grids were imaged (as indicated in figure legends) using an FEI Tecnai T12 electron microscope operating at 120 keV equipped with a Gatan US1000XP CCD camera, or FEI Tecnai F20 electron microscope operating at 200 keV equipped with an FEI Ceta camera.

#### **2.5.5 Grid preparation (Cryo-EM)**

Liquid nitrogen was added to the outer compartment of a polystyrene vessel designed to cool ethane. Once the vessel had cooled sufficiently, gaseous ethane was added to the central compartment and allowed to condense. The vessel was then loaded onto a Vitrobot Mark IV (FEI). Parameters were kept as the default settings except for blotting time (details in text), and chamber humidity was set to 100%. 3  $\mu$ l of the sample was added to a Quantifoil R1.2/1.3 grid, which was then plunge frozen by the Vitrobot Mark IV (FEI) into the liquid ethane. The grid was transferred into liquid nitrogen through the liquid nitrogen vapour and placed into a pre-cooled plastic storage container and subsequently stored in liquid nitrogen.

#### **2.5.6 Electron Microscopy (Cryo-EM)**

Grids were clipped and loaded onto the FEI Titan Krios microscope by the EM staff at the University of Leeds. The FEI Titan Krios microscope was

operating at 300 keV and was equipped with a Falcon II direct electron detector.

### **2.5.7 Processing of Micrographs**

All analyses were carried out using the RELION 3.0. (Scheres, 2012). Processing was performed following recommendations in the user guide. Briefly, particles were extracted manually and then subsequently auto-picked. 2D classification was performed to generate class averages, followed by the generation of an initial model, which was then used for 3D classification. Classes were then subjected to 3D auto-refinement.



## **Chapter 3**

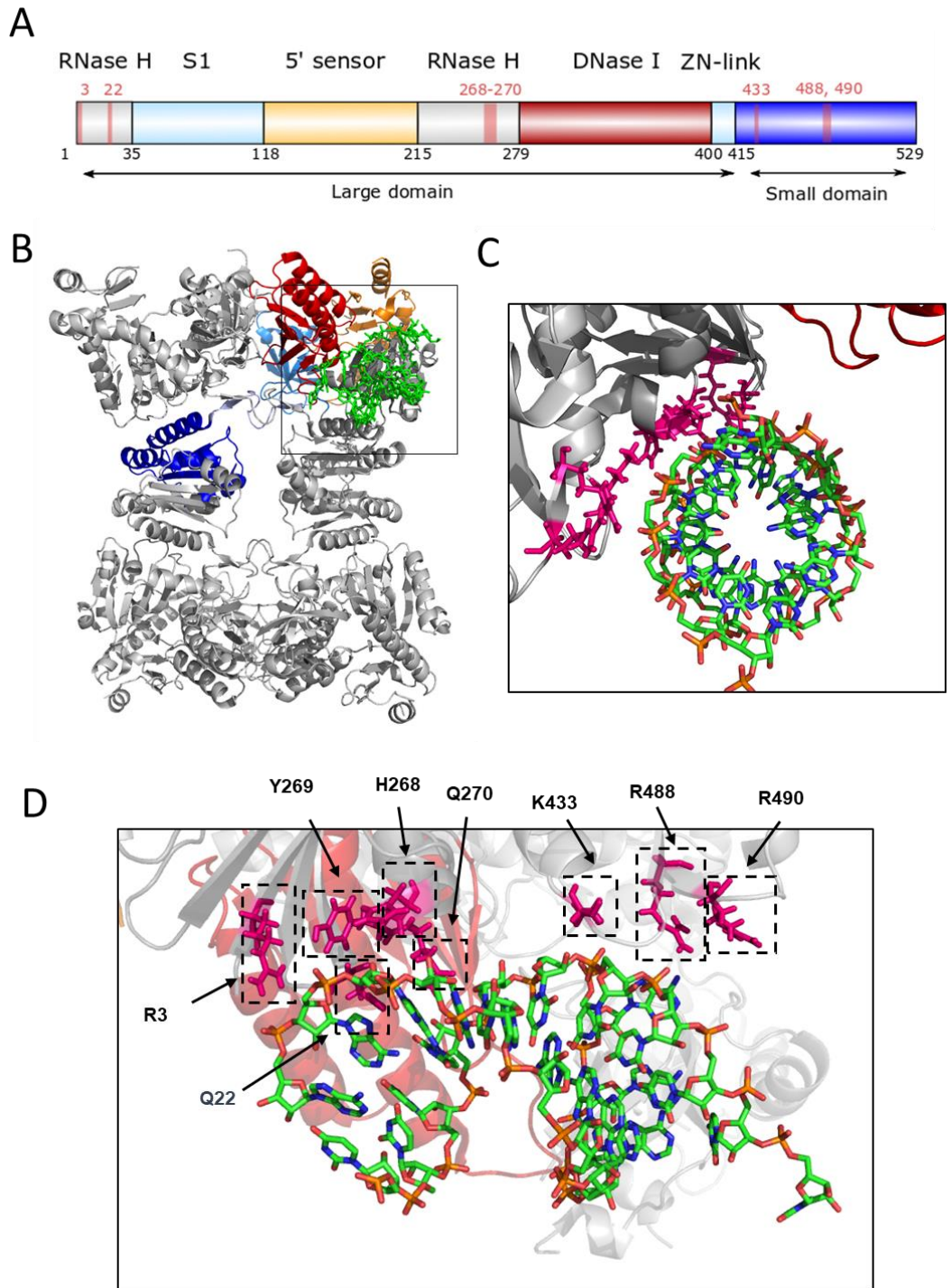
Functional analysis of the alternative RNA-binding site within the N-terminal catalytic half of *E. coli* RNase E

### 3.1 Introduction

In work leading up to this project, it was shown using electrophoretic mobility shift assays that the N-terminal catalytic half (NTH) of RNase E can interact with tRNA using contacts not required for the binding of single-stranded regions (Clarke, 2015). It was envisaged that these contacts would in some cases be sufficient to mediate an interaction with RNA, but in others may function in concert with those that contact single-stranded regions. This study of tRNA processing also produced evidence of allosteric activation of RNase E by “supporting” tRNAs (Clarke, 2015) emphasising the potential for multiple and mixed modes of recognition. In a parallel study, evidence was obtained that supporting tRNAs can be substituted with simple stem-loops, such as the one found in the intragenic region of *rpsO-pnp* mRNA (Kime, pers. comm). This suggested that allosteric activation may not be limited to tRNA processing and may be a more general feature of cleavages mediated by RNase E. Indeed, RNase E cleavage of several mRNA substrates has been shown in early work to be dependent on the presence of stem-loop structures (Ehretsmann et al., 1992; Cormack and Mackie, 1992). This selectivity may allow RNase E to cleave upstream of stem-loops to enable 3'-exonucleases to bypass these stabilising elements (Clarke, 2015).

More recently, demonstration of RNA cleavage directed by *cis*-acting small RNA, such as cleavage of *ompD* mRNA by MicC (Bandyra et al., 2012), prompted interest in the underlying mechanism and macromolecular interactions. The structure of co-crystals of the small RNA RprA and NTH-RNase E was solved to 3.95 Å (Bandyra et al., 2018). This revealed a previously undescribed interaction distal to the site of catalysis. A short

region of duplex RNA presumed from the 5' end of RprA was found to interact with an interprotomer groove. This was composed of the small domain of one protomer and two RNase-H subdomains of a second protomer within the same principle dimer (Bandyra et al., 2018). The density corresponding to the duplex RNA was insufficient to identify specific bases, presumably due to structural disorder and so was modelled as a short duplex of poly-A and poly-U. Potential interacting residues were identified as R3, Q22, H268, Y269, Q270, R433, R488 and R490 (Figure 3.1). Due to the placement of the bases in relation to the residues, the interaction would likely be limited to the phosphodiester backbone. Hydrogen bonds could presumably be made with the 2' OH group of the ribose, and electrostatic interactions could be made between the positively charged amine groups within the arginine side chains and the negatively charged phosphates of the RNA backbone. Interaction with the RNA-binding groove is unlikely to be sequence-specific.



**Figure 3.1 Crystal Structure of NTH-RNase E and the small RNA RprA.** Panel A shows the domains of RNase E. Colouring corresponds to the colouring of the domains in the other panels. The residues associated with sRNA binding are highlighted in red and numbered with their positions. Panel B shows a cartoon of the of NTH-RNase E homotetramer with a single protomer coloured, RNA is coloured in green (PDB:6g63). Panel C shows a magnified view, looking down the RNA helix. Panel D shows a front view of the RNA with residues putatively responsible for interaction shown as sticks, coloured pink and labelled according to the identity and position of the amino acid. Figure generated in PyMOL based on (Bandyra et al., 2018).

Electrostatic interactions are common in RNA biology, particularly due to the fact RNA is a highly charged polyelectrolyte (Lipfert et al., 2014). Indeed, electrostatic surfaces have been used for *in silico* classification of RNA-binding proteins (Shazman and Mandel-Gutfreund, 2007). Electrostatics can have long-range effects, considering they decrease proportional to the distance between the charged atoms, and not exponentially (Lipfert et al., 2014). Electrostatic interactions are dependent on the ionic strength of the solvent, increased concentration of charged ions are able to screen electrostatic interactions between RNA and proteins by adding additional charged species, which compete the interaction.

Previously, a flanking tRNA subunit within a polycistronic tRNA precursor was shown to activate the enzyme by increasing the  $k_{cat}$  without affecting the substrate occupancy (same  $K_M$ ) (Clarke, 2015). Binding of ligands distal to the active site is a common phenomenon in enzymology. Indeed, allostery is the process in which binding to one site can have an effect on another site (Motlagh et al., 2014; Guo and Zhou, 2016; Greener and Sternberg, 2018). This is typified by haemoglobin which displays positive homotropic allostery, in which the initial binding of diatomic oxygen eases subsequent binding of the substrate such that oxygen is both the effector and the ligand (McNamara and El-Khuffash, 2017). Previous suggestions that contacts exist beyond the “catalytic site” have been suggested by cross-linking studies of BR13 in which interaction was seen at amino acids 25-36 within the first RNase H domain additionally RNA was detected crosslinked to amino acids 427-433 (Kim et al., 2014).

To progress the study of the RNA-binding groove of RNase E, it was decided at a joint meeting with Ben Luisi and Kasia Bandyra that the following substitutions would be introduced as part of this project: R3Q, Q22N, H268S, Y269F, Q270N, K433N, R488Q and R490Q. In Cambridge, the 8x RNA-binding groove mutant was shown to have substantially reduced cleavage of a tri-phosphorylated RprA derivative compared with wild-type (Bandyra et al., 2018). Cleavage was also shown to be mostly restored if the substrate was made monophosphorylated, suggesting the mutant is not able to efficiently engage with substrates without a 5' monophosphate. In this chapter, the effects of substitutions within the RNA-binding groove on tRNA processing are described

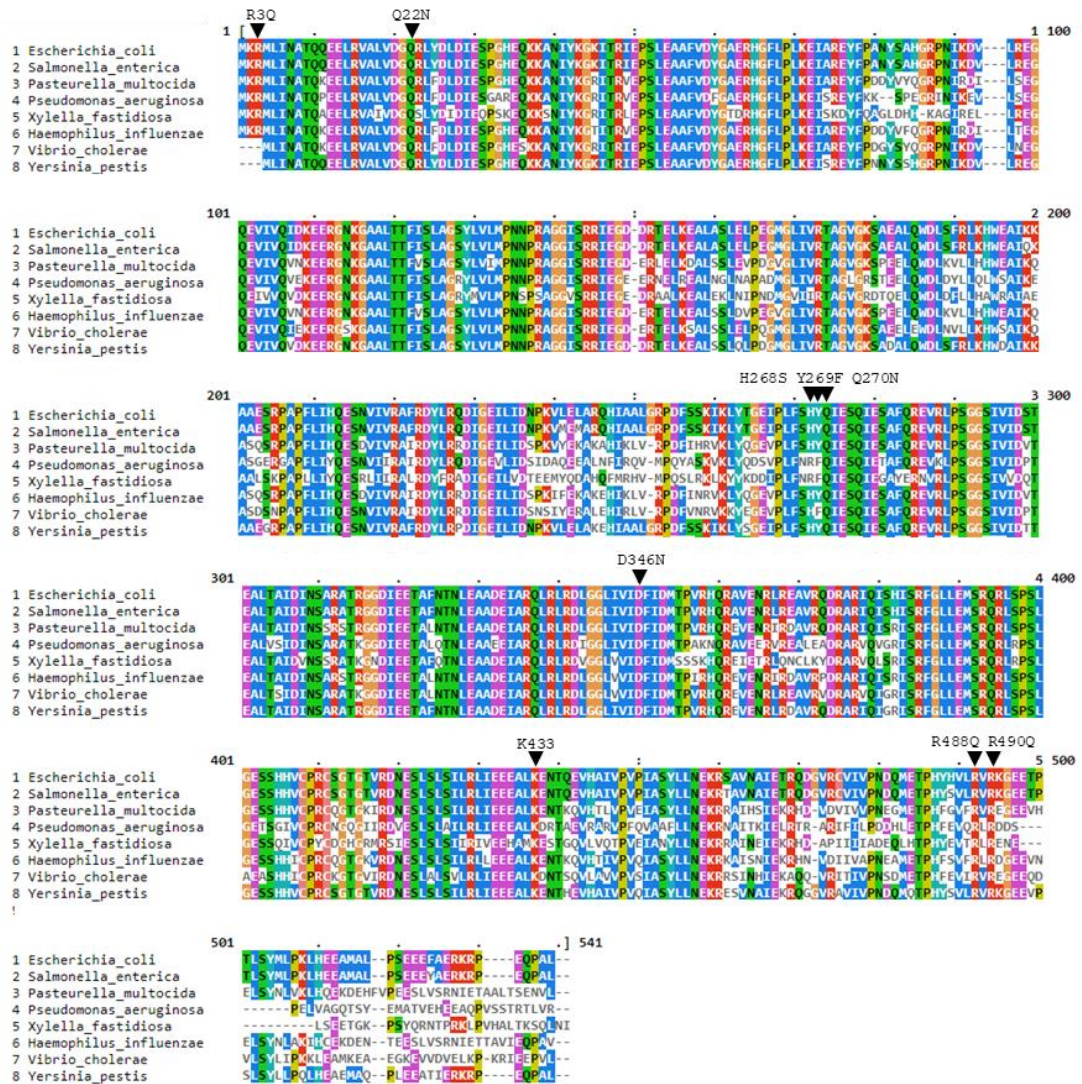
## 3.2 Results

### 3.2.1 Site-directed mutagenesis and over-production of *E. coli* NTH RNase E

To determine whether residues in close proximity to the duplex RNA identified in the RNase E-RprA complex (Bandyra et al., 2018) were evolutionary conserved, amino acid sequences from various members of the  $\gamma$ -proteobacteria, the class of bacteria of which *E. coli* is a member, were aligned. The phylogeny of RNase E is complicated by two factors. First, five forms of RNase E have been described (Aït-Bara and Carpousis, 2015) and secondly, whilst RNase E is essential in *E. coli*, it is non-essential in several organisms due to the presence of additional enzymes that are capable of undertaking similar enzymatic roles such as RNases Y and J (Condon and Putzer, 2002; Aït-Bara and Carpousis, 2015). The presence of additional enzymes that result in catalytic redundancy may have allowed for genetic drift to occur even in regions that are essential to function in *E. coli*. To this end, the analysis was limited to members of the  $\gamma$ -proteobacteria that do not possess RNases Y and J. Sequences were retrieved from NCBI (Pruitt et al., 2007) and aligned using MUSCLE (Edgar, 2004) to residues 1 to 529 of *E. coli* RNase E. Residues 1-529 encode the well-characterised N-terminal catalytic half of RNase E, which is well conserved within the  $\gamma$ -proteobacteria (Kaberdin et al., 1998) and is essential for *E. coli* viability (Baba et al., 2006; Goodall et al., 2018). Of the eight residues in close proximity to the duplex RNA, six were absolutely conserved: R3, Q22, Q270, K433, R488 and R490 (Figure 3.2). One of the two others H268 is replaced by an arginine in

*Pseudomonas aeruginosa* and *Xylella fastidiosa*, which may still facilitate interaction with RNA. The remaining residue Y269 is also not absolutely conserved and is replaced with a phenylalanine in RNase E of *Vibrio cholera* as well as *P. aeruginosa* and *X. fastidiosa*. Both tyrosine and phenylalanine are aromatic amino acids, tyrosine has been previously shown to be critical to RNA interaction in an RNA-binding domain of a viral polymerase (Matsumoto et al., 2019); furthermore, phenylalanine residues in the S1 subdomain of RNase E are critical for alignment of the scissile bond (see main introduction). The conservation of residues indicates the RNA-binding groove may have importance beyond *E. coli*.





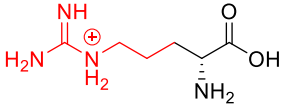
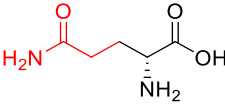
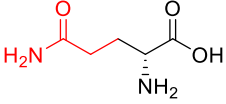
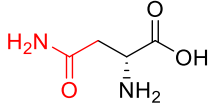
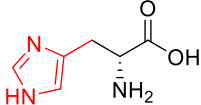

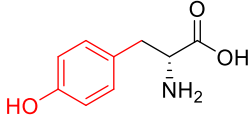
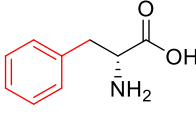
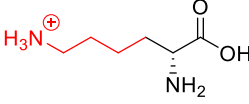
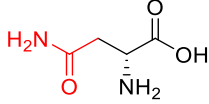
**Figure 3.2 Polypeptide Sequence alignment of members of the RNase E family from  $\gamma$ -proteobacteria.** Sequences from *Salmonella enterica* (2), *Pasteurella multocida* (3), *Pseudomonas aeruginosa* (4), *Xylella fastidiosa* (5), *Haemophilus influenzae* (6), *Vibrio cholerae* (7) and *Yersinia pestis* (8) have been aligned to RNase E from *E. coli* (1) using MUSCLE (Edgar, 2004). Amino acids are highlighted based on conservation and coloured according to physicochemical properties following the CLUSTAL colouring scheme (Blue denotes hydrophobic residues, Red denotes positive residues, magenta denotes negatively charged residues, green denotes polar residues, pink denotes cysteine residues, orange denotes glycine residues, yellow denotes proline residues, cyan denotes aromatic residues and uncoloured residues are not conserved by identity) using MVIEW. Mutated residues are indicated by an arrow along with the mutation introduced at that position, numbering is according to the position in *E. coli* RNase E.

In order to test the biochemical importance of these residues, suitable substitutions were identified in discussion with Prof. Ben Luisi (Cambridge). The substitutions (see Introduction), which were intended to be conservative to minimise unintended effects on local structure, were introduced using QuikChange site-directed mutagenesis in a number of combinations (Table 3.1). The rationale for making the agreed substitution is summarised alongside the structures of the original and resulting amino acid residues (Table 3.2).

**Table 3.1 List of NTH-RNase E Mutants.**

<b>Mutation Designation</b>	<b>Contained Mutations</b>
M3	H268S, Y269F, Q270N
M4	R3Q
M5	Q22N
M6	H268S
M7	Q270N
M8	K433N
M9	R488Q
M10	R490Q
M11	H268S, Y269F, Q270N, R488Q
8x	combined

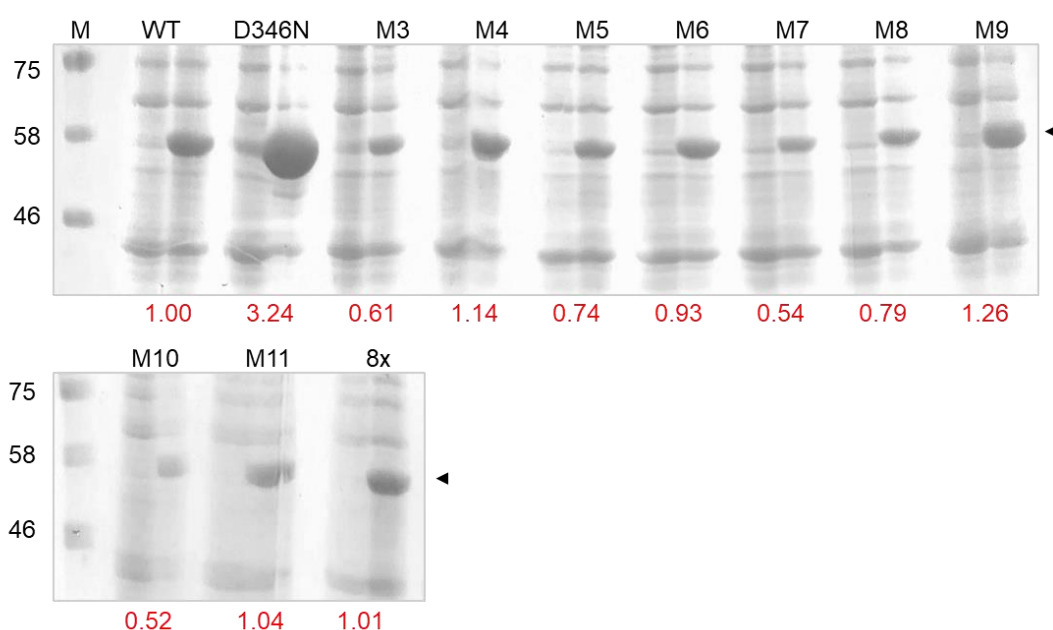
**Table 3.2 Rationale of amino acid substitutions made in RNase E**

Mutation	Original residue	Mutated residue	Details
Arginine -> Glutamine (R3Q, R488Q, R490Q)			Guanidinium group replaced with amide, retains polar character, but removes positive charge.
Glutamine -> Asparagine (Q22N, Q270N)			Reduces carbon chain length by one, retains polar character.
Histidine -> Serine (H268S)			Imidazole group replaced with alcohol group, retains polar character, but is no longer ionisable.
Tyrosine -> Phenylalanine (Y269F)			Alteration of phenol group to phenyl group, maintains aromatic ring but loses polar character.
Lysine -> Asparagine (K433N)			Reduces carbon chain length by two, conversion of amine to amide retains polar character but loses charge.

The plasmid used for site-directed mutagenesis was pRNE529N (Redko et al., 2003), a construct derived from pET16b (Novagen). The mutant D346N, which has a substitution in one of the residues necessary for catalysis (Callaghan, Marcaida, et al., 2005), was also generated as a control for later assays. The substitution and their positions are presented in the context of the alignment of representatives from the  $\gamma$ -proteobacteria (Figure 3.2). The introduction of all the combinations of substitutions (Table 3.1) was confirmed by sequencing (data not shown).

The mutated constructs were subsequently introduced by transformation into *E. coli* BL21 (DE3) cells and an initial expression trial was conducted in which transformants were grown in liquid broth, induced for protein production, lysed, and crude lysates analysed by SDS-PAGE (Figure 3.3). A band corresponding to protein of approximately 58 kDa was detected within the induced samples for each mutant. NTH-RNase E migrates slightly faster than expected for a molecular mass of 62 kDa. It is interesting to note that there appears to be variation in the band intensities for the different mutants. During their induction, T7 RNA polymerase leaves large stretches of RNA uncovered as it outpaces the ribosomes translating behind it, in effect uncoupling transcription and translation (lost et al., 1992). As the recombinant NTH-RNase E is free in the cytosol (due to the lack of the membrane anchor, segment A found within the C-terminal half) it is able to attack effectively its corresponding mRNA, thereby antagonise its own production (Leroy et al., 2002). Therefore, theoretically, activity may be inversely correlated with band intensity. Indeed, the D346N mutant, which is unable to co-ordinate a magnesium ion at the active site (and has been

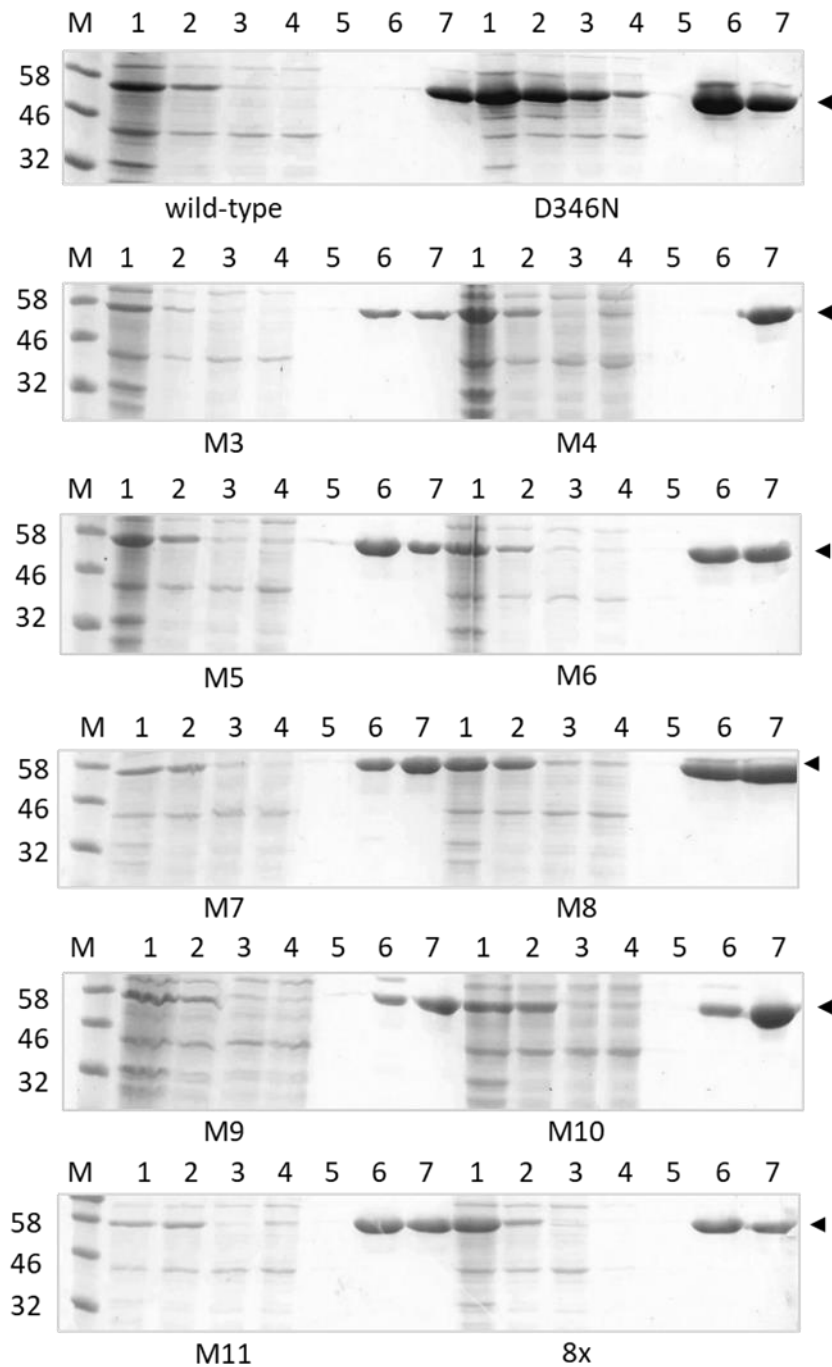
shown to be largely inactive; Callaghan et al., 2005), shows the highest level of production. The other mutants show levels of production more similar to that of NTH-RNase E with wild-type sequence (hereafter simply referred to as NTH-RNase E) suggesting that not only do they retain catalytic activity, but all the functions required to degrade mRNA exposed by the uncoupling of transcription and translation.



**Figure 3.3 SDS-PAGE analysis of *E. coli* BL21 (DE3) cellular extracts taken pre- and post-induction that have been induced to produce mutants of N-terminally tagged NTH-RNase E.** Samples taken pre- and post-induction were separated by electrophoresis on a 15% (w/v) polyacrylamide gel and subsequently stained with InstantBlue™ protein stain. Equal numbers of cells were loaded in each lane based on OD<sub>600</sub>. A pre-stained protein ladder was included to estimate the molecular weight of protein bands. The arrow indicates the position of RNase E and the number in red below each lane indicates the fold change in band intensity compared with wild-type.

### **3.2.2 Purification of mutant RNase E proteins**

In order to assay the effects of mutations of RNase E, it was first necessary to purify the corresponding polypeptides. All the mutants were purified in parallel using immobilised metal affinity chromatography (see section 2.4.2.3 for further details). Samples of the cell lysate, cleared lysate, flow through and wash steps were analysed by SDS-PAGE (Figure 3.4). The purity of proteins was judged by densitometry to be greater than 95% for all samples. Thus, further purification steps were deemed unnecessary for the planned biochemical studies. Final samples of 3.5 ml had concentrations between 2 and 11  $\mu\text{M}$ .



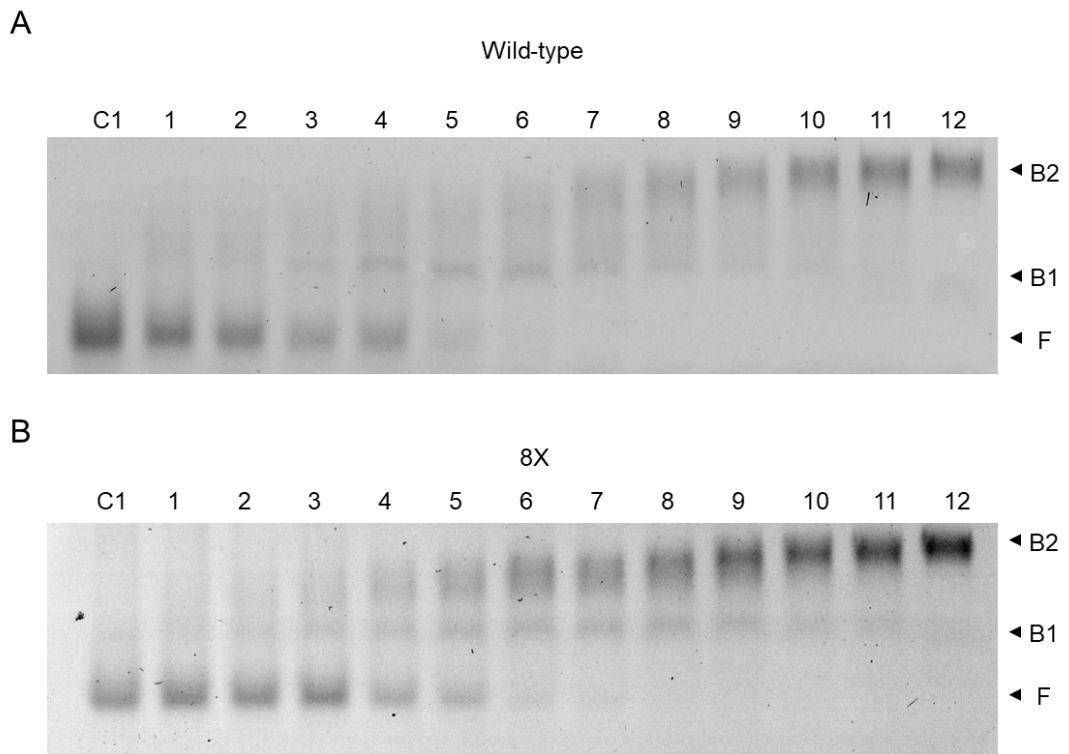
**Figure 3.4 SDS-PAGE analysis of samples obtained during the purification of His-tagged NTH-RNase E by IMAC.** Samples taken during RNase E purification were separated by electrophoresis on a 15% (w/v) polyacrylamide gel alongside a protein ladder and subsequently stained with InstantBlue™ protein stain. The mutant the gel corresponds to is indicated below each gel. The labelling above each lane is as follows; M denotes the marker, lanes 1-7 denote lysate, clarified lysate, flow-through, first wash, high-salt wash, low imidazole wash and eluate, respectively.



### 3.2.3 Analysis of NTH RNase E binding to model RNA substrates

The first substrate used to investigate the contribution of contacts made within the RNA-binding groove was BR15 (5'-GGGGGACAGUAUUG-3'), which has been used previously (Clarke, 2015). The penta-guanosine sequence at the 5' end allows four BR15 oligonucleotides to anneal via non-Watson-Crick, Hoogsteen-type base pairing (Burge et al., 2006) to form an intermolecular G-quadruplex structure (Rhodes and Lipps, 2015), which results in a substrate that presents four single-stranded and no duplex regions. Modelling suggests that a principal dimer of RNase E can interact simultaneously with two of the four single-regions presented by annealed BR15 (Kime et al., 2010). Binding was measured using electrophoretic mobility shift assays (EMSAs), which not only provide estimates of binding affinity but allow the resolution of different complexes (Garner and Revzin, 1981). As found previously, NTH-RNase E binds to BR15 and produces at higher concentrations a second complex (Figure 3.5, panel A). The second complex is thought to correspond to annealed BR15 bound by two tetramers of NTH-RNase E; each tetramer binding two of the four available single-stranded regions (Clarke, 2015; Justin Clarke pers. comm). The second binding event presumably occurs at higher protein concentrations due to steric hindrance by the first RNase E tetramer. The apparent dissociation constant ( $K_d$  values) for the first complex was estimated to be 12 nM using a 1:1 binding model. This value is similar to the value of 8 nM reported previously (Clarke, 2015). Also shown is the result of the equivalent EMSA for the 8x mutant (Figure 3.5, panel B). The binding profile of the 8x mutant was broadly similar to that of NTH-RNase E. The apparent  $K_d$  value was

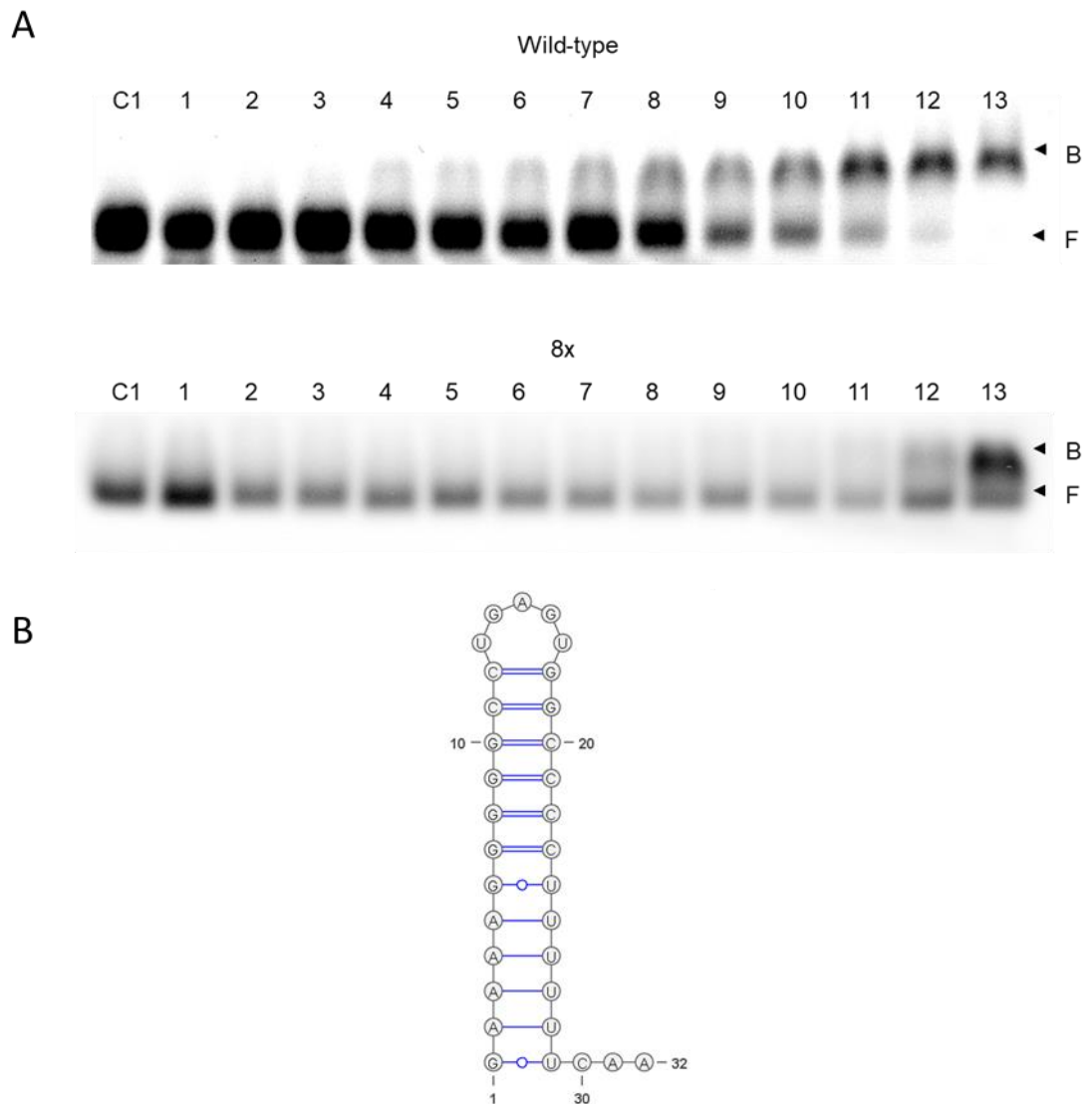
estimated to be 6 nM. All of the mutants were assayed as described above and the corresponding apparent  $K_d$  values estimated (Table 3.3). The results taken together indicated that mutation of the groove distal to the active site of RNase E does not negatively affect the binding of annealed BR15. This was expected as crystallography and modelling studies have indicated that NTH-RNase E can contact single-stranded regions using surfaces presented by the S1 and DNase I domains (Callaghan, Marcaida, et al., 2005). The second complex detected as part of this study is not the result of a second tetramer binding to the first directly. An EMSA using a similar range of protein concentration but a substrate that presents only one single-stranded region produced only one complex (data not shown). The effective binding of the 8x mutant to BR15 suggests that the substitutions have not caused distortion of the N-terminal catalytic domain.



**Figure 3.5 Electrophoretic mobility shift assay of BR15 by NTH-RNase E mutants.** Shown are EMSAs of fluorescein labelled BR15 RNA incubated with increasing concentrations of RNase E and subsequently separated on a 1% agarose gel. The identity of the mutant is shown above each gel. Lanes labelled C1 contains RNA only. The concentrations of protein in lanes 1 to 12 are as follows: 0.49, 0.98, 1.95, 3.91, 7.81, 15.63, 31.25, 62.5, 125, 250, 500 and 1000 nM. BR15 RNA is included in each lane and is 7.5 nM. Free and bound RNA species are labelled with F and B respectively. Numbers were added in cases where multiple bound species (i.e. complex) were detected. Gels were imaged using a Fujifilm FLA-5000 imager and scanned at 473 nm.

The second substrate used to investigate the contribution of contacts made within the RNA-binding groove was the transcriptional terminator of *rpsO* (hereafter referred to simply as *rpsO* RNA) (Evans and Dennis, 1985), which had been used previously in the study of the requirements for efficient RNase E cleavage of tRNA precursors (Kime, unpublished data). In contrast, to what was observed previously for the BR15 substrate, the 8x mutant in comparison to wild-type NTH-RNase E was impaired in the binding of *rpsO* (Figure 3.6). For wild-type NTH-RNase E, the apparent  $K_d$  value for its

interaction with *rpsO* RNA was 517 nM, which is 45-fold higher than the corresponding value for BR15. The lower affinity of the *rpsO* interaction may reflect at least in part the absence of contacts beyond a single RNA-binding groove. Whilst a complex could be detected for the *rpsO* terminator at the highest concentration of the 8x mutant that was used (5000 nM), it migrated slightly faster than the complex detected for wild-type NTH-RNase E. This complex need not correspond to an interaction with the mutated groove, but perhaps another site. All of the other mutants, produced complexes that migrated similar to that of wild-type NTH-RNase E. From the corresponding EMSAs, apparent  $K_d$  values were estimated using a 1:1 binding model (Table 3.3). It seems that as predicted several substitutions are required along the surface of the groove to have sufficient cumulative effect on the binding of duplex RNA.



**Figure 3.6 Electrophoretic mobility shift assay of the *rpsO* terminator by wild-type and 8x NTH-RNase E.** Shown are EMSAs of Cy5 labelled *rpsO* RNA incubated with increasing concentrations of RNase E and subsequently separated on a 1% agarose gel (panel A). The identity of the mutant is shown above each gel. Lanes labelled C1 contains RNA only. The concentrations of protein in lanes 1 to 12 are as follows: 1.22, 2.44, 4.88, 9.77, 19.53, 39.06, 78.13, 156.25, 312.5, 625, 1250, 2500 and 5000 nM. Free and bound RNA species are labelled with F and B respectively. Gels were imaged using a Fujifilm FLA-5000 imager and scanned at 635 nm. Panel B shows the mfold (Zuker, 2003) predicted structure of the substrate.

**Table 3.3 Apparent Binding constant values for BR15 and the *rpsO* terminator RNA.** (Data represents a single measurement)

Mutant	BR15 apparent $K_d$ (nM)	<i>rpsO</i> apparent $K_d$ (nM)
Wild-type	12	517
D346N	26	527
M3	29	520
M4	16	805
M5	11	620
M6	13	740
M7	27	1549
M8	8	504
M9	7	701
M10	4	951
M11	8	1395
8x	6	>5000

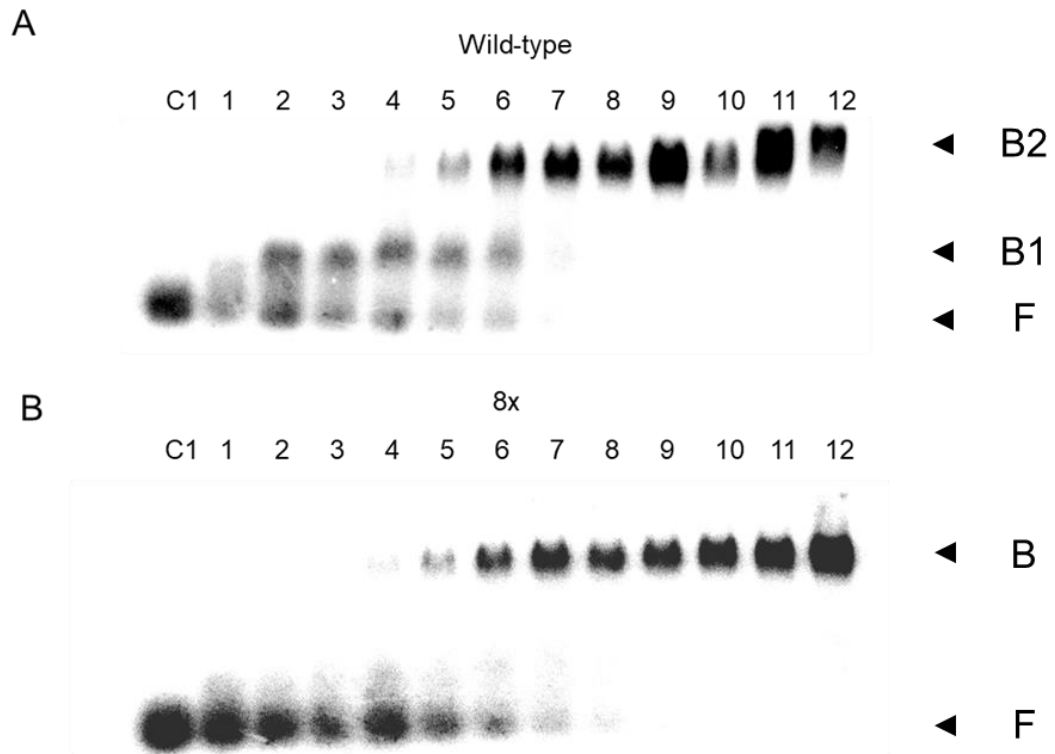
### 3.2.4 RNA-binding groove involvement in tRNA processing

The third substrate used was the *glnW* tRNA subunit, an unmodified tRNA subunit possessing no trailer sequences (hereafter referred to as *glnW*) from the *metT-leuW-glnU-glnW-metU-glnV-glnX* polycistronic tRNA precursor. It was this substrate that provided the first clear biochemical evidence for the existence of a second RNA-binding site on RNase E (see Introduction to chapter). Initially, *glnW* was detected as done previously by staining after the electrophoresis step, but as found previously the presence of sub-stoichiometric amounts of contaminating RNA in preparations of NTH-RNase E could obscure the second of two complexes formed with *glnW* RNA at the highest protein concentrations. Thus, in order to allow the assay of binding at high protein concentrations, 3' FAM-labelled *glnW* RNA was synthesised by phosphoramidite chemistry. However, the presence of the label had a marked effect on binding: only one complex was detected, which migrated at a position similar to the second of the two complexes that were detected when unlabelled *glnW* RNA was used in the binding assays and stained post electrophoresis (discussed further below). Therefore, *glnW* RNA was body-labelled with  $\alpha$ -<sup>32</sup>P UTP during *in vitro* transcription.

EMSA of the interaction of wild-type NTH-RNase E and radio-labelled *glnW* RNA revealed the formation of two distinct complexes (Figure 3.7, panel A), as described previously (Clarke, 2015). The apparent  $K_d$  values for the first and second complexes were 3 nM and 25 nM, respectively. Remarkably, for the 8x mutant, only one complex was detected. The highest affinity interaction detected for *glnW* RNA and NTH-RNase E (fastest migrating complex) was blocked by substitution within the RNA-binding groove. In

addition, the position of the complex formed between 8x and *glnW* RNA was not identical, although similar, to the second of the complexes (slower migrating) formed between *glnW* RNA and NTH-RNase E (see below). The apparent  $K_d$  value for the single interaction detected between 8x and *glnW* RNA was 42 nM. It is speculated that the complex formed by the 8x mutant, given its migration, is possibly *glnW* RNA bound by two tetramers of RNase E. An explanation for the absence of a complex corresponding to *glnW* RNA bound by a single tetramer of 8x is that both binding sites available to 8x on *glnW* RNA are essentially equivalent in terms of the affinity of the corresponding interactions. The region(s) on NTH-RNase E that mediate binding in the presence of the 8x substitutions is not known (see Discussion). The second of the two complexes formed by NTH-RNase E is also thought to be *glnW* RNA bound by two tetramers, but via one high affinity and one low-affinity interaction. In other words, it was concluded the complexes formed by NTH-RNase E and the 8x mutant at high protein concentrations are unlikely to be equivalent. Regardless of the molecular details, the clear loss of the high-affinity interaction for the 8x mutant indicates a role for the RNA-binding groove in the binding of *glnW* RNA.

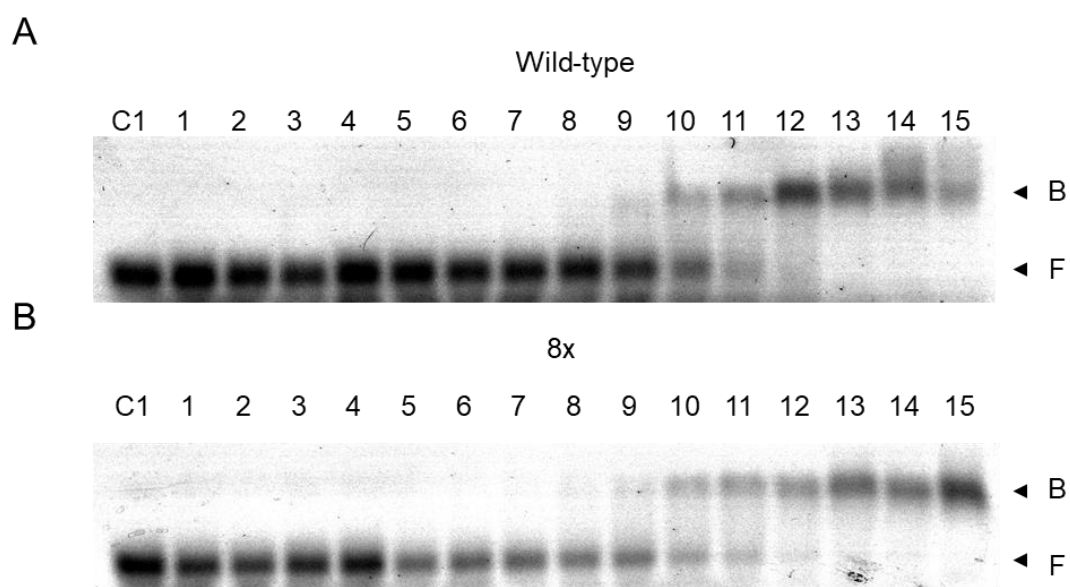




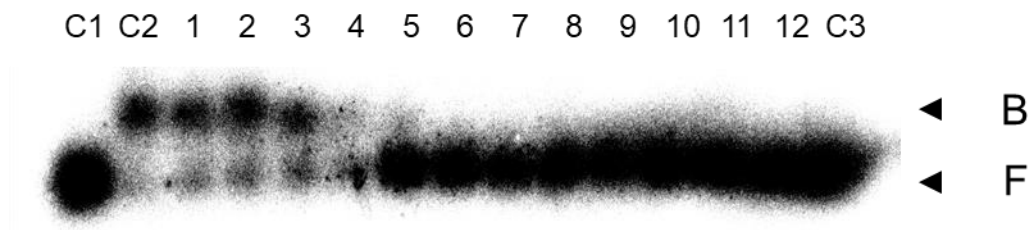
**Figure 3.7 Electrophoretic mobility shift assay of radiolabelled *glnW* RNA subunits by wild-type and 8x NTH-RNase E.** Shown are EMSAs of the lone *glnW* tRNA precursor incubated with increasing concentrations of wild-type (Panel A) and 8x (Panel B) NTH-RNase E and subsequently separated on a 1% agarose gel. C1 contains RNA only, concentrations of protein in lanes 1-12 are as follows; 0.49, 0.98, 1.95, 3.91, 7.81, 15.63, 31.25, 62.5, 125, 250, 500 and 1000 nM. *glnW* RNA of 10 cps is included in every lane. Free and bound species are labelled with F and B respectively. Panel A contains two bound species which are also labelled as B1 and B2 for the first and second species. Dried gels were exposed to a phosphor screen which was subsequently imaged using a Fujifilm FLA-5000 imager and scanned using the 'IP' setting.

Given mutations within the RNA-binding domain were found to disfavour the formation of a complex associated with higher affinity interactions, the binding of 3' FAM-labelled *glnW* RNA was revisited, but this time the analysis included the 8x mutant as well as NTH-RNase E (Figure 3.8). The binding profiles for both proteins were indistinguishable with both lacking the complex associated with the higher affinity interaction. This suggests that the presence of a FAM group at the 3' end of *glnW* RNA may prevent its alignment with the RNA-binding groove. Further evidence that *glnW* RNA

interacts with the RNA-binding groove was provided by a competition assay. Increasing amounts of unlabelled RprA, the substrate with the duplex region shown by crystallography to interact with the RNA-binding groove (Bandyra et al., 2018), was introduced into reactions containing radiolabelled *glnW* RNA and enough NTH-RNase E to form the higher-affinity complex. RprA was able to compete with *glnW* RNA for binding. The concentration of RprA that was able to reduce the abundance of the *glnW* RNA: NTH-RNase E complex by 50% (the IC<sub>50</sub> value) was 13 nM (Figure 3.9).

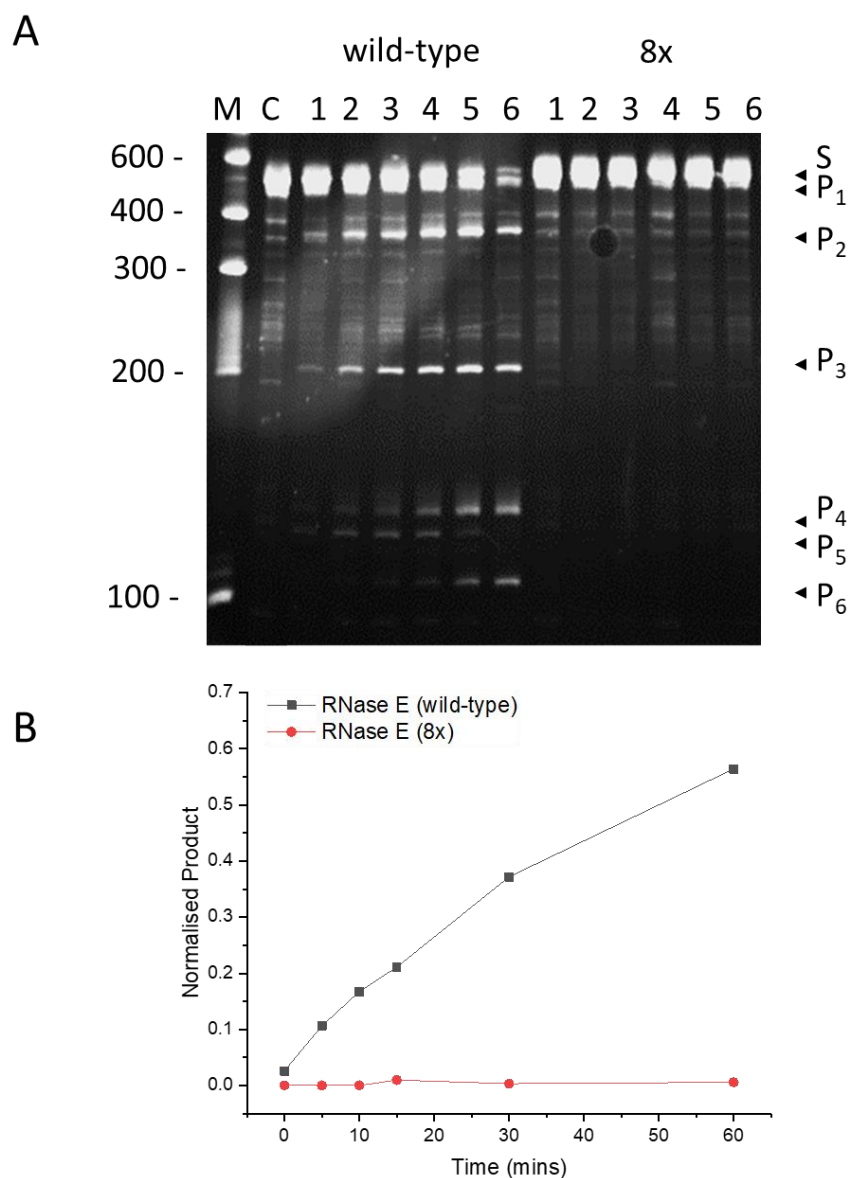


**Figure 3.8 Electrophoretic mobility shift assay of FAM-labelled *glnW* RNA by wild-type and 8x NTH-RNase E.** Shown are EMSAs of the lone *glnW* tRNA precursor labelled with FAM incubated with increasing concentrations of wild-type (Panel A) and 8x (Panel B) NTH-RNase E and subsequently separated on a 1% agarose gel. C1 contains RNA only, concentrations of protein in lanes 1-15 are as follows; 0.31, 0.61, 1.22, 2.44, 4.88, 9.77, 19.53, 39.06, 78.13, 156.25, 312.5, 625, 1250, 2500 and 5000 nM. *glnW* RNA of 20 nM is included in every lane. Bound and free species are indicated as B and F respectively. Gels were imaged using a Fujifilm FLA-5000 imager and scanned at 493 nm.



**Figure 3.9 Competition binding assay of *glnW*-RNase E with RprA.** Shown is a competition EMSA of the lone *glnW* tRNA precursor bound to NTH-RNase E incubated with increasing concentrations of RprA RNA and subsequently separated on a 1% agarose gel. C1 contains *glnW* RNA only, C2 contains NTH-RNase E and *glnW* RNA and C3 contains *glnW* RNA and competitor RNA at 1000 nM. The concentrations of competitor RNA in lanes 1-12 are as follows: 0.49, 0.98, 1.95, 3.9, 7.81, 15.63, 31.25, 62.5, 125, 250, 500 and 1000 nM. *glnW* RNA of 10 cps is included in every lane. NTH-RNase E, when included is at a final concentration of 20 nM. Bound and free species are indicated as B and F respectively. Dried gels were exposed to a phosphor screen which was subsequently imaged using a Fujifilm FLA-5000 imager and scanned using the 'IP' setting.

Substitution of conserved residues within the RNA-binding groove of NTH-RNase E not only affect interaction with *glnW* RNA but the processing of tRNA precursors. This was shown using a discontinuous assay to follow the cleavage of unlabelled polycistronic tRNAs generated by *in vitro* transcription. The substrates and products were visualised by staining with ethidium bromide post electrophoresis. NTH-RNase E but not the 8x mutant was able to cleave the polycistronic *argX-hisR-leuT-proM* precursor (Figure 3.10). Based on estimation of the lowest limits of detection in this system, it was estimated that the reduction in the rate of cleavage of the substrate as a result of multiple substitutions within the RNA-binding groove was >95%. Thus, as previously suggested (Kime et al., 2014), interaction with multiple single-stranded region although required is not sufficient for efficient processing of tRNA precursors.

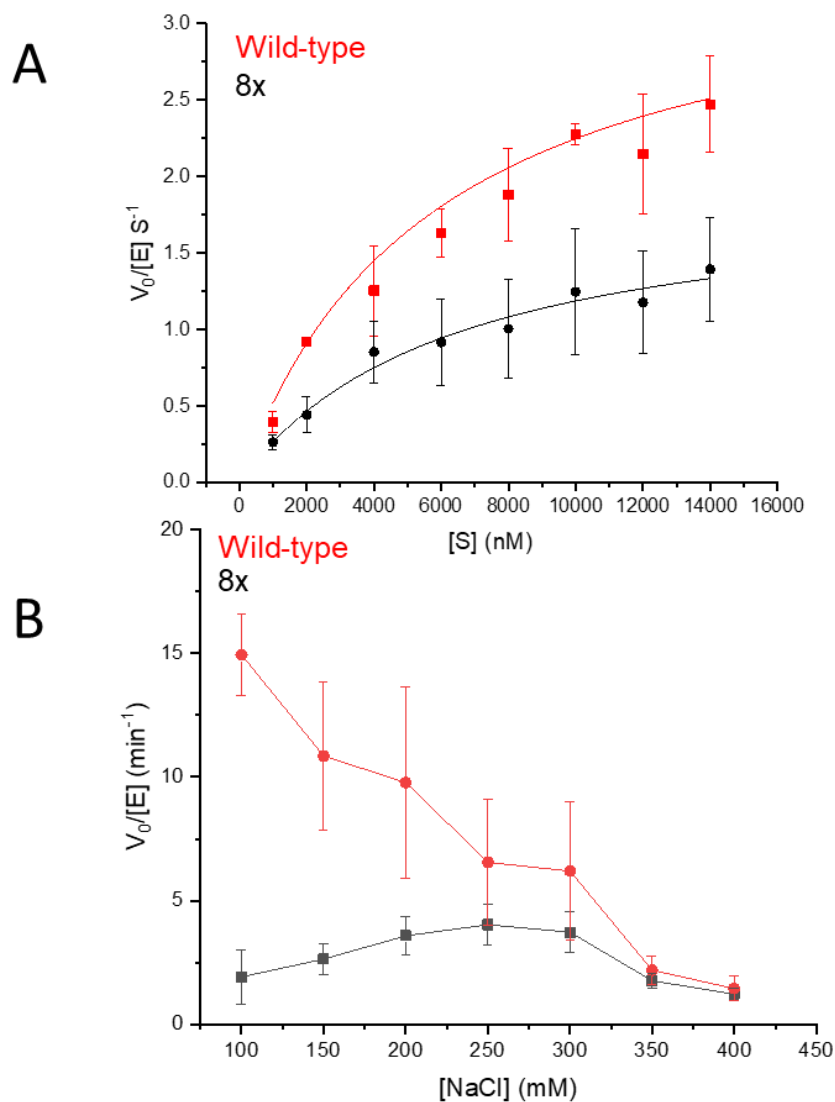


**Figure 3.10 Discontinuous Cleavage assay of a fragment of ArgX tRNA precursor by wild-type and 8x NTH-RNase E.** The 5' triphosphorylated substrate was synthesised by in vitro transcription. The final enzyme and substrate concentrations were 5 nM and 0.2  $\mu$ M respectively. The identity of the mutant enzyme is shown above each gel. Lanes 1-6 contain time points taken at 0, 5, 10, 15, 30 and 60 minutes. Lane M contains an RNA ladder with sizes indicated on the left. Lane C contains a no enzyme control. Samples taken from the reaction at indicated points were quenched by adding to 2x RNA loading buffer, denatured at 95°C and separated by electrophoresis on a 10% (w/v) polyacrylamide gel. The gel was stained by ethidium bromide and imaged using a UV transilluminator. Panel A shows the gel obtained. Panel B shows the increase in amount of product P<sub>3</sub> as a function of time for the wild-type and 8x mutant. A normalised product was calculated by densitometry using the intensity of P<sub>3</sub> relative to the sum of the P<sub>3</sub> and uncleaved substrate. Generation of the 6 products of cleavage by direct entry have been described previously (Kime et al., 2014).

### 3.2.5 Michalis-Menten analysis and dependency on ionic strength

Although substitutions within the RNA-binding groove did not have a marked effect on the binding of substrates that did not present duplex RNA, initial experiments revealed that the 8x mutant was impeded in the cleavage of LU13, another derivative of the widely used substrate BR13 (McDowall et al., 1995), by at least five-fold (see below). Assay of the cleavage activity of all the other mutants at a single substrate concentration did not reveal marked (> 1.5-fold) differences compared with wild-type (data not shown) suggesting that as found for the binding of the *rpsO* terminator and the *glnW* tRNA subunit multiple substitutions are required to produce a marked effect. Like BR15, LU13 is an oligonucleotide substrate but has at its 5' end a GAG motif, followed by the first 10 nucleotides from the 5' end of RNAI, the antisense regulator of the ColE1 replicon (Lin-Chao et al., 1994; McDowall et al., 1994). (5'-GAGACAGUAUUUG-3'). The GAG motif, unlike the GGGGG motif of BR15, does not support quadruplex formation. LU13 was 5' monophosphorylated and was labelled at the 3' end with a fluorescein, which facilitates detection without affecting cleavage (Redko et al., 2003). For the purpose of comparison, the batch of NTH-RNase E used in this analysis was purified using the same protocol used to purify the 8x mutant. Their activities were assayed multiple times using a range of substrate concentrations to allow the determination of Michaelis-Menten parameters (Figure 3.11, panel A). The  $K_M$  and  $k_{cat}$  values for the 8x mutant were  $6.3 \pm 0.8 \mu\text{M}$  and  $1.9 \pm 0.2 \text{ s}^{-1}$ , respectively, whilst the equivalent values for NTH-RNase E were  $5.8 \pm 0.6 \mu\text{M}$  and  $3.6 \pm 0.2 \text{ s}^{-1}$ , respectively. These values for the 8x mutants and NTH-RNase E were more similar than initially expected.

Previously reported  $K_M$  and  $k_{cat}$  values for the cleavage of LU13 by NTH-RNase E were 5.7  $\mu\text{M}$  and 1.1  $\text{s}^{-1}$ , respectively (Kime et al., 2010; Clarke, 2015). The ratio of  $k_{cat}/K_M$  for NTH-RNase E and the 8x mutant were 0.6 and 0.3, respectively, a difference of only two-fold.



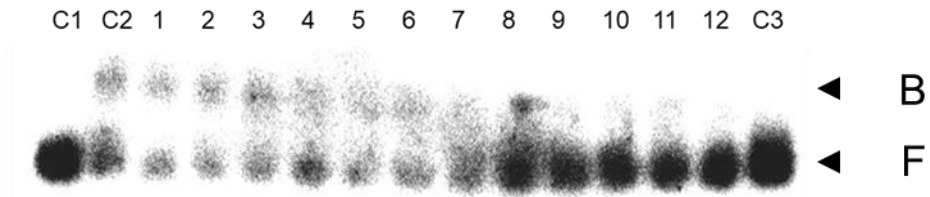
**Figure 3.11 Michaelis-Menten and Salt analysis of wild-type vs 8x mutant RNase E with LU13.** Panel A shows a Michaelis-Menten graph for LU13 cleaved by NTH-RNase E and the 8x mutant. The final concentration of the enzyme was 5 nM. Rates were normalised against enzyme concentration, plotted against substrate concentration and subsequently fitted to the Michaelis-Menten equation. Error bars represent standard error of the mean and are from 3 technical replicates. Panel B shows a graph illustrating the differential salt dependence of wild-type and 8x RNase E. Rates were normalised against enzyme concentration and plotted against sodium chloride concentration. Final enzyme and substrate concentrations were 5 nM and 200 nM, respectively. Error bars represent standard error of the mean and are from 3 technical replicates.

Repeated assay of the cleavage of LU13 at a relatively low substrate concentration (200 nM) under our standard assay conditions (100 mM NaCl) revealed that the activity of 8x was 7.8-fold lower than NTH-RNase E (Figure 3.11, panel B), a much greater difference than that for the ratios of the  $k_{cat}/K_M$  values from the Michaelis-Menten analysis. This suggested that the NTH-RNase E does not strictly obey Michaelis-Menten kinetics and may be subject to allosteric regulation via the interaction of single-stranded RNA with the RNA-binding groove. This might have been evident from the Michaelis-Menten analysis had lower substrate concentrations been included (Berg et al., 2002).

As the RNA-binding groove is thought to mediate largely electrostatic interactions (see Introduction), the effect of increasing the ionic strength of the buffer on the rate of cleavage of LU13 was investigated (Figure 3.11, panel B). This confirmed that, as described previously (Redko et al., 2003), the activity of NTH-RNase E is salt-dependent. More interestingly, the substitutions within the RNA-binding groove largely removed the salt dependency and the activity of the 8x mutant across the range of salt concentrations was similar to NTH-RNase E at the highest salt concentration (500 mM). It is proposed that single-stranded RNA as well as RNA with duplex regions can interact with the RNA-binding groove to stimulate RNA cleavage. Whilst *glnW* RNA was unable to compete with BR15 for binding to NTH-RNase E (Clarke, 2015), substrates displaying single-stranded regions might be able to compete with *glnW* RNA for binding to NTH-RNase E. This prediction, which was based on the assumption that binding at the active site is exclusive to single-stranded regions (i.e. it can accommodate LU13/BR15



but not *glnW* tRNA), was found to be the case (Figure 3.12). Indeed, LU13 is able to compete with *glnW* for binding to NTH-RNase E the  $IC_{50}$  for LU13 was 58 nM, an  $IC_{50}$  value for BR15 could not be determined, however, it was evident that competition does occur (data not shown).



**Figure 3.12 Competition binding assay of *glnW*-RNase E with LU13.** Shown is a competition electrophoretic mobility shift assay of the lone *glnW* tRNA precursor bound to NTH-RNase E incubated with increasing concentrations of LU13 competitor RNA and subsequently separated on a 1% agarose gel. C1 contains *glnW* RNA only, C2 contains NTH-RNase E and *glnW* RNA and C3 contains *glnW* RNA and competitor RNA at 2500 nM. The concentrations of competitor RNA in lanes 1-12 are as follows: 1.2, 2.4, 4.9, 9.8, 19.5, 39.1, 78.1, 156.3, 312.5, 625, 1250 and 2500 nM. *glnW* RNA of 10 cps is included in every lane. NTH-RNase E, when included is at a final concentration of 10 nM. Bound and free species are labelled as B and F respectively. Dried gels were exposed to a phosphor screen which was subsequently imaged using a Fujifilm FLA-5000 imager and scanned using the 'IP' setting.

## Discussion

This chapter has shown that *in vitro* the recently discovered RNA-binding groove of RNase E interacts with the *glnW* tRNA subunit (Figures 3.7 to 3.9) and is required for the cleavage of polycistronic tRNA precursors (Figure 3.10). Evidence is also provided that the RNA-binding groove may interact, depending on the ionic strength of the buffer, with single-stranded regions to promote cleavage (Figures 3.11 and 3.12). Substrates with single-stranded regions can bind independent of the RNA-binding groove, presumably via an interaction that involves the S1 domain (Figures 3.5). It was also shown that a simple stem-loop can be bound by NTH-RNase E provided the RNA-binding groove is not disrupted (Figure 3.6).

Previously, investigation of the processing of tRNA precursors by the NTH-RNase E has revealed interactions beyond those with single-stranded regions that flank the units destined to form tRNA (Clarke, 2015). RNase E cleavage downstream of the *metU* tRNA subunit within the *metT-leuW-glnU-glnW-metU-glnV-glnX* tRNA precursor has been shown to be stimulated by the upstream *glnW* tRNA subunit, at least in *cis* (Clarke, 2015). This suggests the tRNA subunits can have an allosteric role and act as a homotropic positive modulator of cleavage. The finding here that the *glnW* interaction (Figure 3.7, panel B) is affected by mutation of the RNA-binding groove implicates the groove in the allosteric activation of RNase E by an adjacent tRNA. This could be further tested by extending the analysis of cleavage downstream of *metU* tRNA to include the 8x mutant and reactions in which the ionic strength is higher. It is predicted that no cleavage would

occur with the 8x mutant and allosteric activation may be lessened at higher ionic strength.

Previously, based on the analysis of the cleavage downstream of *metU* tRNA in the presence or absence of upstream *glnW* tRNA, it was speculated that blocking allosteric activation by a supporting tRNA would reduce the  $k_{cat}$  by two or three-fold to that of an equivalent monocistronic tRNA precursor (Clarke, 2015). However, analysis of cleavage of the tRNA precursor *argX-hisR-leuT-prom* revealed that the 8x substitutions severely hamper cleavage, estimated to be >95%. This would suggest that the RNA-binding groove has functions beyond allosteric activation and may make a substantial, if not major, contribution to the binding of at least some substrates. This notion is supported by no substantial additional increase in the affinity detected for the binding of *glnW-MetU* or *glnW* with flanking single-stranded regions compared with the *glnW* subunit alone (Clarke, 2015).

In relation to allosteric activation, it would be interesting to repeat the Michaelis-Menten analysis of the cleavage of a single-stranded substrate but using lower substrate concentrations that may reveal evidence of cooperative interactions, which would be manifested as a sigmoidal curve (Berg et al., 2002). It is suggested that such an analysis would benefit from the adoption of a continuous assay system given the effort required to assay cleavage using the discontinuous approach described here which requires the preparation and running of multiple polyacrylamide gels for many hours. Previously, a continuous assay system based on an internal quencher and a 3' fluorophore pair has been trialled (Stead and McDowall, unpublished data)

however the presence of the internal quencher significantly hampered the rate of cleavage (K. McDowall, pers. comms), a similar system has also been published (Jiang and Belasco, 2004). Additionally, a system involving hybridised oligonucleotides involving the 5' monophosphate being present *in trans* and the cleaved RNA is labelled with a fluorophore and quencher pair at the termini has been recently published (Mardle et al., 2019).

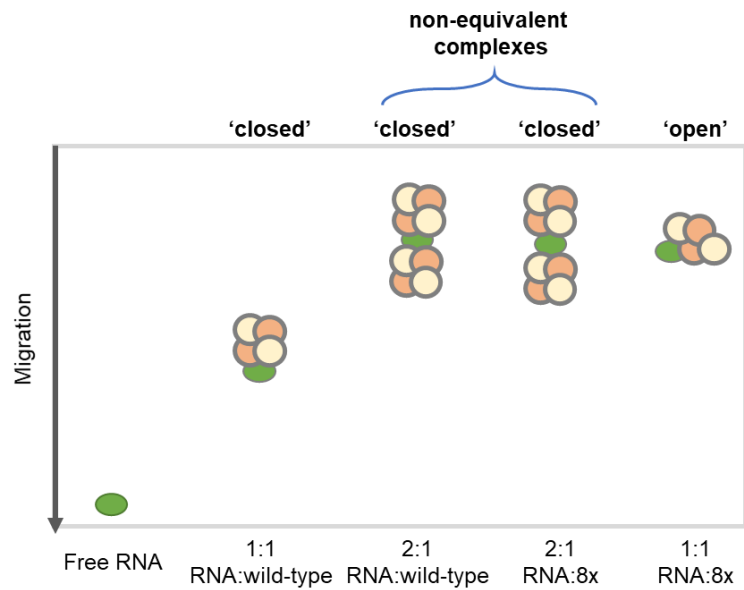
It has been shown that the *rpsO* terminator can mediate RNase E cleavage when substituted for the *hisR* tRNA unit within the *argX-hisR-leuT-proM* polycistronic tRNA precursor (Clarke and Kime, unpubl. data). Consistent with this, it is shown here that a simple stem-loop structure can be bound by NTH-RNase E provided the RNA-binding groove is not disrupted (Figure 3.6). Interestingly, *glnW* tRNA subunit binds with much higher affinity than the *rpsO* terminator which may suggest it makes additional contacts with RNase E beyond the RNA-binding groove. However, *in silico* alignment of a tRNA model with the RNA bound to the groove (PDB:6G63) in PyMOL (Schrödinger, Inc.) did not reveal any obvious additional candidate residues for interaction, suggesting another approach may be necessary to characterise better tRNA binding to the RNA-binding groove (see Chapter 5). Interestingly, the addition of a fluorophore to the 3' end of *glnW* tRNA appeared to block binding to the groove, suggesting that the acceptor arm of the tRNA is, or is in close proximity to, the region that interacts with the RNA-binding groove (Figure 3.8).

The study of the contribution of RNA-binding groove would be aided by mutants that block interaction with the S1 domain. To date, single substitutions have been introduced at multiple sites, without an observable

effect on RNA binding (Callaghan, Marcaida, et al., 2005). It is likely that as found here for the RNA-binding groove that multiple substitutions in the S1 domain are required to produce a marked cumulative effect. Such mutations, perhaps in combination with the 8x substitutions, would shed light on the nature of the complex identified by some of the electrophoretic mobility shift assays (Figure 3.7). It is possible, at least formally, that NTH-RNase E can interact with RNA beyond the RNA-binding groove and contacts involving the S1 domain. Mutations that locked the NTH of RNase E in either the open or closed confirmation would also be of value. It may be possible to achieve this by constraining movement by the use of a bismaleimide crosslinker that could be directed at positions by introducing cysteine residues (Prahlad et al., 2014)

It has been found that the RNA-binding groove has also been implicated in cleavage of MicL sRNA (Updegrave et al., 2019), mutation of the RNA-binding groove results in abolition of cleavage, much like cleavage of the tRNA polycistronic precursors studied as part of this work. Cleavage of MicL was shown to depend on two stable stem-loops proximal to the cleavage site and not dependent on sequence within the cleavage site. It would be interesting to see if the same was true of cleavage of the tRNA precursors by altering the sequence of the flanking regions between tRNA subunits to see if they have any negative effects on cleavage. However, cleavage of the substrates was determined in a qualitative manner so it not clear if the rates of cleavage would change by altering the sequence at the site of cleavage for MicL.

An interesting finding is that whilst the 8x mutant is still able to bind with nanomolar affinity to the *glnW* pre-tRNA the interaction that is made is dissimilar to that made with the wild-type protein as indicated by the presence of a unique complex (Figure 3.7). The 1<sup>st</sup> complex is likely attributed to the RNA-binding groove and it is theorised that the 2<sup>nd</sup> complex occurs via a 2:1 interaction, either via equivalent or non-equivalent interactions. Presumably, if the interactions were equivalent the second interaction occurs at higher concentrations due to steric hindrance. If non-equivalent interactions were occurring, it is likely that the second interaction is weaker and thus occurs at higher protein concentrations. In the EMSA of 8x and *glnW* it is possible that the complex migrating similarly to the 2<sup>nd</sup> complex detected in the EMSA of NTH-RNase E and *glnW* involves interaction with the S1 sub-domain, an ancient RNA-binding domain that can interact with double-stranded RNA (Bycroft et al., 1997; Qu et al., 2012), see (Figure 3.13) for suggested explanations of the complexes seen. Binding via the S1 subdomain alone may lead RNase E to stay in 'open' conformation and thus the complex has much greater retardation in the gel. It could also be possible that there is involvement of a third site or more distributed RNA-binding surface. Previously, other sites of interaction have been identified (Schuck et al., 2009; Kim et al., 2014) (also discussed in chapter 4). A more in-depth characterisation of tRNA interaction would be required to decipher the nature of the complexes seen in the EMSAs.



**Figure 3.13 Hypothetical model of interactions of *glnW* and RNase E.** Shown is the different possible explanations of the complex seen in the EMSA of 8x NTH-RNase E and *glnW*. At low concentrations of wild-type NTH-RNase E bands are seen that represent free RNA and bound species that presumably represent 1:1 binding. At higher concentrations, a second complex is formed that presumably corresponds to a 2:1 interaction. Bound RNA seen in the EMSA of 8x NTH-RNase E and *glnW* migrates similarly to the 2:1 complex seen for the wild-type. This may either be due to a 2:1 interaction or a 1:1 interaction that results in a more open conformation.

## **Chapter 4**

The contribution of the RNA-binding groove to autoregulation and RNase E essentiality.



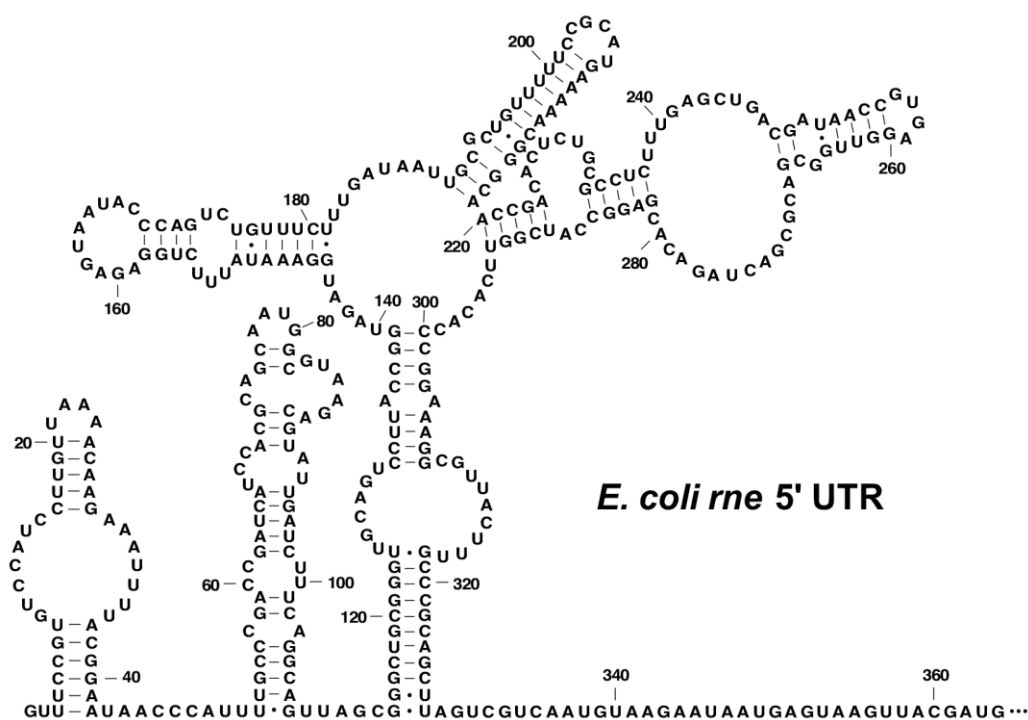
## 4.1 Introduction

The degradation of mRNA is central to the post-transcriptional control of gene expression. Degradation of mRNA is antagonistic to the translation of the RNA by ribosomes and thus the rate at which degradation occurs sets a limit on the steady-state level of proteins. Degradation of RNA in *E. coli* is thought to be orchestrated by RNase E. Indeed, Cellular levels of all classes of RNA are controlled by the degradation and processing functions of RNase E (Mackie, 2013).

RNase E interacts with substrates in two ways, primarily by 'direct entry' but also by the 5' monophosphate dependent pathway (see main introduction for further details). Cleavage of substrates by both pathways can be achieved *in vitro* by the N-terminal half alone (Clarke, 2015). The N-terminal half of RNase E features the small domain that mediates the formation of a homotetramer in which the canonical interaction surface with RNA consists of the S1 and 5'-sensor subdomains of one protomer and the DNase I domain of a second protomer within a principle dimer (Callaghan, Marcaida, et al., 2005). RNase E acts within the context of the degradosome (see main introduction) where it is aided by several other components of the RNA decay apparatus. The C-terminal half is both necessary and sufficient for degradosome assembly (Khemici et al., 2008).

An interesting aspect of the biology of RNase E is autoregulation. *E. coli* have evolved a feedback mechanism to control the global rate of degradation of transcripts such that RNase E autoregulates its own expression (Jain and Belasco, 1995; Jiang et al., 2000; Sousa et al., 2008; Schuck et al., 2009) by tightly controlling cellular levels of the *rne* transcript

the lifetime of which varies (inversely) with RNase E activity. The 5' UTR of the *rne* transcript acts as a cis-regulatory sequence, that confers sensitivity of the transcript to RNase E. The 5' UTR (Figure 4.1) consists of three stem-loops separated by single-stranded regions. Previous studies have shown that the 5' UTR can be fused to reporters which then become particularly susceptible to RNase E mediated degradation (Jain and Belasco, 1995). It has been reported that although the C-terminal half is not necessary for cleavage of RNA it contributes to autoregulation (Jiang et al., 2000).



**Figure 4.1 Structure of 5'UTR of *rne* mRNA.** Shown is a diagram indicating the secondary structure of the *rne* 5' UTR. The Shine-Dalgarno sequence and start codon are underlined. Taken from (Diwa et al. 2000).

RNase E is one of three ribonucleases (see main introduction) that is essential in *E. coli*. It was identified as the enzyme responsible for the processing of the 9S rRNA precursor to 5S rRNA through use of a temperature-sensitive mutant of *E. coli* that results in the accumulation of the

9S precursor (Ghora and Apirion, 1978; Misra and Apirion, 1979). Additionally, RNase E is responsible for the processing of tRNA precursors, which has also been identified as an essential function of RNase E (Ow and Kushner, 2002). A construct of RNase E encompassing amino acids 2-484, the majority of the catalytic domain, has been shown to be unable to complement an RNase E deficient strain unless present at a concentration 8-fold higher (Jiang et al., 2000). This alone suggests that either association of RNase E with the membrane or full formation of the degradosome is necessary for RNase E to carry out its essential functions. The former is precluded by work suggesting that RNase E deficiency can be complemented by RNase E lacking segment A (Khemici et al., 2008). However, it does result in a slow-growth phenotype with a 32% reduction in the rate of growth (Hadjeras et al., 2019). In addition to the processing of the 9S precursor, RNase E also functions to process 16S alongside its paralogue RNase G (Li et al., 1999b). As rRNA processing is essential, the lack of RNase G essentiality implies redundancy exists. RNase E essentiality indicates the paralogue cannot cleave many of the sites that RNase E can.

RNase G is present alongside RNase E in many of members of the  $\beta$ -,  $\gamma$ - and  $\delta$ -proteobacteria (Condon and Putzer, 2002). RNase G shares high sequence similarity (33.7% identity, 67.4% similar in 469 amino acid overlap) with RNase E which sometimes results as homologues being referred to as RNase E/G.

Vast overproduction of RNase G can complement RNase E deficient cells (Lee et al., 2002) although it is not clear to what extent this is true of the

wild-type sequence (Deana and Belasco, 2004). RNase G has a minor contribution to RNA metabolism as it is non-essential (Li et al., 1999b; Wachi et al., 1999). Within *E. coli* RNase G is normally present at a concentration 3% to that of RNase E (Lee et al., 2002).

In this chapter, the effects of the 8x RNase E mutant on cell viability and autoregulation are described. Further to this, comparisons are made to RNase G which is thought to not possess an RNA-binding groove.

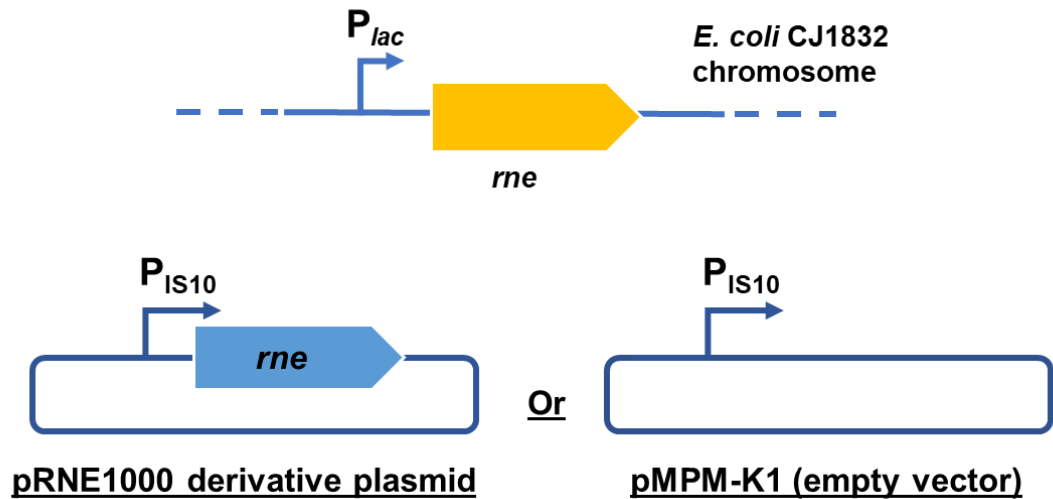
## 4.2 Results

### 4.2.1 Contribution of the RNA binding groove to RNase E essentiality

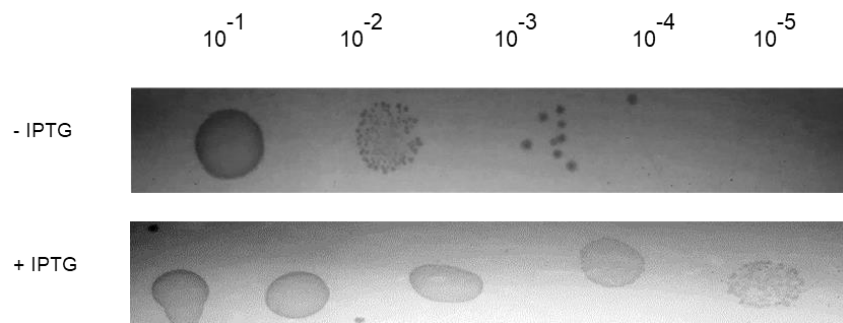
To determine whether the previously described RNA-binding groove contributes to one of the essential functions of RNase E, cell viability assays were conducted. The previously described mutations (Table 3.1) were introduced into the plasmid pRNE1000 (Jiang et al., 2000), which encodes full-length RNase E under the control of the IS10 promoter. This construct has been reported to produce RNase E to a physiological concentration (Jiang et al., 2000). Alongside this, site-directed mutagenesis was used to introduce a stop codon after amino acid 529 to make versions of the plasmid that encode versions of the N-terminal half (NTH) with the wild-type sequence and 8x substitutions. Previously, a version of RNase E with a truncation that is now known to be within the small domain that mediates the interaction of principle dimers, was reported to be unable at normal physiological levels to complement an RNase E-deficient strain (Jiang et al., 2000). It was concluded that this was due to the loss of the C-terminal half, which mediates degradosome. However, the equivalent polypeptide encoding only the first 498 amino acids is prone to aggregation *in vitro* (McDowall and Kaberdin, unpublished observations) raising the alternative possibility that the lack of complementation described above might have been due to defects within the N-terminal catalytic half.

Previously, the essential requirement of RNase E for cell viability or colony-forming activity has been determined using *E. coli* strain CJ1832 (Jain and Belasco, 1995); Figure 4.2). Within this strain, the chromosomal copy of RNase E has been placed under the control of the *lac* promoter. It was confirmed that the growth of this strain was dependent on IPTG, which inactivates the *lac* repressor thereby allowing transcription from the *lac* promoter engineered upstream of the *rne* gene (Figure 4.3). Into this strain, the plasmids described above and pMPM-K1 (Mayer, 1995), an empty vector control, were introduced by transformation. Cells from three independent transformants of each of the resultant strains were then streaked out onto nutrient agar plates with or without IPTG. Growth was detected on all plates in the presence of IPTG indicating that there was no dominant-negative phenotype associated with the presence of the mutants. There were no obvious differences in colony morphology. Significant growth on agar plates lacking IPTG was only detected on the plate streaked with CJ1832 cells containing the plasmid encoding full-length RNase E (Figure 4.4, panel A). The analysis of the resultant strains was extended to liquid cultures (Figure 4.4, panel B). All strains grew in the presence of IPTG with no significant difference in their doubling time (Table 4.1). In the absence of IPTG only the growth of the strain containing the plasmid encoding full-length RNase E approached stationary phase; comparable to the growth of the other strains in the presence of IPTG. Equivalent levels of growth were not detected for the other strains. The inability of full-length RNase E with the 8x substitutions to sustain growth on plates or in liquid media indicates for the first time that the newly identified RNA-binding groove has a function(s) that critical for *E. coli* cell viability. This work also confirms the

earlier suggestion that the C-terminal half of RNase E, the platform for the assembly of the RNA degradosome complex (Vanzo et al., 1998; Kaberdin et al., 1998), is likely critical for *E. coli* cell viability under conditions where the production of RNase E is fixed at normal physiological levels, i.e. not subject to autoregulation.

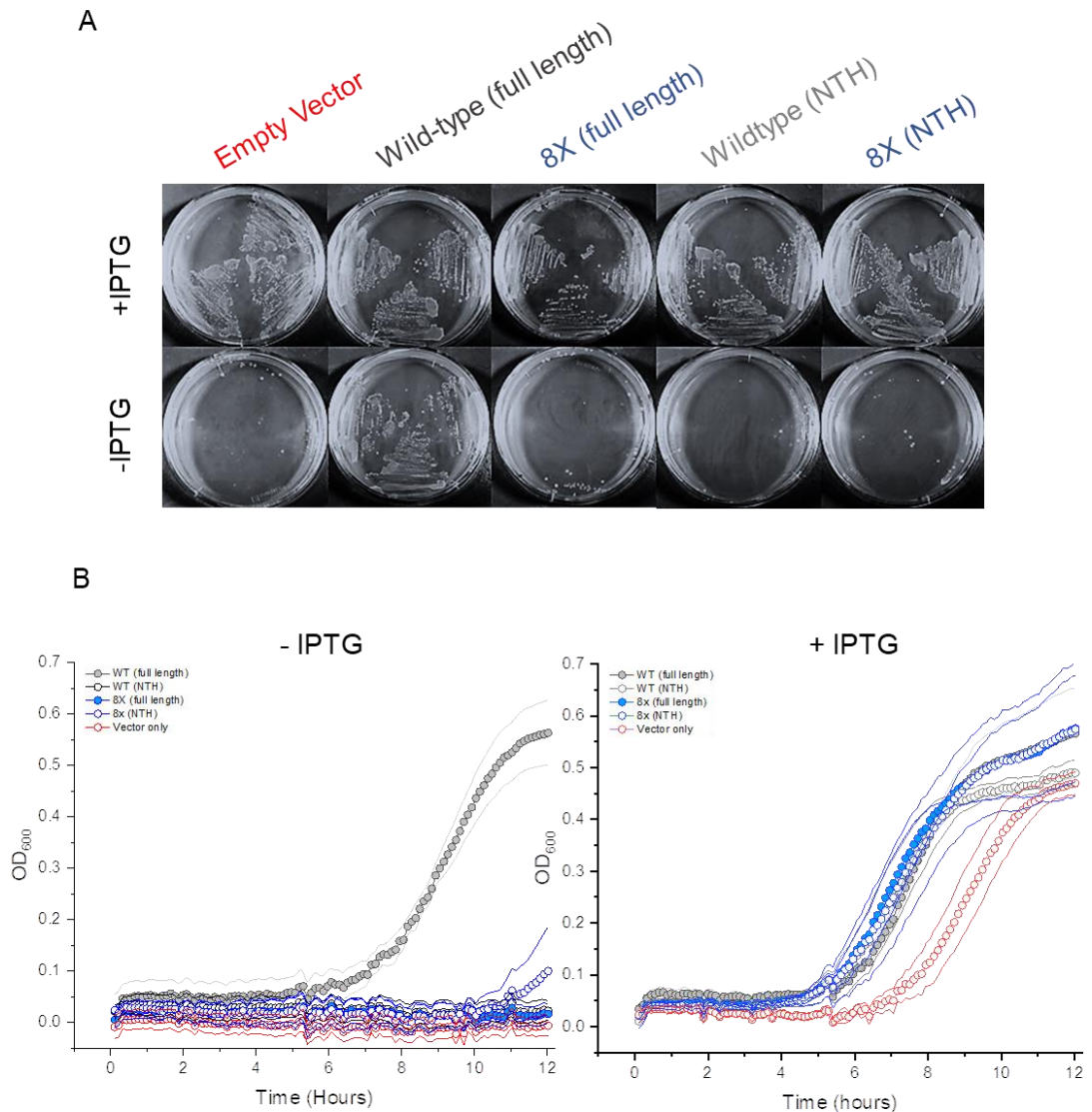


**Figure 4.2 Schematic representation of *E. coli* strain CJ1832.** The chromosomal copy of the RNase E gene (*rne*) is under the control of the lac promoter ( $P_{lac}$ ). Cell viability assay involved CJ1832 harbouring pMPM-K1 (Mayer, 1995) or pRNE1000 (Jiang et al., 2000) or derivatives of the latter.



**Figure 4.3 Assaying IPTG dependence and colony-forming ability of *E. coli* CJ1832** Viability testing on *E. coli* CJ1832 to confirm IPTG dependence. CJ1832 grown overnight at 37°C in the presence of IPTG was serially diluted in PBS and spotted onto agar with or without IPTG. The dilutions are indicated above the panels.





**Figure 4.4 RNase E complementation assay.** Cell viability was assessed for CJ1832 strains containing plasmids encoding full-length and N-terminal half RNase E with the wild-type sequence and 8x substitutions. CJ1832 containing the empty pMPM-K1 vector was included as a control. Panel A shows LB agar plates streaked with three separate colonies of the indicated strains both with or without IPTG supplementation. Panel B shows growth curves from liquid culture measured at OD<sub>600</sub> with or without IPTG supplementation. Closed circles indicate full-length RNase E, whilst open circles indicate NTH constructs. Polypeptides with wild-type sequence are shown in grey, whilst those with the 8x substitutions are shown in blue. The control corresponding to the empty pMPM-K1 vector is depicted by red open circles. Three separate replicates were used for growth curves. The mean OD<sub>600</sub> values are indicated by the circles and the standard error by solid lines.

**Table 4.1 Doubling times of *E. coli* CJ1832 strains**

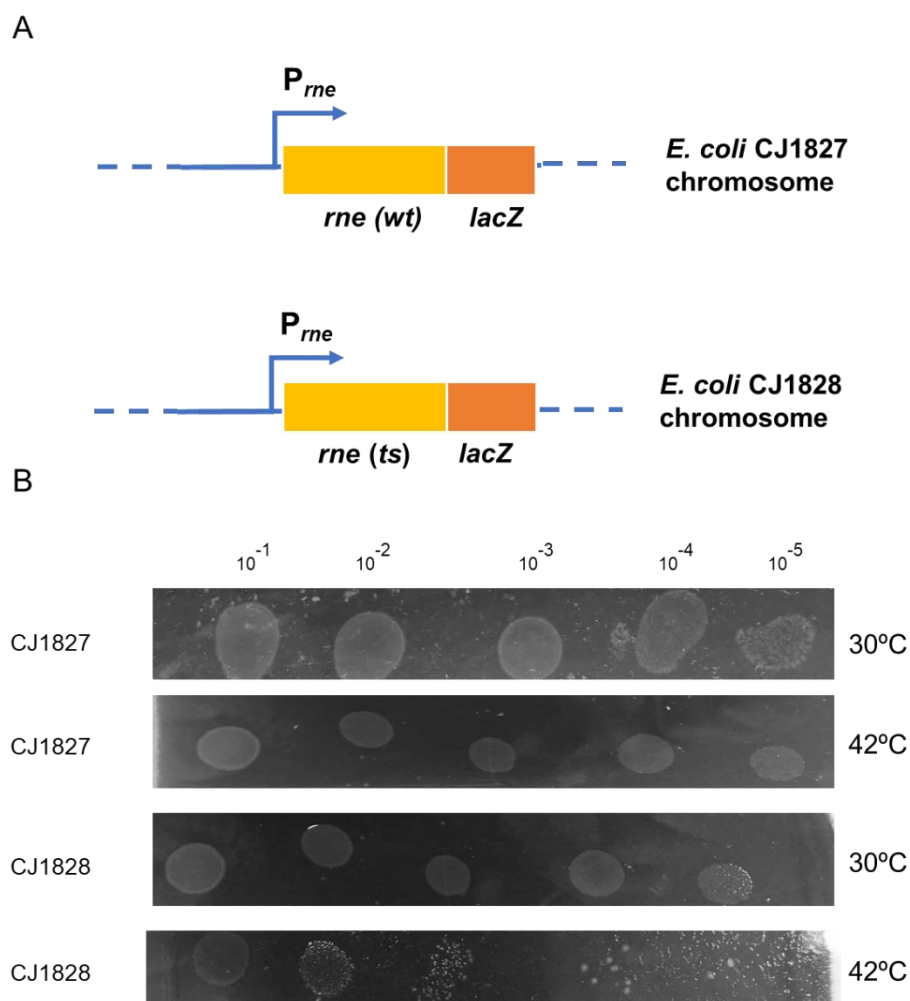
RNase E variant	IPTG	Doubling time (mins)
Wild-type (full length)	-	87.79±14.1
	+	79.06±11.46
Wild-type (NTH)	-	n/a
	+	86.48±5.77
8x (full length)	-	n/a
	+	79.1±5.13
8x (NTH)	-	n/a
	+	84.9±12.33
Empty vector (pMPM-K1)	-	n/a
	+	95.57±11.27

#### 4.2.2 Contribution of the RNA-binding groove to autoregulation of RNase E

RNase E is normally able to adjust its own expression via a feedback regulation system that efficiently regulates the degradation of its own mRNA (Mudd and Higgins, 1993; Jain and Belasco, 1995). Autoregulation has been explicitly linked to the complex secondary structures found within the 5' UTR of RNase E (see Introduction), a region that might be recognised at least in part using the RNA-binding groove. This possibility was investigated using a *rne-lacZ* translational fusion that has been previously used to study autoregulation (the fusion incorporates the full-length *rne* gene). To this end, the plasmids used in the previous complementation study were introduced into *E. coli* strain CJ1828, which contains the *ez1* reporter (Jain and Belasco, 1995) plus the temperature-sensitive *rne-1* mutation (Ono and Kuwano, 1979) of RNase E (Figure 4.5, panel A). This strain that can support growth at 37°C but is unable to fully repress *ez1* (Jiang et al., 2000) indicating a deficiency in RNase E function even at temperatures permissive for growth. At temperatures above 42°C, strains harbouring the *rne-1*

mutation are unable to grow (Ono and Kuwano, 1979). This was confirmed for CJ1828 (Figure 4.5) (Goldblum and Apririon, 1981).

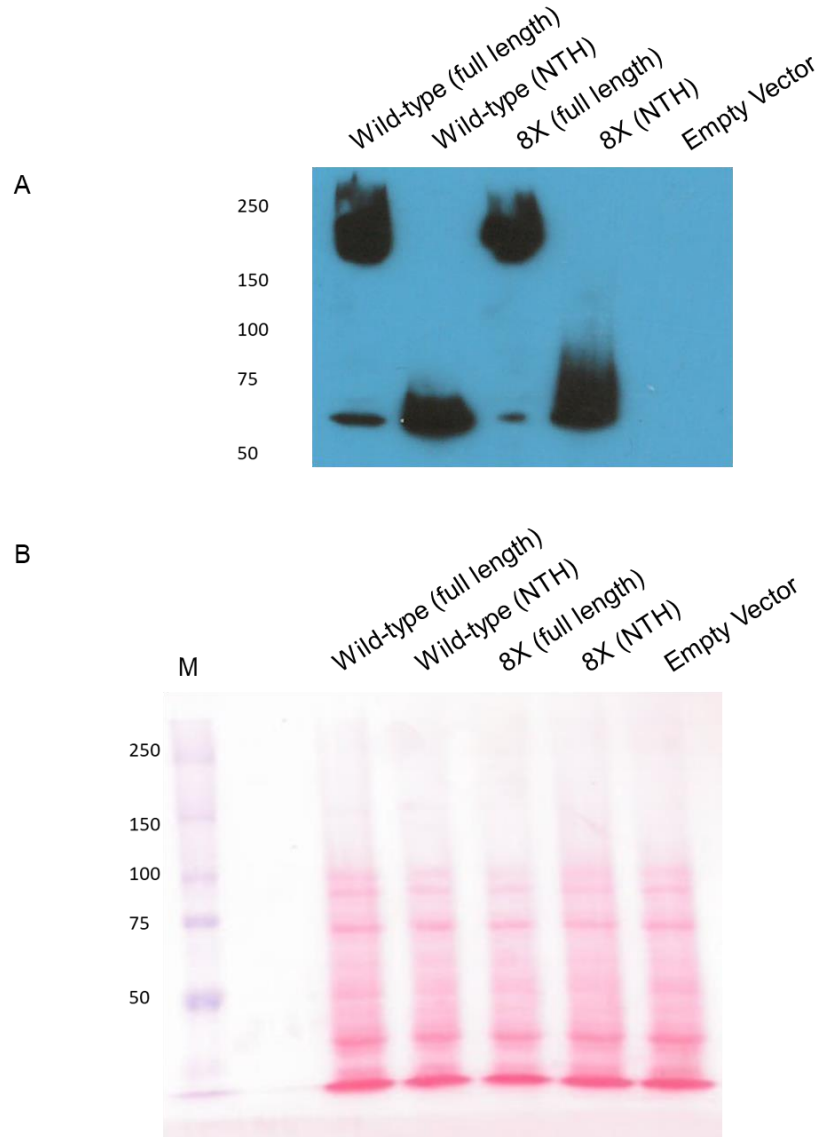
$\beta$ -Galactosidase assays utilising the  $\beta$ -Glo system (Promega) were used to investigate the effects of the 8x substitutions on the repression of *ez1*. The data were normalised to the CJ1827 strain (Jain and Belasco, 1995), which is the congenic wild-type *rne* partner of CJ1828 and should have a normal level of autoregulation. The substitution of residues within the RNA-binding groove of full-length RNase E did not result in a statistically significant difference in  $\beta$ -galactosidase activity indicating that the RNA-binding groove does not make a critical contribution to autoregulation. In contrast, deletion of the C-terminal half resulted in a statistically significant increase in  $\beta$ -galactosidase activity indicating that the N-terminal catalytic half of RNase E is insufficient for normal autoregulation. The actual level of  $\beta$ -galactosidase activity associated with the N-terminal catalytic half was statistically different from that of the temperature-sensitive *rne-1* mutant (p-value of 0.04). Substitutions within the RNA-binding groove of the N-terminal catalytic half of RNase E did not result in further, statistically significant lowering of  $\beta$ -galactosidase activity (p-value of 0.46). For each strain, the average value of the associated  $\beta$ -galactosidase activity was used as the denominator to calculate a relative level of repression using the equivalent average value for full-length RNase E in strain CJ1827 as the numerator (Table 4.2). Values lower than 1.0 indicate a reduction in the ability to repress the expression of the *ez1* reporter. Correspondingly, the N-terminal half does not appear to make a critical contribution to autoregulation. A near two-fold decrease was seen for deletion of the C-terminal half in the contexts of the wild-type and 8x RNase E variants in comparison with CJ1827.



**Figure 4.5 *E. coli* CJ1827 and CJ1828 temperature sensitivity.** Panel A shows a schematic of the two strains. Panel B shows viability testing of *E. coli* CJ1837 and CJ1828 to confirm temperature sensitivity. Strains were grown overnight at 30°C in LB broth and subsequently serially diluted in PBS and spotted onto agar and incubated at 30 °C or 42°C.

Western blots were subsequently performed on cell extracts to ensure data from  $\beta$ -galactosidase assays were not affected by significant differences in cellular levels of RNase E (Figure 4.6). Full-length RNase E, as described previously migrates slower than expected for a 124 kDa protein and migrates between 150-250 kDa (Khemici et al., 2008), whilst the NTH-RNase E migrates to the expected position of a 63 kDa protein. The times for effective western blotting of full-length RNase E and the N-terminal half vary considerably (McDowall, unpublished data). Thus, no attempt was

made to compare the cellular level of the two full-length polypeptides with those of the two N-terminal half polypeptides. Instead, the focus was on comparing the cellular levels of the full-length polypeptides and separately comparing the levels of the N-terminal half polypeptides. A comparison was done using three independent blots of three samples of cell lysates corresponding to each of the RNase E polypeptides. The results for key stages during a representative immunoblot are shown (Figure 4.6). Three independent blots were used and probed with chemiluminescence-generating antibodies for different periods of time to prevent the results from being skewed by under- or over-exposure. From each blot, the densitometry values for polypeptides with 8x substitutions and wild-type sequence were used as the numerator and denominator respectively to calculate a relative cellular level. The average of three such estimates were then determined (Table 4.2). No marked difference in protein level was associated with the 8x substitutions. Nevertheless, the value of the relative cellular level was used to normalise the values of the relative level of repression (Table 4.2). This reduced the already small arithmetical difference between the full-length constructs with the 8x substitutions or wild-type sequence (Table 4.2).



**Figure 4.6 Western Blot of c-Myc tagged RNase E from CJ1828 strains .** Approximately  $3.2 \times 10^6$  cells (equivalent to 10  $\mu$ l of OD<sub>600</sub> of 4) were resuspended in 1 x SDS loading dye and then boiled for 5 min at 95°C. Lysates were loaded and separated on an 8% (v/v) polyacrylamide-SDS gel. Proteins were transferred onto an activated PVDF membrane by semi-dry transfer. Panel A shows a western blot of the membrane indicated with sizes and CJ1828 strains. The membrane was blotted using an anti-c-Myc antibody, which was visualised using an HRP-labelled secondary antibody. Panel B shows an image of the membrane that was stained with Ponceau S prior to blotting.

**Table 4.2 Summary of  $\beta$ -Galactosidase-Autoregulation assay.**

Strain <sup>A</sup>	Protein	$\beta$ -Galactosidase activity (RLU $1 \times 10^6$ ) <sup>B</sup>	p-values (comparison with CJ1827)	Relative repression to CJ1827 <sup>C</sup>	Relative repression to CJ1828(pMPM-K1) <sup>D</sup>	Relative protein concentration <sup>E</sup>	Relative specific activity <sup>F</sup>
CJ1827	Wild-type	5.08 $\pm$ 0.11	1	1 <sup>X</sup>	2.40 $\pm$ 0.10	1	2.40 $\pm$ 0.10
CJ1828 (pMPM-K1)	n/a	12.19 $\pm$ 0.26	3.35E-8	0.42 $\pm$ 0.02	1 <sup>Y</sup>	n/a	n/a
CJ1828 (pRNE1000)	Wild-type (full length)	5.02 $\pm$ 0.63	0.9385	1.01 $\pm$ 0.15	2.43 $\pm$ 0.36	1	2.43 $\pm$ 0.36
CJ1828 pNRNE1000	Wild-type (NTH)	10.35 $\pm$ 0.57	7.13E-05	0.49 $\pm$ 0.04	1.18 $\pm$ 0.09	1	1.18 $\pm$ 0.09
CJ1828 (pRNE1008)	8x (full length)	5.79 $\pm$ 0.38	1.86E-1	0.88 $\pm$ 0.08	2.11 $\pm$ 0.19	0.90 $\pm$ 0.13	2.34 $\pm$ 0.54
CJ1828 (pNRNE1008)	8x (NTH)	11.4 $\pm$ 0.94	6.18E-4	0.45 $\pm$ 0.05	1.07 $\pm$ 0.11	0.81 $\pm$ 0.06	1.32 $\pm$ 0.24

**A.** *E. coli* K-12 derivative strains CJ1827 (*rne*) and CJ1828 (*ams-1*) contain chromosomal *rne-lacZ* fusions ref. Plasmids pRNE1000, pNRNE1000, pRNE1008 and pNRNE1008 are derived from the pMPM-K1 vector, they encode wild-type RNase E (full length), wild-type RNase E (NTH), 8x RNase E (full length) and 8x RNase E (NTH) respectively.

**B.** The  $\beta$ -galactosidase activity of each strain is proportional to *rne-lacZ* expression. Results are the averages of 5 biological replicates  $\pm$  standard error from these measurements.

**C.** Relative repression to CJ1827 was calculated by dividing the  $\beta$ -galactosidase activity of CJ1827, wild-type RNase E by each value. Therefore, the ratio of (x) is set to 1.

**D.** Relative repression to CJ1828 (pMPM-K1) was calculated by dividing the  $\beta$ -galactosidase activity of CJ1828 (pMPM-K1), empty vector control by each value. Therefore, the ratio of (y) is set to 1.

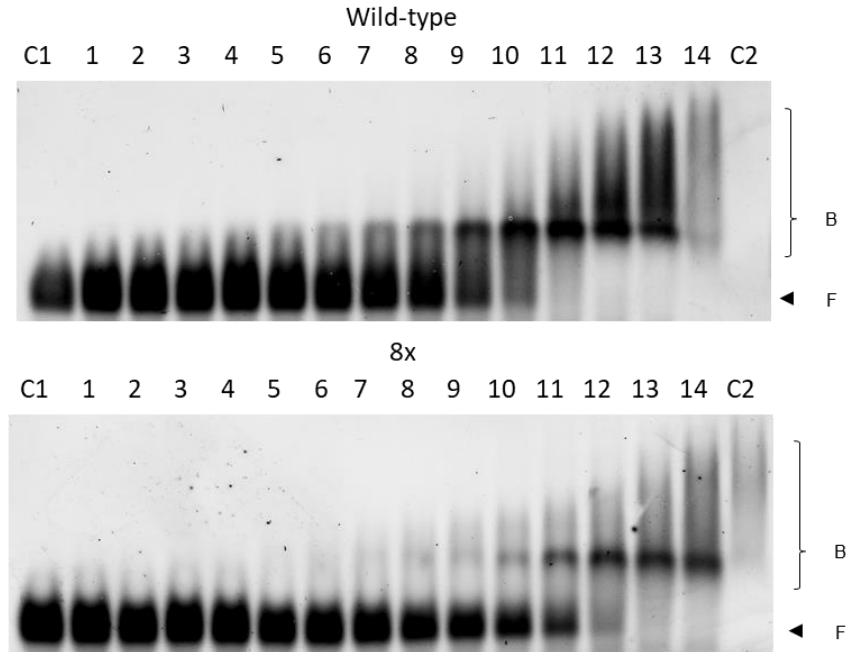
**E** Relative protein concentrations were determined by western blot using anti-C-myc antibodies. As CJ1827 was not c-Myc tagged, the relative concentration was set to 1 as it has been previously shown to be expressed to the same level as RNase E in CJ1828 (pRNE1000) (Jiang et al., 2000). CJ1828 (pMPM-K1) has no tagged RNase E so there is no concentration value reported. Differences in transfer efficiency make relative quantitation of NTH and full-length RNase E difficult, both wild-type RNase E variants were set to 1 and 8x NTH and full length were expressed as a relative concentration to these. The calculated relative concentrations are a result of three technical replicates  $\pm$  standard error from these measurements (Figure 4.6).

**F.** Relative specific activity was calculated as a ratio of **C/E** where **C** is the relative repression to CJ1828 (pMPM-K1) and **E** is the relative protein concentration. No value was calculated for CJ1828 (pMPM-K1) as there is no concentration value available.

Errors were calculated by calculating % error for each step and adding them before re-expressing them as an absolute error value.

The analysis was extended using EMSAs to compare the binding of NTH-RNase E with 8x substitutions and wild-type sequence to the 5' UTR (-361 to +134) of the *rne* transcript (Figure 4.7). NTH-RNase E with 8x substitutions bound to the 5' UTR with an apparent  $K_d$  of 256 nM, which was 2.7-fold higher than the apparent  $K_d$  of 96 nM for the wild-type equivalent. As the 8x substitution in the context of the NTH, as well as full-length RNase E, did not have a significant effect on autoregulation (see above), this might reflect a level of redundancy *in vivo* where for example additional or alternative contacts might be mediated by the generation of a 5'-monophosphorylated end. Combined the *in vivo* and *in vitro* results suggest that the RNA-binding groove is not critical for RNase E to interact with the 5' UTR of its own mRNA.



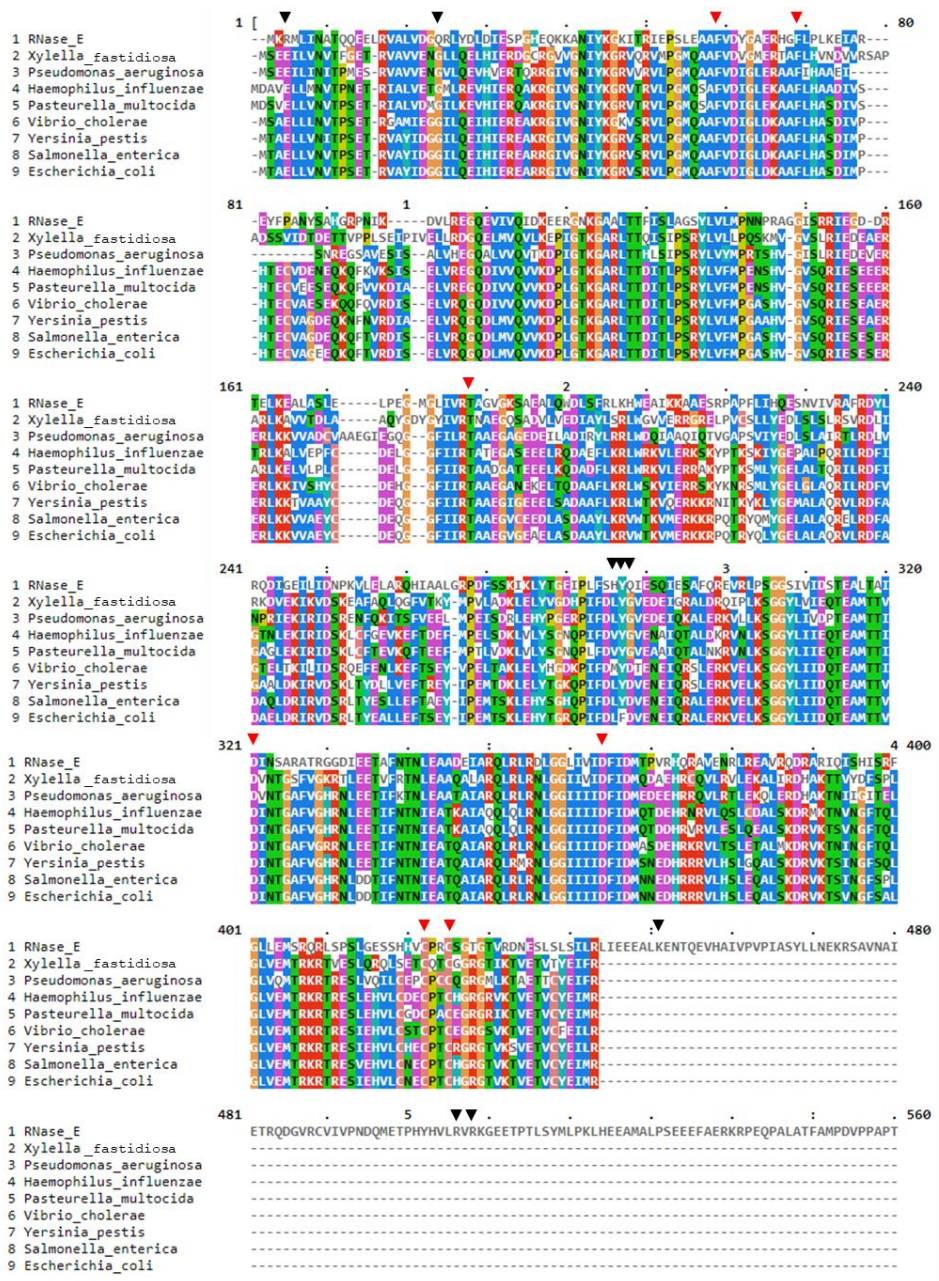


**Figure 4.7 Electrophoretic mobility shift assay of 5'UTR of the *rne* transcript.** Shown is an EMSA of regions -361 to +134 of the *rne* transcript. Identity of the variant of RNase E used is above each gel. RNA was incubated with increasing concentrations of RNase E and subsequently separated on a 1% agarose gel. C1 contains RNA only, concentrations of protein in lanes 1-14 are as follows; 0,31, 0.61, 1.22, 2.44, 4.88, 9.77, 19.53, 39.06, 78.13, 156.25, 312.5, 625, 1250 and 2500 nM. RNA is included in every lane and is 20 nM. Arrows indicate free RNA and bound species labelled F and B respectively. Gels were stained with SYBR gold and imaged using a Fujifilm FLA-5000 imager and scanned at 473 nm.

#### 4.2.3 Sequence analysis and purification of RNase G

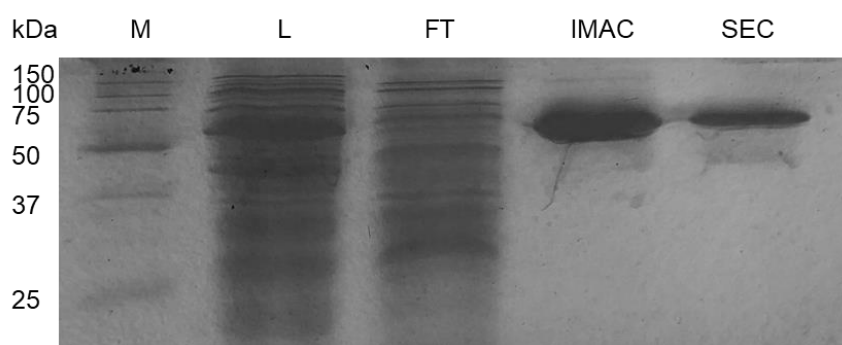
It was noticed during sequence analysis that RNase G does not possess many of the residues associated with the RNA-binding groove. This was confirmed by aligning sequences of RNase G from select organisms from the  $\gamma$ -proteobacteria with RNase E from *E. coli* (Figure 4.8). As can be seen, the arginine at position 3 in RNase E is conserved as an aspartate in RNase G, which reverses the charge at this position. The glutamine at position 22 in RNase E is conserved as a glycine in RNase G, which would eliminate a potential hydrogen bond between the R group of the glutamine and the RNA. The histidine at position 268 in RNase E is present as leucine, valine or methionine in RNase G, all of which would be unable to form hydrogen

bonds with RNA. The tyrosine as position 269 seems to be conserved. The glutamine as position 270 is present as either glycine or aspartate in RNase G. The alignment ends prior to residues K433, R488 and R490, the last three residues associated with the RNA-binding groove, which could further eliminate contacts made with RNA via charged interactions. In contrast, residues involved in the 5' monophosphate interaction (T170), catalysis (F57, F67, D303, D346) and the Zn-link (C404, C407) are conserved in RNase G. Yet it would seem that RNase G would be incompatible with binding RNA distal to the site of catalysis, at least with the RNA-binding groove.



**Figure 4.8** Sequence alignment of RNase G from select members of the  $\gamma$ -proteobacteria with RNase E from *E. coli*. 1) RNase E from *E. coli* has been aligned to RNase G from 2) *X. fastidiosa*, 3) *P. aeruginosa*, 4) *H. influenzae*, 5) *P. multocida*, 6) *V. cholerae*, 7) *Y. pestis*, 8) *S. enterica* and 9) *E. coli* using MUSCLE (Edgar, 2004). Amino acids are highlighted based on conservation and coloured according to physicochemical properties following the CLUSTAL colouring scheme (Blue denotes hydrophobic residues, Red denotes positive residues, magenta denotes negatively charged residues, green denotes polar residues, pink denotes cysteine residues, orange denotes glycine residues, yellow denotes proline residues, cyan denotes aromatic residues and uncoloured residues are not conserved by identity) using MVIEW. Key residues associated with catalysis and the zinc link are indicated by red arrowheads, RNA-binding groove residues are indicated by black arrowheads.

In order to confirm that interactions facilitated by the RNA-binding groove are unique to RNase E, it was first necessary to obtain purified, active RNase G for *in vitro* analysis. The plasmid pCafA was used for the overproduction of RNase G (Jourdan, 2008). BL21 (DE3) cells harbouring the pCafA plasmid were grown to mid-log phase, induced and subsequently harvested after three hours of induction. RNase G was purified by IMAC and size exclusion chromatography (see methods). During purification samples were taken after lysis, application to the column (flow-through), elution and post size-exclusion and analysed by SDS-PAGE to confirm successful purification of RNase G (Figure 4.9). The purity of protein was judged by densitometry scanning to be greater than 95% by IMAC alone.

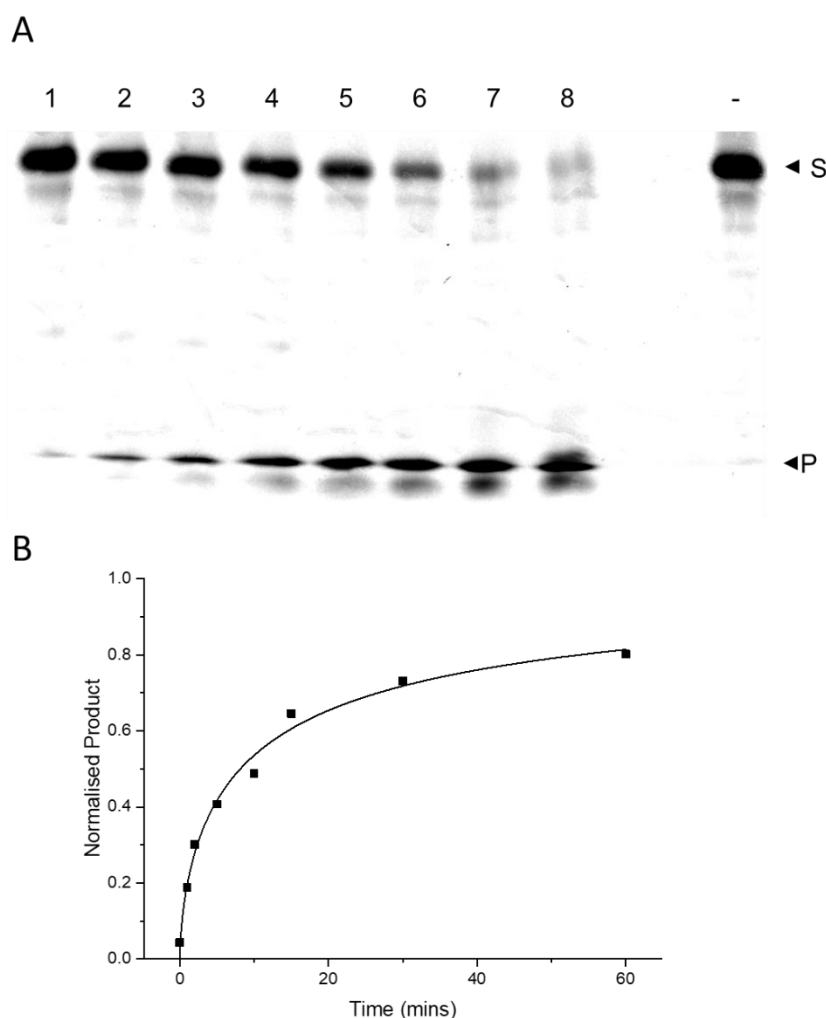


**Figure 4.9 Analysis of samples taken during purification of RNase G by SDS-PAGE.** Samples taken during RNase G purification were separated by electrophoresis on a 15% (w/v) polyacrylamide gel alongside a protein ladder and subsequently stained with InstantBlue™ protein stain. Lanes are labelled as follows M denotes the marker, L denotes lysate, FT denotes the flow-through, IMAC denotes the sample taken after purification by IMAC and SEC denotes the sample taken after size exclusion.

#### 4.2.4 Biochemical analysis of RNase G

Before investigating the RNA-binding capabilities of RNase G, the catalytic activity of the preparation was confirmed using conditions that from previous work would be expected to result in 50% of the LU13 substrate being cleaved within 5 to 10 min (Jourdan and McDowall, 2007). From the gel

corresponding to the RNase G preparation of this study (Figure 4.10, panel A), densitometry scan of the amount of the LU13 substrate remaining indicated that 50% was cleaved in 9.7 mins (Figure 4.10, panel B).

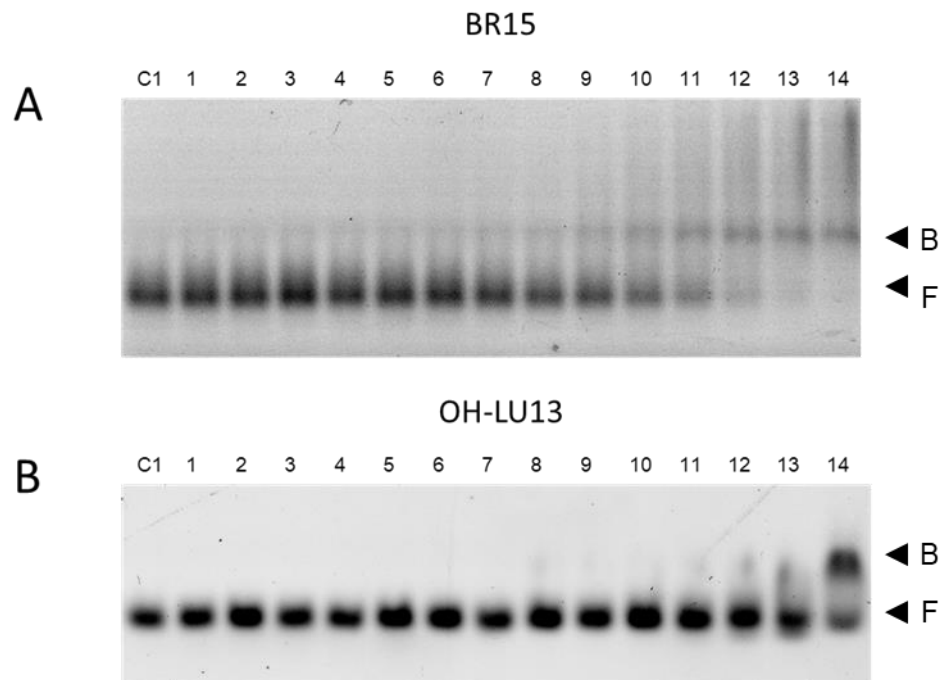


**Figure 4.10 Confirmation of RNase G activity by discontinuous cleavage of LU13.** The 5' monophosphorylated substrate was synthesised by Eurogentec. The final enzyme and substrate concentrations were 5 nM and 200 nM respectively. Panel A shows a polyacrylamide gel. Lanes 1-8 contain time points taken at 0, 1, 2, 5, 10, 15, 30 and 60 minutes. Lane labelled '-' contains a no-enzyme control. Arrows labelled S and P indicate substrate (LU13) and product, respectively. Samples taken from the reaction at indicated points were quenched by adding to 2 x RNA loading buffer, denatured at 95°C and was separated by electrophoresis on a 20% (w/v) polyacrylamide gel. The gel was imaged using a Fujifilm FLA-5000 imager and scanned at 473 nm. Panel B shows a graph of the normalised product against time. The normalised product was calculated as the intensity of the product relative to the sum of the intensities of the substrate and product, produced.

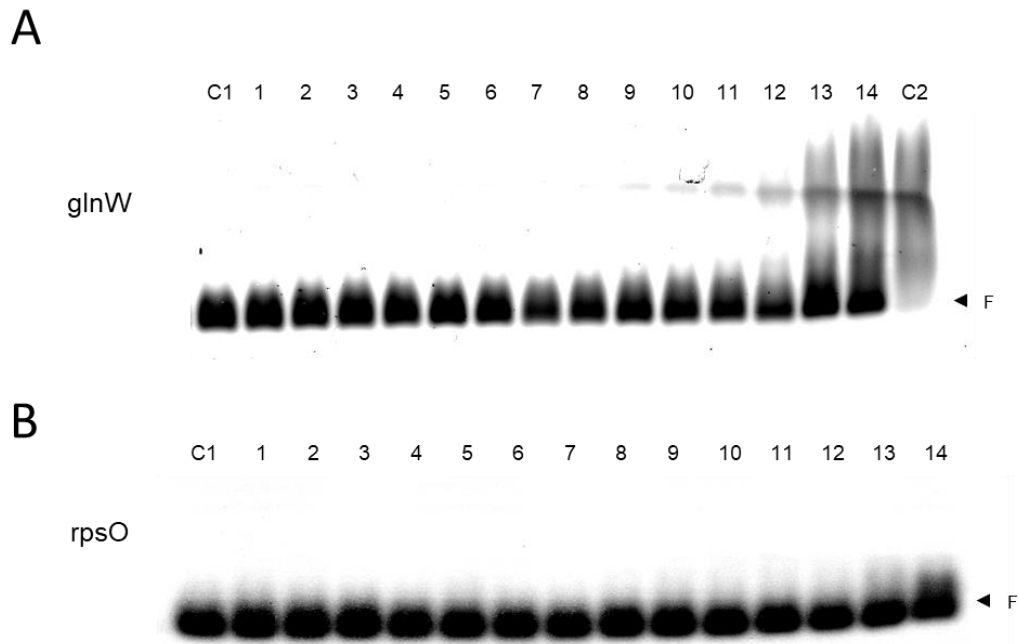
Next the binding of RNase G to substrates lacking regions of duplex RNA (Figure 4.11), which have been shown to interact with the RNA-binding groove of RNase E (Bandyra et al., 2018; Updegrave et al., 2019), was investigated using EMSAs as done previously for RNase E (see Chapter 3). As found for RNase E, RNase G binds with considerably higher affinity to BR15, which presents multiple single-stranded regions, than 5' hydroxylated LU13, which presents only one (and lacks a group that could interact with the 5' sensor). Binding to LU13 was only detected at the highest RNase G concentration that was used (2.5  $\mu$ M), whilst approximately 50% of BR15 was bound at 159 nM, which provides an estimate of the apparent  $K_d$  of this interaction. The considerably higher affinity of RNase G for BR15 suggest that as proposed for RNase E it is able to contact more than one single-stranded region in this substrate simultaneously. Compared to RNase E, the affinity of RNase G for BR15 is around 12-fold lower (apparent  $K_d$  value of 149 nM vs 12 nM for RNase E). Thus, although both enzymes appear to be able to interact co-operatively with single-stranded regions, the register of the corresponding reading heads, presumed composed at least in part from the S1 domains (see Introduction), may differ, with that of RNase E being better suited to the binding of BR15.

Whilst NTH-RNase E was shown earlier to bind to *glnW* and *rpsO* RNA substrates, both of which have regions of duplex RNA, with apparent  $K_d$  values of 3 nM and 517 nM, respectively (Figure 3.7 and Figure 3.6), no binding of RNase G to these substrates was detected at the highest concentration used (2.5  $\mu$ M, Figure 4.12). This is consistent with the notion,

stemming from an alignment of their sequences, that unlike RNase E, RNase G is unable to interact with regions of duplex RNA.



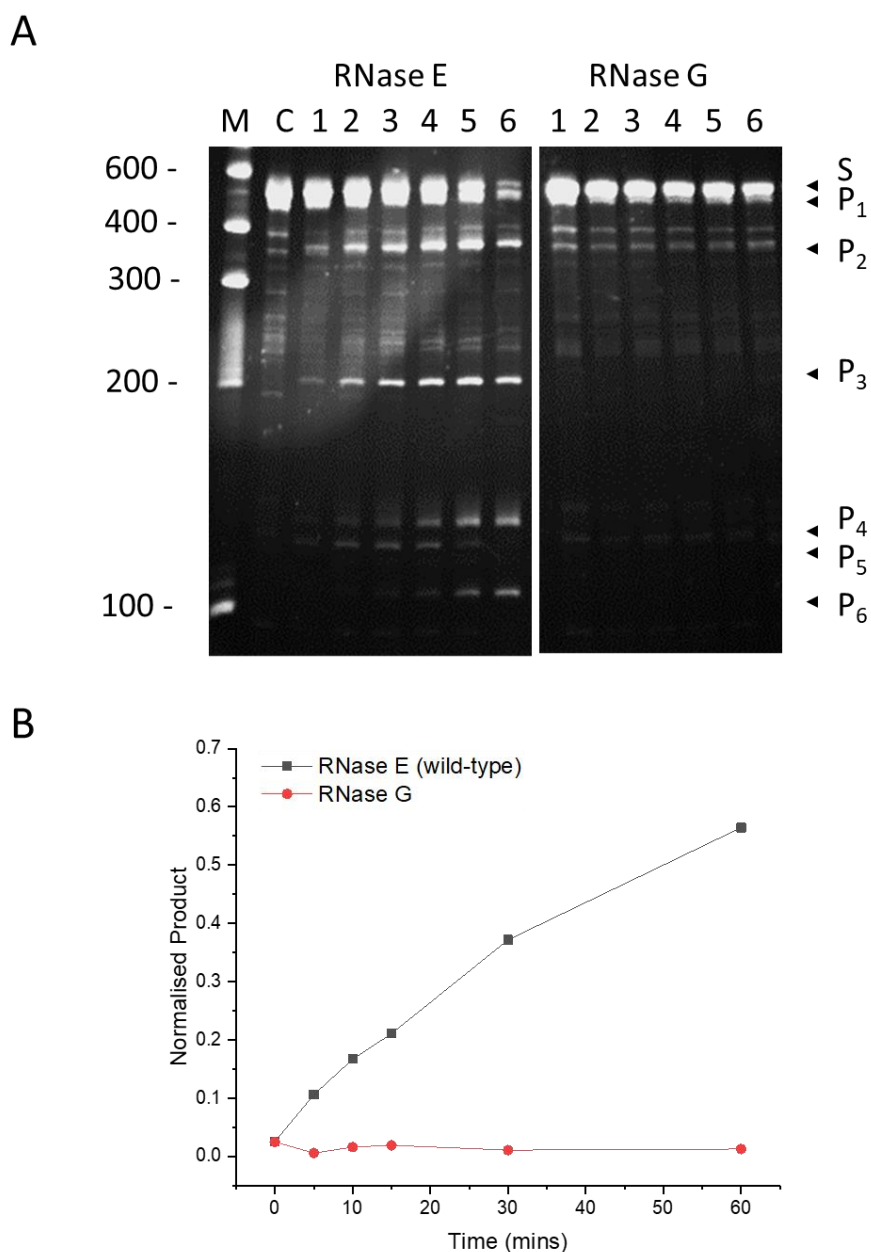
**Figure 4.11 Electrophoretic mobility shift assay of BR15 and OH-LU13 by RNase G.** Shown is an EMSA of BR15 and OH-LU13 RNA incubated with increasing concentrations of RNase G and subsequently separated on a 1% agarose gel. C1 contains RNA only, concentrations of protein in lanes 1-14 are as follows; 0,31, 0.61, 1.22, 2.44, 4.88, 9.77, 19.53, 39.06, 78.13, 156.25, 312.5, 625, 1250 and 2500 nM. RNA is included in every lane and is 7.5 nM and 20 nM for BR15 and OH-LU13, respectively. Arrows indicate free RNA and bound species labelled F and B respectively. Gels were imaged using a Fujifilm FLA-5000 imager and scanned at 473 nm.



**Figure 4.12 Electrophoretic mobility shift assay of *glnW* and *rpsO* by RNase G.** Panel A shows an EMSA of *glnW* and panel B shows an EMSA of the Cy5 labelled *rpsO* transcriptional terminator. RNA was incubated with increasing concentrations of RNase G and subsequently separated on a 1% agarose gel. C1 contains RNA only, concentrations of protein in lanes 1-14 are as follows; 0,31, 0.61, 1.22, 2.44, 4.88, 9.77, 19.53, 39.06, 78.13, 156.25, 312.5, 625, 1250 and 2500 nM. RNA is included in every lane and is 20 nM. Arrows indicate free RNA and labelled F. Panel A included an additional C2 control of protein only as it was stained with SYBR™ Gold nucleic acid stain. Gels were imaged using a Fujifilm FLA-5000 imager and scanned at 473 nm (panel A) and 633 nm (panel B).

To see if the inability of RNase G to bind to structured regions of RNA precluded cleavage of direct entry substrates discontinuous assays were setup with a direct entry substrate that have been studied previously, the full-length polycistronic *argX-leuT-hisR-proM* (Figure 4.13). (Data was collected at the same time as Figure 3.10 in chapter 3, the wild-type comparison features in both figures). Consistent with the results from the binding assays, RNase G was not able to cleave the substrate.



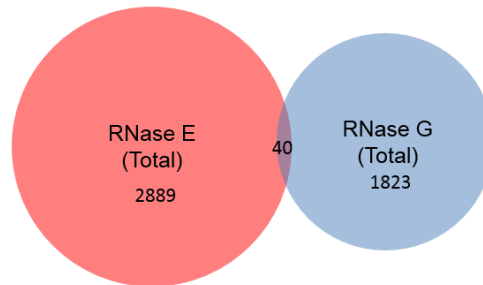


**Figure 4.13 Discontinuous cleavage of *argX-leuT-hisR-prom* tRNA precursor by RNase E and RNase G.** The 5' tri-phosphorylated substrate was synthesised by in vitro transcription. The final enzyme and substrate concentrations were 5 nM and 0.2  $\mu$ M respectively. The identity of the enzyme is shown above each gel. Lanes 1-6 contain time points taken at 0, 5, 10, 15, 30 and 60 minutes. Lane M contains an RNA ladder with sizes indicated on the left and lane C contains a no enzyme control. Samples taken from the reaction at indicated points were quenched by adding to 2x RNA loading buffer, denatured at 95°C and separated by electrophoresis on a 10% (w/v) polyacrylamide gel. The gel was stained by ethidium bromide and imaged using a UV transilluminator. Panel A shows the gel obtained. Panel B shows the increase in amount of product P<sub>3</sub> as a function of time for the wild-type and 8x mutant. A normalised product was calculated by densitometry using the intensity of P<sub>3</sub> relative to the sum of the P<sub>3</sub> and uncleaved substrate. Generation of the 6 products of cleavage by direct entry have been described previously (Kime et al., 2014).

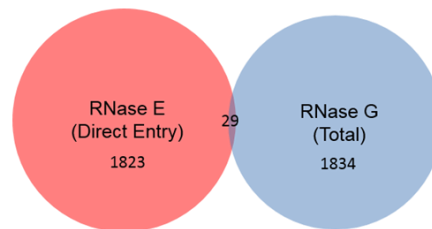
Using previously published *in vivo* RNA-seq data of RNase G, (Clarke et al., 2014), the congruence of RNase G cleavages and RNase E direct entry cleavages was investigated on a transcriptome-wide scale. Total RNase E *in vivo* and RNase E direct entry cleavages were assigned in previous work (Clarke et al., 2014; Clarke, 2015). *In vivo* RNase G cleavages were obtained by comparing RNA-seq data from a strain with inactivation of *rng* (*E. coli* GM11) with data from the parental wildtype strain and identifying sites where cleavages were depleted (Clarke, 2015). Comparison of cleavages made by RNase E direct entry, as well as total RNase E cleavages *in vivo*, with RNase G *in vivo* was then attempted. As expected there are only 29 RNase E direct entry sites that are also assigned as RNase G cleavages (Figure 4.14). However, the dataset is limited in that some cleavages may be efficiently made by RNase E in the wild-type strain and thus RNase G could make these cleavages, but they are not detectable. It may be possible that many sites that can be cleaved by both RNase E direct entry and RNase G could be missed from the analysis if both enzymes can substitute for each other fully. In this case, a Weblogo was generated to see if the sites of cleavage identified from either dataset had any sequence similarity. It appears that RNase E has some sequence specificity for AU-rich regions spanning from the cleavage site up to 4 nt downstream (Figure 4.15), in agreement with previous work (McDowall et al., 1994). Given that the model for direct entry requires multiple single-stranded regions of RNA to engage the principle dimer of RNase E simultaneously, sequence specificity for AU-rich regions, which tend to be associated with unpaired regions of RNA, around the cleavage site is not surprising. In contrast, RNase G has

no sequence specificity, further supporting the findings that RNase G does not cleave RNA via direct entry.

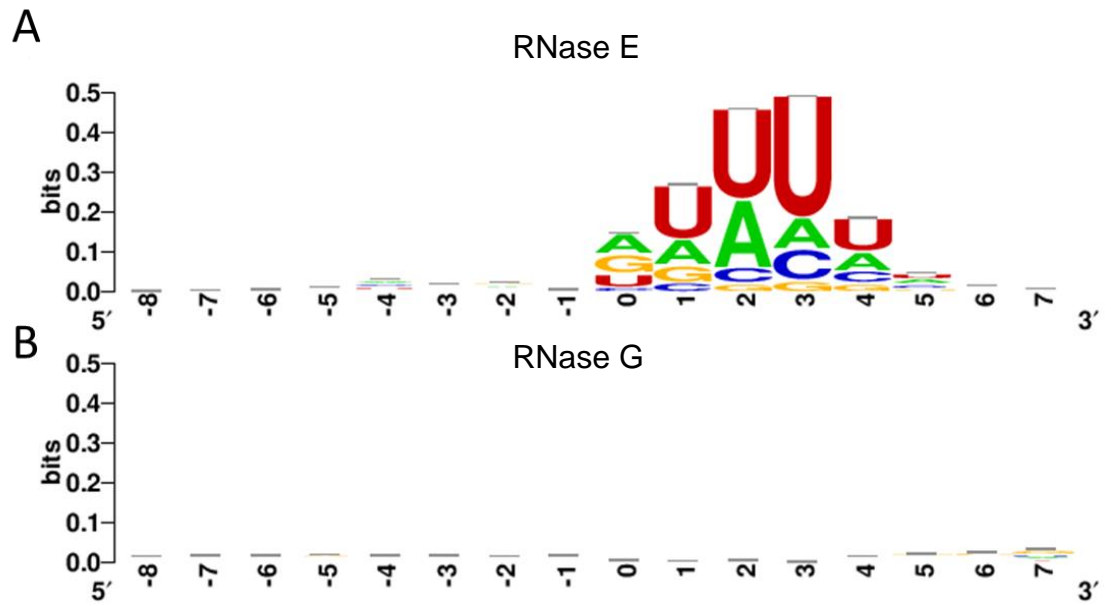
A



B



**Figure 4.14 Congruence of RNase E and RNase G cleavage.** Panel A shows a Venn diagram of the total RNase E cleavages *in vivo* compared to total RNase G cleavages *in vivo*. Panel B shows a Venn diagram of the RNase E cleavages assigned as direct entry sites compared to total RNase G cleavages. Diagram was created using the BioVenn web application (Hulsen et al., 2008).



**Figure 4.15 Conservation of RNase E and G cleavage site motif.** Shown are Weblogos of the regions around the cleavage sites of RNase E (panel A) and RNase G (panel B) calculated from in vivo data published by (Clarke et al., 2014). The height at each position indicates the level of conservation. Nucleotide positions are labelled relative to the cleavage site, where 0 represents the nucleotide just upstream of the cleavage site in the phosphodiester backbone. Weblogo was produced using the Berkley Weblogo application (Crooks et al., 2004).

### 4.3 Discussion

This chapter has found that the RNA-binding groove of *E. coli* RNase E is not required for autoregulation (Table 4.2) but is required for a function(s) essential for cell viability (Figure 4.4). The work in this chapter has also found that RNase G, whilst appearing able to make co-operative interactions with RNA by engaging multiple single-stranded regions much like RNase E (Figure 4.11), is unable to bind and cleave RNAs that evidence suggests interact with RNase E at least in part via contact between duplex regions and the RNA-binding groove (Figure 4.12 and Figure 4.13). This is consistent with the absence in RNase G of residues conserved in the RNA-binding groove of RNase E (Figure 4.8). Furthermore, reanalysis of published sequencing data (Clarke et al., 2014; Clarke, 2015) has revealed that RNase G seems to have little congruence with RNase E cleavages (Figure 4.14) in terms of the sequences of sites within which cleavage occurs (Figure 4.15).

The inability of the 8x mutant to complement an RNase E-deficient strain may reflect a critical role for the RNA-binding groove in the processing of stable RNA, which includes the maturation of 50 of the 86 tRNA species (Li and Deutscher, 2002; Ow and Kushner, 2002). This notion is supported by *in vitro* assays which showed the 8x mutant is impeded in the binding of *glnW*, and the cleavage of *argX-hisR-leuT-proM* (Figure 3.7 and Figure 3.10). The role of RNase E in the processing of tRNA has been studied *in vivo* through northern blot comparison of total RNA samples of *rne<sup>ts</sup>* strains of *E. coli* and their congenic wild-types resolved by PAGE (Li and Deutscher, 2002; Ow and Kushner, 2002). The inclusion of comparisons by primer

extension assays allowed specific sites of cleavage to be studied (Ow and Kushner, 2002). It is suggested that a similar approach should be used to compare a strain defective in the RNA-binding groove of RNase E with a congenic wild-type partner. As *E. coli* strains with 8x substitutions are inviable upon withdrawal of induction of the wild-type copy (Figure 4.4) consideration needs to be given to the strains that would be compared to analyse the function of the RNA-binding groove. The same strains used here to assess the effects of the 8x substitutions on RNase E autoregulation and cell viability in *E. coli* could be used to assay tRNA processing. The comparison would be based on samples taken following a temperature upshift and rifampicin addition that would, inactivate the temperature-sensitive form of RNase E and halt transcription (respectively). Whilst this approach is sensitive to indirect effects caused by the loss of viability, the use of *rne<sup>ts</sup>* mutants has shed much light on the overall function of RNase E (Ghora and Apirion, 1978; Wachi et al., 1997; Ow and Kushner, 2002; Clarke et al., 2014; Chao et al., 2017).

It is possible that a reduced number of substitutions within the RNA-binding groove may still perturb function but not sufficiently to prevent the growth of *E. coli*. Thus, it is suggested that RNase E mutants with fewer substitution are assayed for cell viability with a view to identifying one or perhaps more that are sufficient to support growth, but growth that appears compromised. Conclusions on the role of the 5' sensor of RNase E have been drawn from the study of a mutant that had impeded growth (Garrey and Mackie, 2011). The same set of mutants could also be used to assess whether the RNA-binding groove is required for the normal processing of 9S rRNA to produce

pre-5S rRNA, the original step for which RNase E was proposed to be essential (Ghora and Apirion, 1978), and indeed any other specific function. Mutation of the RNA-binding groove has been shown by others to reduce markedly the efficiency of *in vitro* cleavage of both tri- and monophosphorylated 9S, without loss of specificity (Bandyra et al., 2018). The processing of 9S rRNA, like tRNA, can be followed *in vivo* using a combination of northern blotting and primer extension (Ow and Kushner, 2002). An assay using next-generation sequencing is discussed in the final chapter. Essentially, there is a need to confirm that the findings of biochemical assays in relation to the RNA-binding groove are relevant *in vivo*. However, it should be remembered that any mRNA enrichment may impose limits on the analysis of the RNA processing central to ribosome biogenesis. The processing of 16S like 9S RNA involves RNase E (Li et al., 1999b). The corresponding cleavages within their rRNA precursors are likely mediated by a 5'-monophosphorylated end-dependent pathway, considering the initiating event is cleavage by RNase III (see main introduction) (Young and Steitz, 1978). It may be useful for repeats of *in vitro* 9S processing cleavage assays to be performed to provide quantitative information in terms of the fold change in the rate of cleavage and perform *in vivo* analysis (discussed below) to understand effects on ribosome biogenesis.

Degradation of mRNA has been previously shown to be one of the essential functions of RNase E (Hammarlöf et al., 2015) through isolation of genetic suppressor mutants. It has also been shown that deletion of four to five of the seven *rrn* operons alleviates the synthetic lethal phenotype of CTH-

deletion in combination with *rppH* or the R169Q RNase E mutation, implying that reduced abundance of stable RNA allows diversion of impaired RNase E to mRNA degradation (Himabindu and Anupama, 2017). Other suppressor mutations have been isolated such as deletion of *nusG* and *rho* which leads to an increase in R-loop formation due to impaired rho-dependent transcription termination (Anupama et al., 2011), presumably this alleviates RNase E necessity by allowing RNase H to initiate cleavages that allow for entry by exonucleases. Given these examples, it is suggested that the isolation of suppressor mutants of the 8x substitutions may allow further mechanistic understanding of the contribution of the RNA-binding groove to the essential function of RNase E.

RNA-seq approaches have revealed that the majority of cleavages can be made *in vitro* by T170V NTH-RNase E, which is not able to engage with substrates via the 5' monophosphorylated end-dependent pathway (Clarke et al., 2014). Repeating the above analysis with an 8x mutant would allow for further investigation into how widespread consequences were for disruption of the RNA-binding groove. If absolutely critical for direct entry, the RNA-binding groove would have far-reaching consequences on post-transcriptional regulation and nucleotide recycling.

Sequence analysis (Figure 4.8) suggests that RNase G does not possess the conserved residues associated with the RNA-binding groove, which is corroborated by its inability to bind *glnW* tRNA (Figure 4.12) and cleave the *argX-hisR-leuT-proM* polycistronic tRNA precursor *in vitro* (Figure 4.13). This may also explain why RNase G is not able to complement RNase E following inactivation of the latter in *E. coli*. Introduction of substitutions into



RNase G that correspond to those in the RNA-binding groove of RNase E using site-directed mutagenesis may alleviate its inability to complement RNase E deficiency as well as substitute for RNase E during tRNA processing. When placed under the RNase E promoter, RNase G possessing either V219F or E248K mutations in the second RNase H domain is able to complement RNase E deficiency (Chung et al., 2010) these residues are proximal to residues identified within RNase E to be associated with the RNA-binding groove, although mechanistically it is not clear how the individual mutations would allow complementation.

Extending the *in vivo* analysis of the RNA-binding groove to its contribution during autoregulation revealed the 8x substitutions had no observable effect (Table 4.2). Whilst the simplest conclusion is that the RNA-binding groove does not contribute to autoregulation, it should be remembered that many processes in bacteria have a level of redundancy (Mahadevan and Lovley, 2008). Thus, the finding that the apparent  $K_d$  value for interaction with the *mne* 5' UTR was 2.7-fold higher for the 8x mutant compared with NTH-RNase E (Figure 4.7) may point to function *in vivo*. One possibility is that through the production of a 5' monophosphate group on the nascent 5' end of *mne* mRNA, RNase E is able to bind via a second mode that is not dependent on interaction involving the RNA-binding groove. This could be investigated by repeating the *in vivo* reporter assay in a strain deficient in RppH or utilising the T170V RNase E genetic background and the *in vitro* binding assay with 5' monophosphorylated RNA. These assays would disrupt and promote any mode of binding that was dependent on a 5'-monophosphorylated end, respectively. Consistent with the 5' monophosphorylated end of the *mne* transcript contributing to the interaction with RNase E, it has been shown

that the R169A mutant results in a 4.5-fold increase in the level of the *rne* transcript as measured by the same *ez1* reporter assays described here (Schuck et al., 2009).

Although the 8x mutant had a higher value of apparent  $K_d$ , it still bound the 5' triphosphorylated *rne* 5' UTR. The binding activity remaining following disruption of the RNA-binding groove may have been mediated interaction with regions of single-stranded character within the *rne* 5' UTR. This includes the region referred to as hp3 (see Chapter 4 introduction), which has been shown to play a major role in autoregulation (Diwa et al., 2000) and appears to interact strongly with NTH-RNase E (Clarke 2015).

Crosslinking analysis has suggested that the region referred to as hp2 of the 5' UTR of *rne*, which has been shown to contribute significantly to autoregulation, interacts with N323 within the DNase I domain of RNase E (Schuck et al., 2009). This was suggested by differential crosslinking to an N323A RNase E mutant. Given the distant proximity of N323 to the RNA-binding groove, this may suggest a more distributed RNA-binding surface. Thus, in further study of the role of the RNA-binding groove in autoregulation and binding of the 5' UTR of *rne* mRNA, the substitutions should be extended to residue N323. During this work, an *in vitro* transcription/translation system was designed (Shimizu et al., 2001) for further dissection of components of autoregulation of the 5' UTR of the *rne* transcript. However, despite repeated attempts, no translation of any of the constructs was achieved

The finding that our NTH-RNase E construct, which extends from residues 1 to 529, is insufficient for cell viability confirms the conclusion of others that

functions within the C-terminal half are required for cell viability (Jiang et al., 2000). As indicated above, the C-terminal deletion of the previous study, which only left residues 1 to 498, may have affected the ability of the catalytic domain to form a stable tetramer and cleave RNA. It would be interesting to determine whether the NTH-RNase E used here (residues 1 to 529) is sufficient for cell viability in the presence of autoregulation. The extent, if any, to which increased expression as a result of decreased autoregulation can facilitate cell viability has not been quantified. There is a report that residues 1 to 395 are sufficient to complement the *rne<sup>ts</sup>* mutant (i.e. support growth), but this was when produced from an expression plasmid; furthermore a number of longer constructs from the same study failed to complement RNase E deficiency (Caruthers et al., 2006). To our knowledge, the longest “NTH” construct that supports cell viability in the presence of autoregulation extends from residues 1 to 584 (Kido et al., 1996). When production is fixed and not subject to increases resulting from autoregulation, it would also be interesting to determine the extent to which parts of the C-terminal half of RNase E are essential for cell viability and contribute to autoregulation as measured using the *ez1* reported construct. Regions of the CTH of RNase E required for assembly of the degradosome and membrane association have been mapped (Mackie, 2013; Bandyra et al., 2013). As found here for the RNA-binding groove (Table 4.2), functions of RNase E beyond the N-terminal catalytic domain that are required for autoregulation and cell viability need not be the same.

## **Chapter 5**

### Initial structural studies of RNase E by Electron Microscopy

## 5.1 Introduction

### 5.1.1 Insight into NTH-RNase E function through structural studies

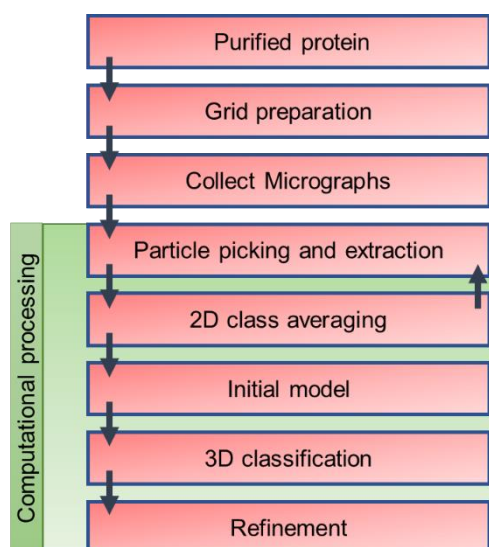
A comparison of the 'open' (Callaghan, Marcaida, et al., 2005) and 'closed' (Koslover et al., 2008) structures of RNase E solved by X-ray crystallography has revealed that the enzyme is capable of performing large conformational changes during interaction with RNA (Figure 1.4). Additionally, the data used to identify the RNA-binding groove (Bandyra et al., 2018) also reveals an alternative 'closed' conformation. Full characterisation of differences between the two 'closed' conformations has yet to be achieved. Previously, the study of RNase E by X-ray crystallography has allowed elucidation of key residues associated with function such as residues that interact with bases adjacent to the scissile bond, residues constituting the monophosphate binding pocket and residues that coordinate the magnesium ion required for catalysis (Callaghan, Marcaida, et al., 2005).

The RNA-binding groove identified in crystals of the complex of sRNA RprA and NTH-RNase E (Bandyra et al., 2018) gave an indication of RNA interaction beyond the active site and the 5' sensor, which binds 5'-monophosphorylated ends. However, as only a section of the RprA RNA could be resolved, it likely only provides a limited view of the interaction of sRNA with RNase E, which could possibly extend well beyond the identified groove. This is likely due to the RNA being quite flexible. To this end, further study of complex substrates with NTH-RNase E could inform our understanding of the contacts that facilitate the binding of this essential ribonuclease to its substrates and the extent to which substrates can span

the full tetramer. The latter notion presumes that the evolution of RNase E to form tetramers rather than dimers, like RNase G (Briant et al., 2003), is likely to be of functional significance.

### **5.1.2 Electron Microscopy as a tool for structural biology**

Structural elucidation of proteins by single-particle electron microscopy relies on the collection of many micrographs, and subsequent processing and averaging of thousands of particles. Particles are extracted and are subsequently computationally grouped into 2D classes, which can then be used to generate an initial model. That model can then be used to reclassify extracted particles to generate 3D reconstructions, which can then be subjected to further refinement (Figure 5.1).



**Figure 5.1 Single-particle EM workflow.** Steps necessary for structure determination by electron microscopy. Protein is purified and applied to grids at  $\sim 0.02$  mg/ml for negative-stain EM and 0.2-2 mg/ml for cryo-electron microscopy (cryo-EM) (Thompson et al., 2016; Takizawa et al., 2017). Samples are fixed either with heavy metal stains (negative-stain) or by vitrification (cryo-EM). Micrographs are then collected by electron microscopy either manually or by automated data collection. Micrographs are subsequently computationally processed with software such as RELION (Scheres, 2012).

Apparent homogeneity, as deduced by SDS-PAGE and size-exclusion chromatography, does not exclude samples appearing heterogenous in electron-microscopy due to alternative conformations that have equivalent molecular weight and similar hydrodynamic radii. Negative-stain EM can be used as a further characterisation step prior to cryo-EM to gauge whether a sample is likely to be amenable to study. Additionally, negative-stain EM can provide low-resolution information in which overall architectures of a complex can be determined/inferred, such as oligomeric state and whether a substrate-analyte complex is formed (Ohi et al., 2004). As samples are stained with heavy metals, they have a theoretical maximum resolution of 20 Å (Scarff et al., 2018).

Cryo-EM involves plunge freezing samples to form vitreous ice, in which freezing is performed at  $\sim 10^6 \Delta^\circ\text{Cs}^{-1}$  (Dubochet et al., 1988). Such rapid freezing does not allow water molecules to rearrange to form hexagonal lattices, which is found in crystalline ice, resulting in a phase of ice that has much higher clarity. As samples do not need to be stained, the resolution limit is almost 10-fold lower (Lyumkis, 2019). Cryo-EM structures of apoferritin are among the top-ten highest resolved structures, owing to its structural homogeneity and its octahedral symmetry, and usually have a resolution of around 2 Å (Lawson et al., 2011).

Thus far the majority of structural data informing the molecular biology of RNase E has come from X-ray crystallography. As a technique, it is limited in that it requires the generation of crystals. Sample preparation to meet the concentration requirements of crystallography of some ribonucleoparticles (RNPs) can be an additional challenge (Dessau and Modis, 2010), as well as the fact that the introduction of RNA substrates can influence crystallisation conditions. In addition, as stated above, more complex and flexible regions of both the protein and RNA can be difficult to resolve, and in some cases, may not even represent the natural conformation, and just represent an artefact caused by crystal packing. Cryo-EM allows the structural study of macromolecular complexes in a semi-native environment and has allowed for the solving of structures of proteins to near-atomic resolution (Cheng et al., 2015). Cryo-EM also allows species to be grouped into classes, to better understand structural changes that may occur during complex formation. A better understanding of how RNase E interacts with more complex substrates may help augment existing biochemical studies

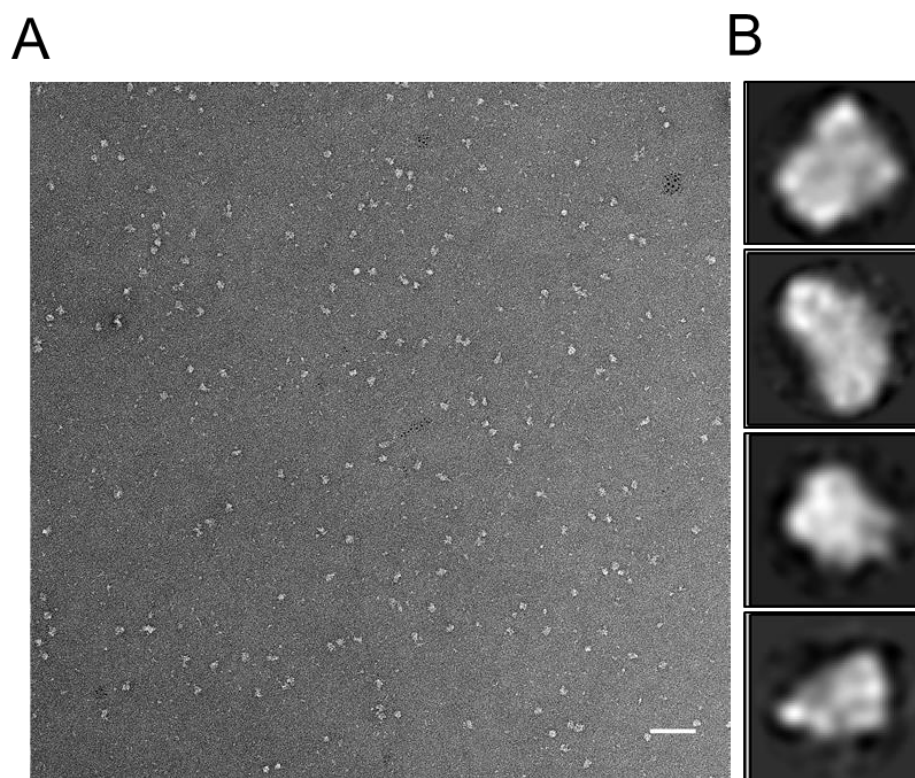


produced as part of this thesis and by others, thus this chapter aims to initiate studies of RNase E by electron microscopy.

## 5.2 Results

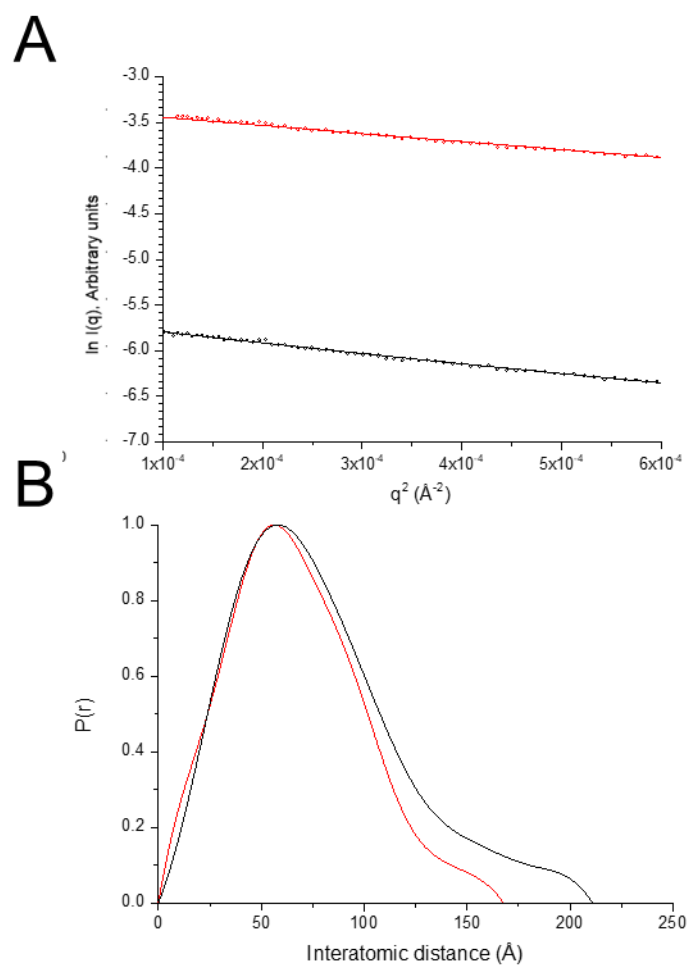
### 5.2.1 Negative-stain Electron Microscopy of BR15 in complex with NTH-RNase E

To initiate the study of RNase E by cryo-EM, it was first necessary to see how samples performed in negative-stain EM. Purified NTH-RNase E was mixed with BR15 at a molar ratio of 1:1 and applied to a standard carbon-coated copper grid at a concentration of 25  $\mu\text{g/ml}$ . Subsequently, micrographs were collected using a transmission electron microscope (Figure 5.2, panel A). Micrographs were processed using the REgularised LIkelihood OptimisatiON (RELION) software (Scheres, 2012), whereby particles were extracted and subjected to 2D classification into 10 classes. Of these, four of the 2D class averages (2913 particles out of 9810 total particles) resembled RNase E (Figure 5.2, panel B), seeming to be roughly of the appropriate size range, discarded classes contained particles that were too small to be RNase E (data not shown). The shown class averages resemble the 'closed' structure of RNase E (PDB:2C0B). However, the maximum dimension of these class averages is approximately 210  $\text{\AA}$ , which is larger than that of the closed structure at 140  $\text{\AA}$  (as measured in PyMOL of PDB:2C0B). The possibility of the observed particle being two tetramers of RNase E interacting with a single molecule of BR15 RNA should not be excluded



**Figure 5.2 Negative-stain electron microscopy of BR15 in complex with NTH-RNase E.** BR15 and NTH-RNase E was mixed in 1:1 molar ratio at 25  $\mu\text{g/ml}$  and applied to a carbon-coated copper grid. Panel A contains a typical micrograph taken on a Technai T12 electron microscope, scale bar indicates 100 nm (1000  $\text{\AA}$ ). Panel B shows 2D class averages of particles generated in RELION.

It is important to note that large areas of the grid contained protein that had aggregated either in solution or during grid preparation (data not shown). Small-angle X-ray scattering (SAXS), as part of a rapid-access service provided by Diamond Light source, was used to check the size distribution of the particles in both samples of apoprotein and NTH-RNase E in complex with BR15 (Figure 5.3). A straight line in the Guinier plot (Figure 5.3, panel A) indicated that both samples were monodisperse, and therefore not aggregating in solution. The plot also provided a radius of gyration ( $R_g$ ), which represents the square root of the squared mean of distances to the centre of density in the protein, providing information on the size of the protein.



**Figure 5.3 Small-angle X-ray Scattering of NTH-RNase E apoprotein and BR15 RNP.** Panel A contains a Guinier plot together with the fit of the data of NTH-RNase E apoprotein (red) and RNP (black) the y-axis represents  $\ln(\text{intensity})$  and has arbitrary units the x-axis represents the square of the scattering angle. Panel B contains a distance distribution function, which was used to determine the  $D_{\max}$ . The X-axis represents paired distances between two points in a particle, the Y-axis represents the proportion in which those distances occur on the particle.  $D_{\max}$  is calculated by the x-intercept. Data was processed in ATSAS (Franke et al., 2017).

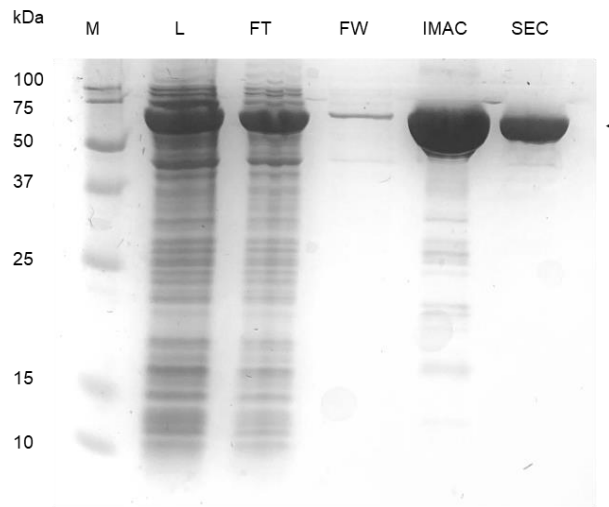
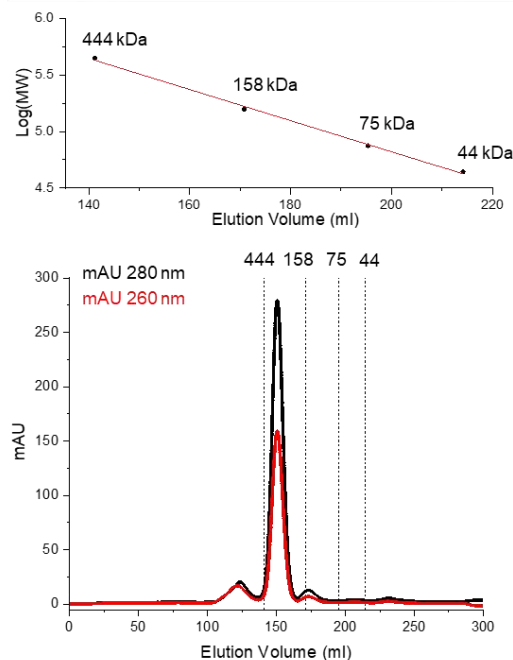
The  $R_g$  values for the apoprotein and RNP of NTH-RNase E with BR15 were 54  $\text{\AA}$  and 61  $\text{\AA}$ , respectively. The value for the apoprotein is comparable, although slightly larger than previous estimates of the apoprotein of 51  $\text{\AA}$  and 50  $\text{\AA}$  reported by others (Callaghan et al., 2003; Mardle et al., 2019). The distance distribution function, which enabled measurement of

interatomic distances within the sample, provided a maximum dimension ( $D_{\max}$ ) of 168 Å for the apoprotein, which was comparable with previous results that show a  $D_{\max}$  of 160 Å and 161 Å, (respectively) (Callaghan et al., 2003; Mardle et al., 2019). The value of  $D_{\max}$  for the complex of NTH-RNase E and BR15 was 208 Å. The values of  $D_{\max}$  and  $R_g$  are higher than the equivalent values for the apoprotein, consistent with the majority of NTH-RNase E being present as a complex with BR15, a complex in which the RNA protrudes from NTH-RNase E and hence results in an increase in the  $D_{\max}$ . In fact, the  $D_{\max}$  value of 208 Å from the SAXS data correlates with  $D_{\max}$  calculated using the measured size of the particles seen within the class averages from electron microscopy (Figure 5.2, panel B). Furthermore, the values obtained are consistent with RNase E not being dissociated into dimers or monomers.

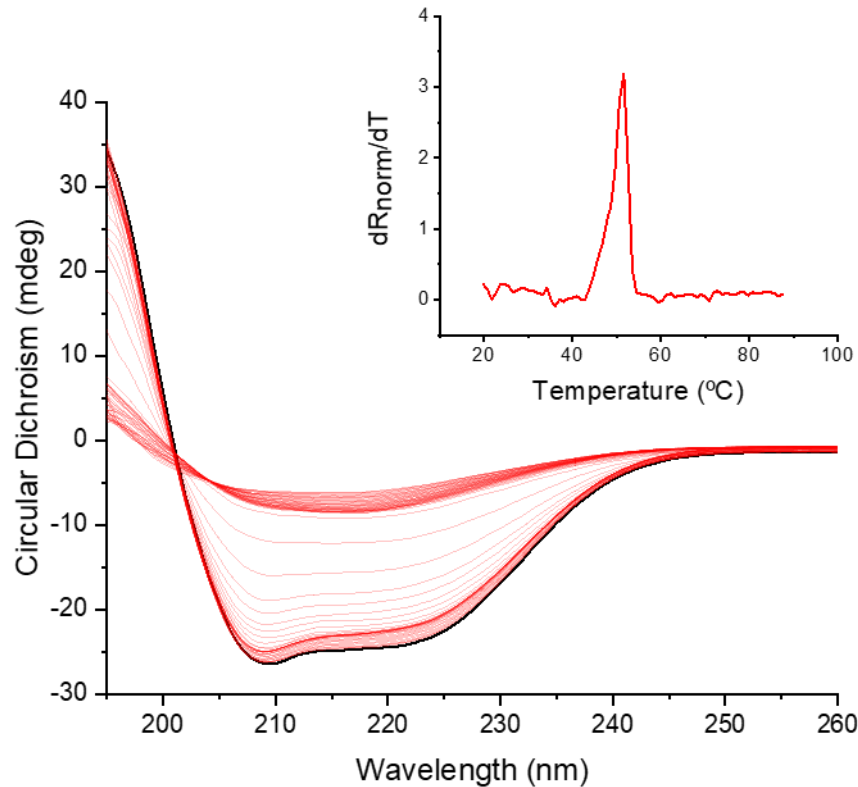
### **5.2.2 Negative-stain Electron Microscopy of *glnW-metU* bicistronic tRNA precursor fragment in complex with D346N NTH-RNase E**

Next, the preliminary analysis was extended to the bicistronic tRNA precursor fragment, *glnW-metU*, which is a natural substrate for RNase E and has been shown to make additional contacts with RNase E (Clarke, 2015). The substrate incorporates the two unmodified tRNA subunits, *glnW* and *metU* separated by a trailer sequence and a further 3' trailer sequence. To prevent the cleavage of the substrate, NTH-RNase E with the D346N substitution, which inactivates catalysis was used (Callaghan, Marcaida, et al., 2005). Fresh batches of the D346N mutant were purified, and grids were prepared immediately after purification, as it was suggested from empirical observation that this tended to promote sample homogeneity and increase

the reproducibility of electron microscopy (Emma Hesketh, pers. comms.). The SDS-PAGE analysis of a typical purification of D346N is shown (Figure 5.4, Panel A). It should be noted that size exclusion chromatography was employed as a polishing step (Figure 5.4, panel B). A single major peak eluted between the time points for markers of 158 and 444 kDa. The peak eluted at the time point expected for protein of 313 kDa, derived from a calibration curve produced using the elution points of the markers. This was consistent with results obtained previously for NTH-RNase E with wild-type sequence and also consistent with the sample being a tetramer (Callaghan et al., 2003). Circular dichroism was performed (Figure 5.5) to confirm that the D346N mutant was folded correctly, strong negative inflection at 208 nm and 222 nm is indicative of  $\alpha$ -helical character. Positive values at 195 nm and negative values at 218 nm are contributed by  $\beta$ -sheets within the protein. A temperature ramp was also performed to generate an unfolded state to compare with the native, which results in a reduction of the magnitude of inflections at the above wavelengths as the secondary structure of the protein melts. A plot was generated of the first differential of the normalised response at 222 nm as a function of temperature (Figure 5.5, inset), which contains a single peak at 50.5°C, suggesting only one transition state occurs during the unfolding of RNase E. This is in agreement with previous work that shows that RNase E activity is inactivated irreversibly by heating samples to 50°C (Misra and Apirion, 1979)

**A****B**

**Figure 5.4 Purification of D346N NTH-RNase E for structural studies.** Panel A shows analysis of samples by SDS-PAGE. Samples were analysed by electrophoresis using a 15% (v/v) polyacrylamide gel and subsequently stained with InstantBlue™ protein stain. Lanes are labelled as follows: M denotes protein marker, L denotes Lysate, FT denotes the flow-through, FW denotes the first wash, IMAC denotes elution after IMAC purification, SEC denotes pooled sample after size-exclusion chromatography. The band consisting of NTH-RNase E monomer is highlighted with an arrow. Panel B shows the size-exclusion profile of D346N NTH-RNase E (bottom panel) during purification along with a calibration curve (Top panel), derived using the HMW calibration kit (GE Healthcare).

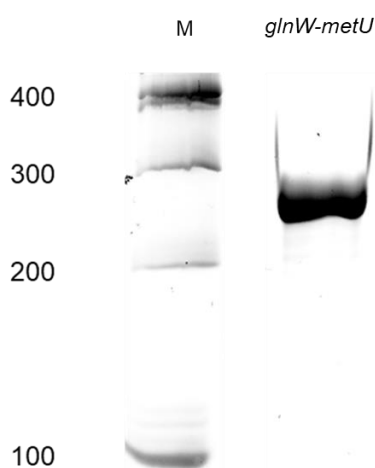


**Figure 5.5 Circular Dichroism of D346N NTH-RNase E.** D346N NTH-RNase E was buffer exchanged into 5 mM Tris-Acetate (pH 8.3), 100 mM NaSO<sub>4</sub> and 10 mM MgSO<sub>4</sub> at 0.25 mg/ml. The average CD spectrum at 37°C (black) was calculated from 2 replicates. CD spectra in red correspond to those obtained at several temperatures between 20 and 87°C. The inset shows the first differential of a normalised response at 222 nm.

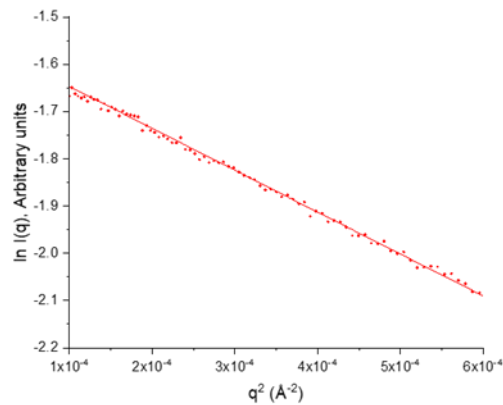
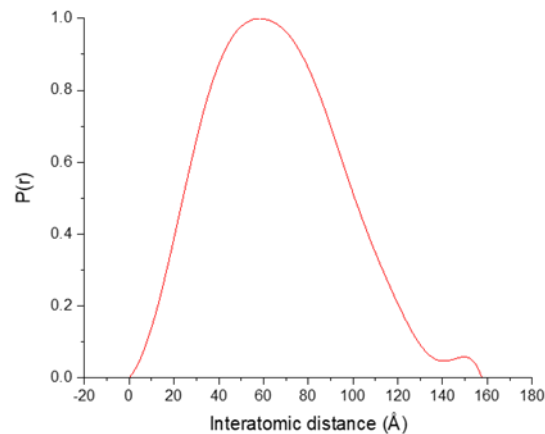
The *glnW-metU* substrate was generated by *in vitro* transcription and purified by gel-extraction following polyacrylamide gel electrophoresis. The purity was deemed to be >95% using densitometry (Figure 5.6). SEC-SAXS was employed for quality assurance using D346N apoprotein and the *glnW-metU* with D346N complex, prepared as with the wild-type RNase E and BR15 complex (Figure 5.7). The measured  $D_{\max}$  and  $R_g$  values of the D346N mutant apoprotein were 158 Å and 51 Å, respectively. These values are slightly lower than those reported herein for NTH-RNase E with wild-type sequence and closer to values reported previously by others (Callaghan et al., 2003; Mardle et al., 2019). Importantly, the linear scaling of Guinier plot



indicates the sample of the D346N mutant is monodisperse in solution and the measured  $D_{max}$  and  $R_g$  values are consistent with RNase E being a tetramer. The complex of NTH-RNase E D346N and *glnW-metU* RNA was also sent for analysis by SAXS, but unfortunately, the sample precipitated prior to loading; thus, no data could be collected.



**Figure 5.6 Analysis of the purification of *glnW-metU* RNA.** The substrate was synthesised by *in vitro* transcription. Lane M contain an RNA ladder and lane *glnW-metU* contains 500 ng of indicated RNA. Samples were mixed with equal volumes of 2 x RNA loading buffer, denatured at 95°C and analysed by electrophoresis using a 10% (w/v) polyacrylamide gel containing 7 M urea. The gel was stained with SYBR<sup>TM</sup> Safe stain and viewed using a Fujifilm FLA-5000 imager with the scanner set at 473 nm.

**A****B**

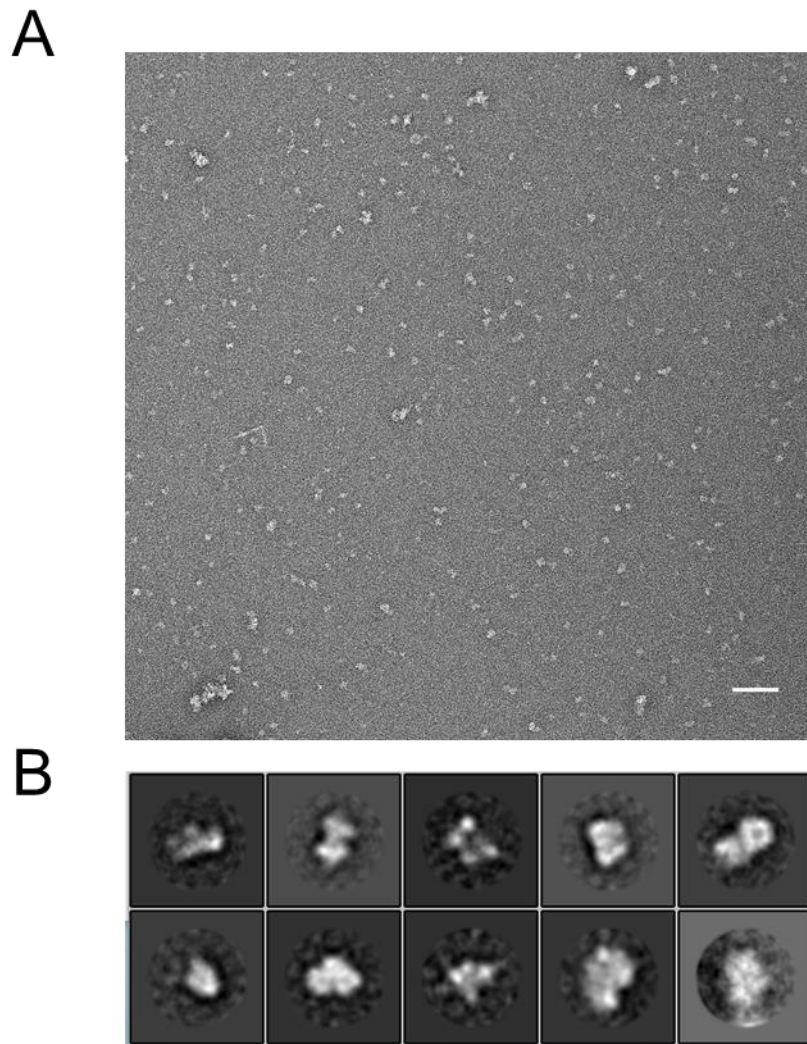
**Figure 5.7 Small-angle X-ray Scattering of D346N NTH-RNase E apoprotein.** Panel A contains a Guinier plot together with the fit of the data of D346N NTH-RNase E apoprotein the y-axis represents  $\ln(\text{intensity})$  and has arbitrary units. The x-axis represents the square of the scattering angle. Panel B contains a distance distribution function, which was used to determine the  $D_{\max}$ . The X-axis represents paired distances between two points in a particle, the Y-axis represents the proportion in which those distances occur on the particle.  $D_{\max}$  is calculated by the x-intercept. Data was processed in ATSAS (Franke et al., 2017)

As before, negative-stain EM grids were prepared using a 1:1 ratio of RNase E and substrate and micrographs were collected on a Technai TF20 electron microscope (Figure 5.8, panel A). A reasonable distribution of particles was observed and micrographs were processed in RELION (Figure 5.8, panel B). Particles were extracted and sorted into ten 2D classes. All of which seemed to all be of the appropriate size for NTH-RNase E; consequently, these were

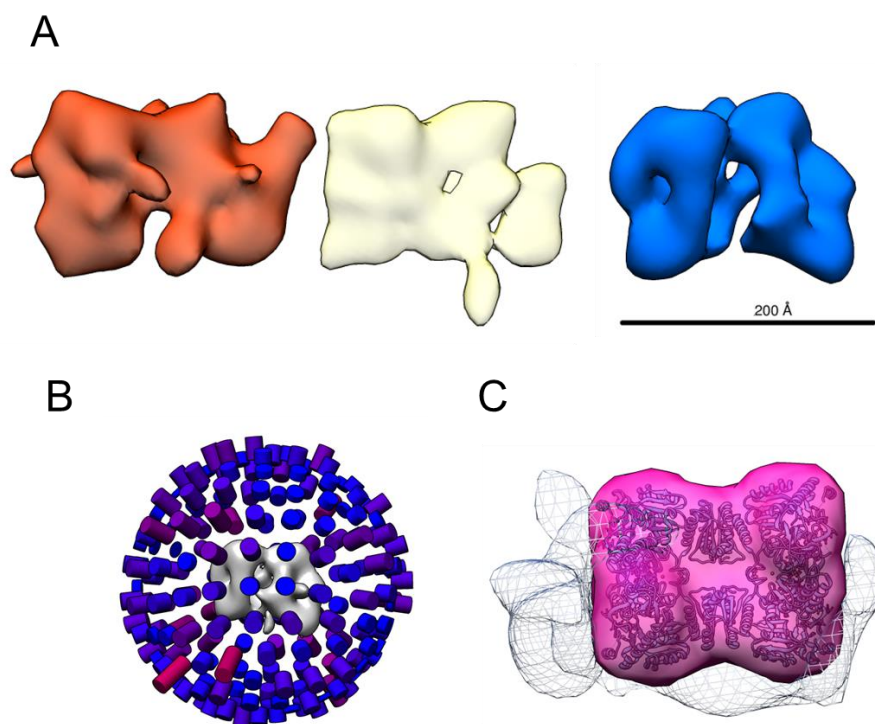
subjected to further processing. An initial model was generated from the 2D class averages, which was then used for 3D reconstructions. Following recommended guidelines provided in the RELION tutorial (Scheres, 2012), 3D classification was performed, with 3 classes chosen as a starting point (Figure 5.9). For all three classes, the 3D reconstructions appear to have additional density relative to the apo form of NTH-RNase E. One potential cause of additional density could be angular imbalance of projections, caused by a bias in the orientation that RNase E adheres to the grid which can result in stretching of the 3D reconstruction on sides opposite to the favoured view (Sorzano et al., 2001). Therefore, to confirm that additional density was not an artefact the angular distribution file was inspected (Figure 5.9, Panel C). The angular distribution of projections are not solely concentrated in any one area and are reasonably well distributed, suggesting no elongation of the model. Thus, it was concluded the additional density likely corresponds to bound tRNA substrate. To better visualise the additional density, a 'closed' NTH-RNase E structure (PDB: 2COB) was fitted into one of the classes by generating a simulated map from the crystal structure with a resolution of 35 Å and, using the "fit in map" tool within Chimera (Pettersen et al., 2004), the simulated map was then subtracted from the experimental map produced within RELION (Scheres, 2012) (Figure 5.9, Panel C).

Next, 3D auto-refinement was performed, with the final resolution of the map being 35 Å, calculated from the Fourier Shell Correlation (FSC) from independently refined half-reconstructions (Figure 5.10, panel A). The final map is shown fitted with 'closed' NTH-RNase E (Figure 5.10), and shows additional density in an elongated form spanning the tetrameric interface.

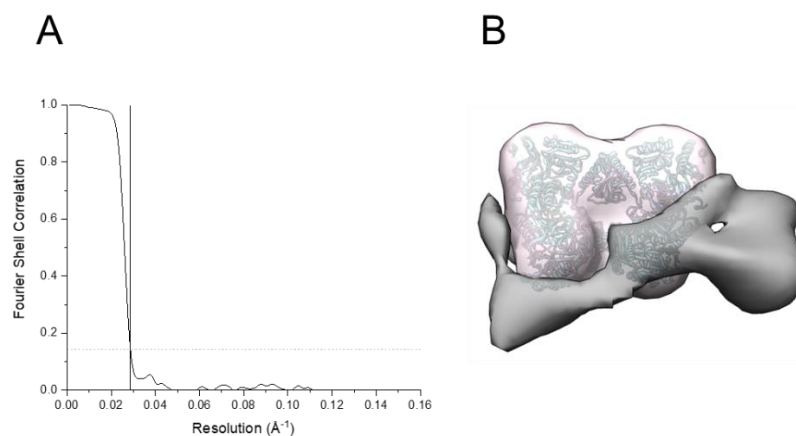
The additional density is of the appropriate size to accommodate tRNA. RNase E alongside tRNA is provided as a size comparison (Figure 5.11). However, whilst this result was encouraging, it should not be over-interpreted, A map of higher resolution is required to identify the various subdomains of RNase E, let alone the molecular contacts that might mediate the interaction between NTH-RNase E and the tRNA-based substrate. Therefore, priority was given to extending the analysis to cryo-EM.



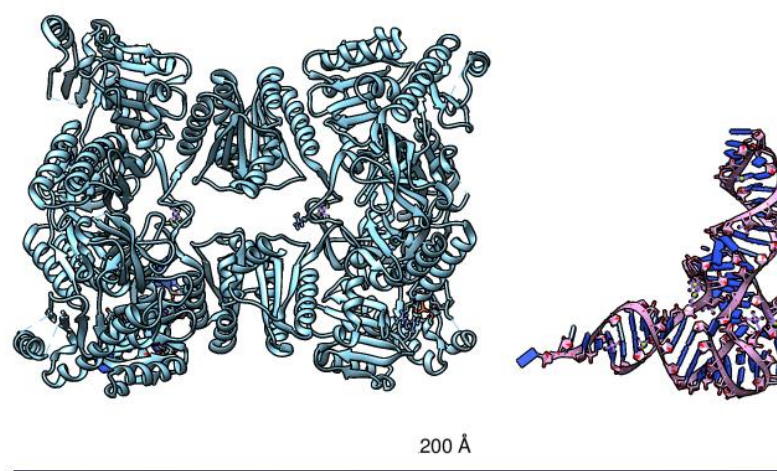
**Figure 5.8 Negative-stain electron microscopy of *glnW-metU* RNA in complex with NTH-RNase E.** NTH-RNase E and *glnW-metU* were mixed in 1:1 molar ratio at 0.02 mg/ml and applied to a carbon-coated copper grid. Panel A contains a typical micrograph taken on a Technai TF20 electron microscope, scale bar indicates 100 nm (1000 Ångstrom). Panel B shows the ten 2D class averages generated in RELION.



**Figure 5.9 3D classification of NTH-RNase E in complex with *glnW-metU*.** Panel A shows the three classes generated using 3D classification in RELION along with a 200 Å (20 nm) scale bar. Panel B shows the angular distribution of views that contribute to the class shown in blue within panel A. Panel C shows a (blue) class within panel B with simulated density of RNase E fitted into the map and additional density displayed as a mesh.



**Figure 5.10 3D auto-refinement of NTH-RNase E in complex with *glnW-metU*.** Panel A shows the Fourier shell correlation curve, showing the resolution of the dataset is 35 Å, the horizontal line indicates the FSC cut-off of 0.143, the solid vertical line indicates the resolution dictated by the cut-off (0.0286 Å<sup>-1</sup>). Panel B shows the final map generated by subtraction of the 'closed' structure map (light grey) and 3D auto-refinement, with the additional density is shown in grey.



**Figure 5.11 Size comparison of tRNA and RNase E.** Shown are structures of RNase E (PDB: 2C0B) and tRNA (PDB: 1EHZ) for comparison of size. Scale bar represents 200 Å (20 nm).

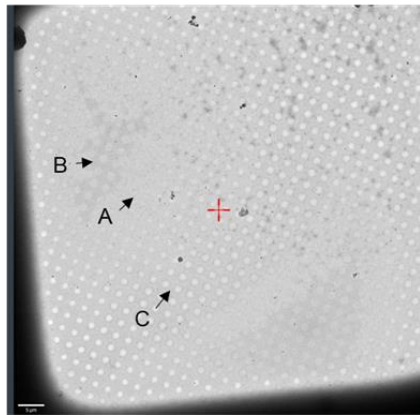
### 5.2.3 Initial screening of RNase E by cryo-EM

NTH-RNase E (with the D346N substitution) and *glnW-metU* were mixed as before at a 1:1 molar ratio for initial screening purposes by cryo-EM. However, the concentration of both macromolecules was increased substantially to meet the requirements of cryo-EM. Unfortunately, at concentrations between 0.5 and 5 mg/ml, substantial precipitation occurred for samples of the complex but not apoprotein. It was concluded that the cause was likely two or perhaps more tetramers associating via binding to a shared *glnW-metU* transcript at the higher concentrations. Consistent with this conclusion, higher-order complexes were observed in EMSAs when concentrations of NTH-RNase E were in excess over substrates (Chapter 3). However, increasing the concentration of transcript until it was in eight-fold excess over NTH-RNase (1 mg/ml) did not abrogate the precipitation (data not shown). Thus, interaction with the bicistronic tRNA substrate may alter the solubility of individual tetramers, rather than being a consequence of multiple tetramers associating.

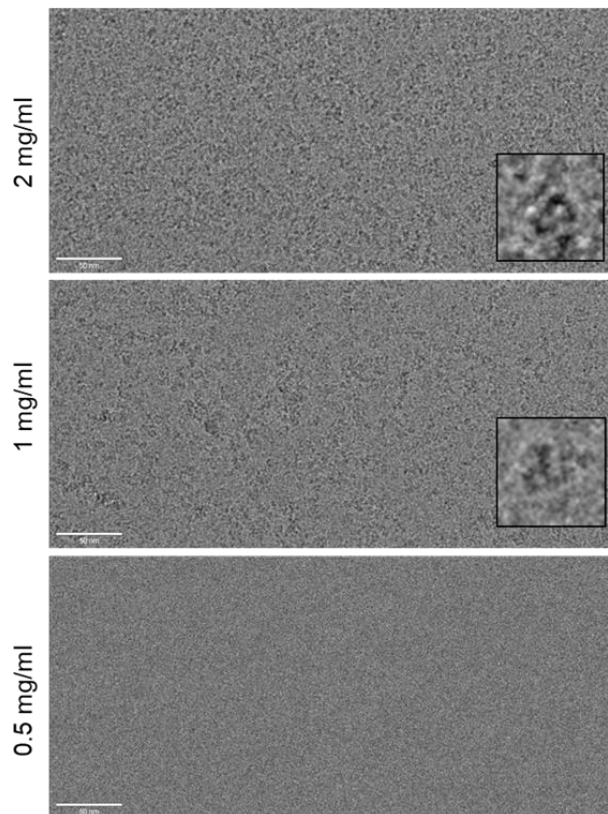
As the apo form of NTH-RNase E had already been prepared, grids were prepared using concentrations of 0.5, 1 and 2 mg/ml using two blotting parameters (3- and 6-second blot). Grids were screened on a Krios G3i Cryo-TEM. All grids produced with a blot time of 3 seconds had ice that was impenetrable by the electron beam (data not shown). Increasing the blotting time to 6 seconds produced ice of a range of thicknesses (ice of a higher opacity was thicker) (Figure 5.12, panel A); NTH-RNase E could be seen on these grids at both 1 and 2 mg/ml (Figure 5.12, panel B). No protein was visible at 0.5 mg/ml. At 2 mg/ml, NTH-RNase E was far too clustered on the grid for data collection. However, at 1 mg/ml particles were discrete enough to collect a dataset (Dan Maskell, pers. comms). Thus whilst beyond the scope of this study, others may wish to perform a data collection and subsequently process the resultant data.



A



B



**Figure 5.12 Initial screening by Cryo-EM.** Cryo-EM grids were prepared with NTH-RNase E at 2 mg/ml, 1 mg/ml and 0.5 mg/ml. Panel A contains an atlas view of a typical grid with thick, medium and thin ice labelled A-C, respectively. Scale bar is 5  $\mu\text{m}$  (5000 nm). Panel B shows typical micrographs with the concentration of NTH-RNase E indicated on the left. Scale bar is 50 nm. An inset showing a magnified particle is shown in the bottom right in a 20 x 20 nm box.

### 5.3 Discussion

Through the use of negative-stain EM it has been shown that a polypeptide of the N-terminal catalytic half of RNase E can be prepared in a manner that is suitably pure for studies by cryo-EM (Figure 5.8). Quality control was performed by SEC-SAXS (Figure 5.7) to ensure RNase E is monodisperse and of the expected dimensions. Additional density that is seen in the map that corresponds to bound *metU-glnW* RNA; however, at the resolution achieved it is not possible to comment on the nature of the underlying interactions.

The general structure of the additional density seems to cross the tetramer of RNase E which would suggest that both principle dimers of the tetramer contribute to the interaction of *metU-glnW* RNA. This is the first time this suggestion has been made, however models of RNA making multiple contacts with RNase E do not exclude this, they have just limited the idea to interaction with both protomers within the same principle dimer (Clarke et al., 2014).

Differences were seen in the calculated values from SAXS of the wild-type NTH-RNase E compared with previously published values for wild-type (Callaghan et al., 2003; Mardle et al., 2019). A study of different RNase E homologues from five different species produced values of  $D_{\max}$  ranging from 149-183 Å, despite high sequence similarity of these species, which highlights the variability of the data produced (Mardle et al., 2019). This is not surprising considering the 5' sensor and S1 subdomains are very dynamic, as can be seen by the changes that occur between the 'open' and 'closed' forms (see main introduction).

The above work has laid the foundations of the study of RNase E through cryo-EM. Conditions were found in which the apo-form of NTH-RNase E is visible as discrete particles within vitreous ice and is of sufficient quality to perform a data collection. Determination of the cryo-EM structure of the apo form alone would provide further insight into the structure of RNase E in its 'open' form. So far, sources of structural information of the apo form are limited to SAXS data (Callaghan et al., 2003; Mardle et al., 2019) and X-ray crystallography data, mostly completed using molecular replacement (Koslover et al., 2008). Previously, cryo-EM of the BAM complex has revealed conformational rearrangements relative to structures solved by X-ray crystallography, further suggesting the worth of further characterisation of the apo form of RNase E (Iadanza et al., 2016). Additionally, some of the challenges in the generation of RNPs with RNase E have been highlighted. For example, the presence of long single-stranded regions, while more physiologically relevant as a substrate, results in an RNP that has reduced solubility and therefore is not amenable to study by cryo-EM.

It may be possible to overcome the issues of RNP solubility by changing the preparation of the complex. Perhaps one method could include the preparation of RNPs at lower concentrations to preclude aggregation, fixation of the RNP complex (Stark, 2010), and then gradual concentration of the complex to suitable concentrations for studies by EM. Another approach could involve pre-application of RNase E to the grids and RNA could be added to form the RNP on the grids immediately before plunge freezing (Hurdiss et al., 2018). This would presumably generate some RNPs whilst potentially reducing the time for aggregation to occur. Another approach may be to try and improve the solubility of the complex by screening different

buffer conditions, potentially by changing the buffer pH or salt concentrations. In addition, the inclusion of small amounts of detergent has been shown to increase the solubility of proteins that were studied by cryo-EM (Sgro and Costa, 2018). Screening of other substrates may prove useful in the identification of a soluble complex such as the 5' UTR from the *mne* transcript. Alternatively, extending the construct to include parts of the C-terminal half may yield a more soluble polypeptide, although this would have to be determined empirically. Perhaps the study of the entire degradosome as a whole could be considered.

In the absence of acquiring further structural data through cryo-EM, other approaches may be necessary. UV cross-linking of RNA to RNase E, followed by mass spectrometry fingerprinting, has been previously used to identify sites of interaction (Kim et al., 2014). Hydrogen-deuterium exchange followed by mass spectrometry (HDX-MS) (Kostyukevich et al., 2018) could also be a viable alternative, in which the solvent accessibility of sites on the protein is measured. Comparing apoprotein to RNA-bound protein would reveal residues that are no longer susceptible to deuteration, due to occlusion of the surface either through conformational change or ligand binding. Understanding the points of interaction of tRNAs that extend beyond the identified RNA-binding groove would help to direct future functional and structural studies.

Study of RNase E bound to previously identified small molecule inhibitors (Kime et al., 2015) by cryo-EM would allow better characterisation of them and possibly aid improvement of them. The resultant small molecules could potentially be used as antimicrobials, at the very least they could provide

useful tools for the study of RNase E through chemical genetics approaches (discussed in chapter 6).

## **Chapter 6**

### Discussion and future work

## 6.1 Summary of work

Work conducted as part of this thesis has shown that mutation of the RNA-binding groove within RNase E affects its binding to structured RNA substrates, such as *glnW* pre-tRNA (Figure 3.7) and the *rpsO* transcriptional terminator (Figure 3.6). Cleavage of polycistronic tRNA precursors was disrupted by mutation of the RNA-binding groove (Figure 3.10), which could suggest that this site plays a role in direct entry (Clarke, 2015). Additionally, mutation of the RNA-binding groove has minimal effects on the interaction of a single-stranded RNA oligonucleotide, LU13, where it was found that the  $K_M$  remains unchanged (Figure 3.11).

The *in vivo* significance of the RNA-binding groove was also established, as it was found that the 8x mutant of RNase E was not able to restore growth of an RNase E deficient strain (Figure 4.4). If absolutely critical for direct entry it would be predicted that the 8x mutant could not complement an RNase E deficient strain unless heavily overexpressed much like complementation by RNase G (Lee et al., 2002). Furthermore, the role of the RNA-binding groove does not appear to extend to autoregulation (Table 4.2). The hairpins within the 5' UTR of the *rne* transcript have been implicated as the major components that mediate RNase E autoregulation, most likely through direct interaction with the enzyme (Schuck et al., 2009). However, although the RNA-binding groove has been associated with interaction with duplex RNA, no significant effect on autoregulation was found by mutating the 8 residues. Additionally, data in this thesis corroborates previous work that suggests that the C-terminus, which is not required for RNA-degradation, makes a substantial contribution to autoregulation (Table 4.2).

Protein sequence analysis revealed that RNase G, whilst sharing high sequence homology with RNase E, has little chemical conservation compared to RNase E in the residues that are associated with the RNA-binding groove (Figure 4.8) Indeed, RNase G also is unable to cleave tRNA precursors (Figure 4.13) by the direct entry pathway. Reanalysis of published RNA-seq data reveals that RNase G seems to make a unique set of cleavages (Figure 4.14) and, unlike RNase E, has little sequence specificity for RNA cleavage (Figure 4.15).

An initial foray into the study of RNase E by electron microscopy highlighted issues with the ability for RNase E to form higher-order complexes with some substrates. However, distinct particles of the apoprotein were observed by Cryo-EM (Figure 5.12), suggesting that solving a structure by EM may be possible in the future and would presumably require optimisation of the preparation of the RNP complex or re-design of the substrate choice.

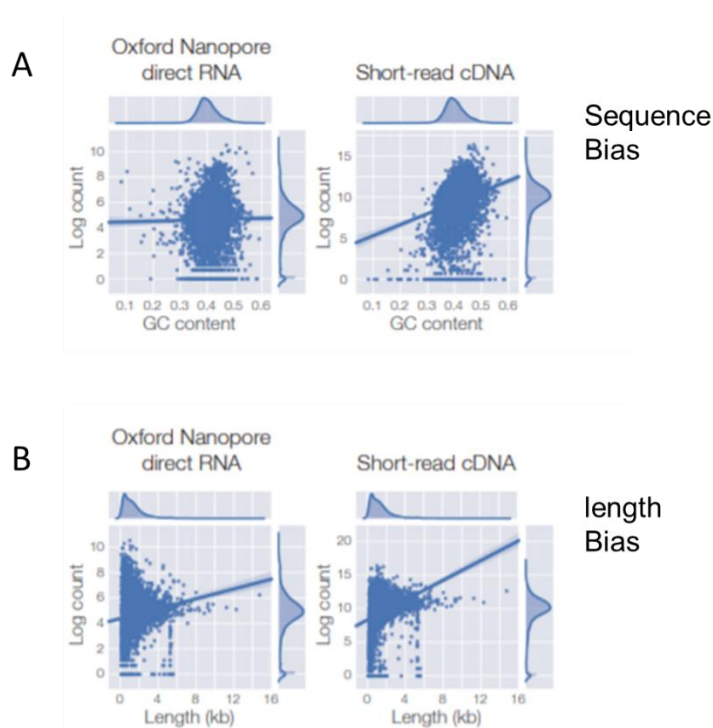


## 6.2 Future work

As discussed in chapter 5, one of the major limitations of performing EM is the solubility of RNase E in complex with RNA. One potential solution is to form the complex directly on the grids rather than in solution, which would hopefully allow vitrification prior to aggregation. Improving the conditions for EM would allow more complex substrates to be studied, such as RNase E bound to polycistronic tRNA or the *rne* 5' UTR. Alternative structural methods could also be used, such as cross-linking or foot-printing studies, which would at least illuminate further interactions that may be made beyond the established RNA-binding groove. Hydrogen-Deuterium exchange (HDX) (Kostyukevich et al., 2018) or fast photo-oxidation of proteins (FPOP) (Johnson et al., 2019) would provide information on residues that change their surface exposure due to RNA interaction or conformational change, which could be augmented by crosslinking mass-spectrometry studies (Urlaub et al., 2008).

Currently, RNA-Seq approaches to study RNase E have utilised the Illumina-based sequencing-by-synthesis methods (Clarke et al., 2014; Chao et al., 2017) and also the temperature-sensitive mutant (Ono and Kuwano, 1979). Additionally, cleavage sites have been inferred by enrichment of 5' ends rather than directly called from the RNA. The use of Nanopore long-read sequencing (Oxford Nanopore Technologies) would allow for direct measurement of RNA, which would result in less susceptibility to length and sequence bias, providing a more quantitative assessment of the transcriptome (Figure 6.1). Furthermore, the entire RNA strand can be read in a single read, providing more direct information on cleavage sites, as the

end of a read would indicate the end of the RNA strand. Long-read sequencing has also been used for structure-probing of RNA (Zhang et al., 2017). Another advantage of this long-read sequencing technology is that RNA modifications can be detected. Therefore, it would be interesting to exploit this property to determine if there exists RNA modifications at sites where RNase E cleavage occurs. The sugar pucker of the ribose group on RNA has been directly implicated in the selection of substrates for cleavage; a C2'-endo conformation of the ribose of the nucleotide just upstream of the site of cleavage has been shown to be required (Redko et al., 2003). Thus, it could be possible that the modification of RNA residues provides a further tuning step to gene regulation.



**Figure 6.1 Length and Sequence bias of Illumina vs Oxford Nanopore sequencing technologies.** Panel A shows graphs of log(count) against the GC content. Panel B shows graphs of log(count) against the length of RNA (Figure is taken from (Oxford Nanopore Technologies, 2018)).

The temperature-sensitive (ts) mutant of RNase E has been exploited extensively in several studies, whereby rapid inactivation of RNase E allows

depletion of RNase E cleavages, which can be mapped using RNA-seq strategies (Clarke et al., 2014; Chao et al., 2017). However, one drawback to this system is that inactivation of the ts mutant by incubation at non-permissive temperatures would also induce the heat-shock response, resulting in the rapid production of heat shock proteins and thereby potentially altering gene expression (Arsène et al., 2000). In addition, an increase in temperature may affect the secondary structure of RNAs, which could result in changes to the susceptibility of these RNAs to cleavages by ribonucleases such as cleavage of dsRNA by RNase III and direct entry cleavages by RNase E. An alternative method could involve the use of previously-published small-molecule inhibitors of RNase E (Kime et al., 2015) to assign cleavages *in vivo* which may then be further probed by seeing how the cleavages are affected by mutants *in vitro*. Development of inhibitors would be beneficial beyond generating a more robust RNA-sequencing dataset as RNase E, being an essential protein found in several human pathogens, thus a novel target for antibiotic development. It may be interesting to perform further characterising of RNase E cleavages *in vivo* by utilising an Affimer (Tiede et al., 2014) that binds to the RNA-binding groove. Libraries of affimers could be screened for binding wild-type RNase E then counter-selected against the 8x mutant. Presumably, this would remove any affimers from the pool that bind to RNase E distal to the RNA-binding groove. If the affimer had an antagonistic effect on RNase E, it would be a useful tool to look at effects on inactivating the RNA-binding groove *in vivo*. It would be useful to map the binding sites of RNase E that are dependent on the RNA-binding groove in a transcriptome-wide manner. This would require generating a strain of RNase E in which the RNA-binding groove has

been mutated but still results in viability; this could be achieved either through overexpression or utilising a different mutant. *In vivo* crosslinking by UV irradiation has been previously used to identify the small RNA interactome of RNase E (Waters et al., 2017), following a similar method and comparing crosslinking of mutant and wild-type RNase E would presumably reveal binding sites that depend on the RNA-binding groove.

Binding studies during this thesis have been performed by EMSA, which only gives an apparent  $K_d$  and therefore is limited in terms of quantitation of kinetic parameters. SwitchSENSE<sup>®</sup> has been used previously to look at RNA-binding proteins (Webster et al., 2019). SwitchSENSE<sup>®</sup> allows for real-time measurement of the rate constants  $k_1$  and  $k_{-1}$ , thereby allowing  $K_d$  values to be accurately calculated. Additionally, it provides information on the hydrodynamic radius of the bound particle. SwitchSENSE<sup>®</sup> allows for a ‘molecular ruler’ mode, which may allow inference on the region binding is occurring on the RNA. Studies performed under conditions that allow cleavage to occur could allow real-time measurement of the rate of RNA cleavage, allowing  $k_2$  to be calculated. More accurate measurements of binding could be made that would allow better comparison mutant and wild-type RNase E.

## **Chapter 7**

### References

- Aït-Bara, S. and Carpousis, A.J. 2015. RNA degradosomes in bacteria and chloroplasts: classification, distribution and evolution of RNase E homologs. *Molecular Microbiology*. **97**(6), pp.1021–1135.
- Aït-Bara, S., Carpousis, A.J. and Quentin, Y. 2015. RNase E in the  $\gamma$ -Proteobacteria: conservation of intrinsically disordered noncatalytic region and molecular evolution of microdomains. *Molecular Genetics and Genomics*. **290**(3), pp.847–862.
- Andrade, J.M., Hajnsdorf, E., Régnier, P. and Arraiano, C.M. 2009. The poly(A)-dependent degradation pathway of rpsO mRNA is primarily mediated by RNase R. *RNA (New York, N.Y.)*. **15**(2), pp.316–26.
- Anupama, K., Leela, J.K. and Gowrishankar, J. 2011. Two pathways for RNase E action in Escherichia coli in vivo and bypass of its essentiality in mutants defective for Rho-dependent transcription termination. *Molecular Microbiology*. **82**(6), pp.1330–1348.
- Apirion, D. 1978. Isolation, genetic mapping and some characterization of a mutation in Escherichia coli that affects the processing of ribonucleic acid. *Genetics*. **90**(4), pp.659–671.
- Apirion, D. and Lassar, A.B. 1978. A conditional lethal mutant of Escherichia coli which affects the processing of ribosomal RNA. *Journal of Biological Chemistry*. **253**(5), pp.1738–1742.
- Apirion, D., Neil, J. and Watson, N. 1976. Consequences of losing ribonuclease III on the Escherichia coli cell. *MGG Molecular & General Genetics*. **144**(2), pp.185–190.
- Aristarkhov, A., Mikulskis, A., Belasco, J.G. and Lin, E.C. 1996. Translation of the adhE transcript to produce ethanol dehydrogenase requires

- RNase III cleavage in *Escherichia coli*. *Journal of bacteriology*. **178**(14), pp.4327–32.
- Arsène, F., Tomoyasu, T. and Bukau, B. 2000. The heat shock response of *Escherichia coli*. *International Journal of Food Microbiology*. **55**(1–3), pp.3–9.
- Baba, T., Ara, T., Hasegawa, M., Takai, Y., Okumura, Y., Baba, M., Datsenko, K.A., Tomita, M., Wanner, B.L., Mori, Hirotsada and Mori, H. 2006. Construction of *Escherichia coli* K-12 in-frame, single-gene knockout mutants: the Keio collection. *Molecular Systems Biology*.
- Babitzke, P., Granger, L., Olszewski, J. and Kushner, S.R. 1993. Analysis of mRNA decay and rRNA processing in *Escherichia coli* multiple mutants carrying a deletion in RNase III. *Journal of Bacteriology*. **175**(1), pp.229–239.
- Babitzke, P. and Kushner, S.R. 1991. The Ams (altered mRNA stability) protein and ribonuclease E are encoded by the same structural gene of *Escherichia coli*. *Proceedings of the National Academy of Sciences of the United States of America*. **88**(1), pp.1–5.
- Bakshi, S., Siryaporn, A., Goulian, M. and Weisshaar, J.C. 2012. Superresolution imaging of ribosomes and RNA polymerase in live *Escherichia coli* cells. *Molecular Microbiology*. **85**(1), pp.21–38.
- Bandyra, K.J., Bouvier, M., Carpousis, A.J. and Luisi, B.F. 2013. The social fabric of the RNA degradosome. *Biochimica et Biophysica Acta - Gene Regulatory Mechanisms*. **1829**(6–7), pp.514–522.
- Bandyra, K.J., Said, N., Pfeiffer, V., Górna, M.W., Vogel, J. and Luisi, B.F. 2012. The Seed Region of a Small RNA Drives the Controlled

- Destruction of the Target mRNA by the Endoribonuclease RNase E. *Molecular Cell*. **47**(6), pp.943–953.
- Bandyra, K.J., Wandzik, J.M. and Luisi, B.F. 2018. Substrate Recognition and Autoinhibition in the Central Ribonuclease RNase E. *Molecular Cell*. **72**, pp.275–285.
- Bayas, C.A., Wang, J., Lee, M.K., Schrader, J.M., Shapiro, L. and Moerner, W.E. 2018. Spatial organization and dynamics of RNase E and ribosomes in *Caulobacter crescentus*. *Proceedings of the National Academy of Sciences*. **115**(16), pp.E3712–E3721.
- Belasco, J.G. 2010. All things must pass: Contrasts and commonalities in eukaryotic and bacterial mRNA decay. *Nature Reviews Molecular Cell Biology*. **11**(7), pp.467–478.
- Berg, J., Tymoczko, J. and Stryer, L. 2002. *The Michaelis-Menten Model Accounts for the Kinetic Properties of Many Enzymes* [Online]. Available from: <http://www.ncbi.nlm.nih.gov/books/NBK22430/>.
- Bernstein, J.A., Khodursky, A.B., Lin, P.-H.P., Lin-Chao, S. and Cohen, S.N. 2002. Global analysis of mRNA decay and abundance in *Escherichia coli* at single-gene resolution using two-color fluorescent DNA microarrays. *Proceedings of the National Academy of Sciences of the United States of America*. **99**(15), pp.9697–702.
- Braun, F., Le Derout, J. and Régnier, P. 1998. Ribosomes inhibit an RNase E cleavage which induces the decay of the rpsO mRNA of *Escherichia coli*. *The EMBO journal*. **17**(16), pp.4790–7.
- Briant, D.J., Hankins, J.S., Cook, M.A. and Mackie, G.A. 2003. The quaternary structure of RNase G from *Escherichia coli*. *Molecular*



*Microbiology*. **50**(4), pp.1381–1390.

- Bruce, H.A., Du, D., Matak-Vinkovic, D., Bandyra, K.J., Broadhurst, R.W., Martin, E., Sobott, F., Shkumatov, A. V and Luisi, B.F. 2018. Analysis of the natively unstructured RNA/protein-recognition core in the Escherichia coli RNA degradosome and its interactions with regulatory RNA/Hfq complexes. *Nucleic Acids Research*. **46**(1), pp.387–402.
- Burge, S., Parkinson, G.N., Hazel, P., Todd, A.K. and Neidle, S. 2006. Quadruplex DNA: sequence, topology and structure. *Nucleic acids research*. **34**(19), pp.5402–15.
- Bycroft, M., Hubbard, T.J.P., Proctor, M., Freund, S.M.V. and Murzin, A.G. 1997. The solution structure of the S1 RNA binding domain: A member of an ancient nucleic acid-binding fold. *Cell*. **88**(2), pp.235–242.
- Callaghan, A.J., Aurikko, J.P., Ilag, L.L., Günter Grossmann, J., Chandran, V., Kühnel, K., Poljak, L., Carpousis, A.J., Robinson, C. V., Symmons, M.F. and Luisi, B.F. 2004. Studies of the RNA degradosome-organizing domain of the Escherichia coli ribonuclease RNase E. *Journal of Molecular Biology*. **340**(5), pp.965–979.
- Callaghan, A.J., Grossmann, J.G., Redko, Y.U., Ilag, L.L., Moncrieffe, M.C., Symmons, M.F., Robinson, C. V., McDowall, K.J. and Luisi, B.F. 2003. Quaternary Structure and Catalytic Activity of the Escherichia coli Ribonuclease E Amino-Terminal Catalytic Domain. *Biochemistry*. **42**(47), pp.13848–13855.
- Callaghan, A.J., Marcaida, M.J., Stead, J.A., McDowall, K.J., Scott, W.G. and Luisi, B.F. 2005. Structure of Escherichia coli RNase E catalytic domain and implications for RNA turnover. *Nature*. **437**(7062), pp.1187–

1191.

- Callaghan, A.J., Redko, Y., Murphy, L.M., Grossmann, J.G., Yates, D., Garman, E., Ilag, L.L., Robinson, C. V., Symmons, M.F., McDowall, K.J. and Luisi, B.F. 2005. 'Zn-Link': A metal-sharing interface that organizes the quaternary structure and catalytic site of the endoribonuclease, RNase E. *Biochemistry*. **44**(12), pp.4667–4675.
- Del Campo, C., Bartholomäus, A., Fedyunin, I. and Ignatova, Z. 2015. Secondary Structure across the Bacterial Transcriptome Reveals Versatile Roles in mRNA Regulation and Function A. Toledo-Arana, ed. *PLOS Genetics*. **11**(10), p.e1005613.
- Cao, G.J. and Sarkar, N. 1992. Identification of the gene for an Escherichia coli poly(A) polymerase. *Proceedings of the National Academy of Sciences of the United States of America*. **89**(21), pp.10380–4.
- Carpousis, A.J. 2007. The RNA Degradosome of *Escherichia coli*: An mRNA-Degrading Machine Assembled on RNase E. *Annual Review of Microbiology*. **61**(1), pp.71–87.
- Caruthers, J.M., Feng, Y., McKay, D.B. and Cohen, S.N. 2006. Retention of Core Catalytic Functions by a Conserved Minimal Ribonuclease E Peptide That Lacks the Domain Required for Tetramer Formation. *Journal of Biological Chemistry*. **281**(37), pp.27046–27051.
- Celesnik, H., Deana, A. and Belasco, J.G. 2007. Initiation of RNA Decay in Escherichia coli by 5' Pyrophosphate Removal. *Molecular Cell*. **27**(1), pp.79–90.
- Chandran, V. and Luisi, B.F. 2006. Recognition of enolase in the Escherichia coli RNA degradosome. *Journal of Molecular Biology*. **358**(1), pp.8–15.

- Chandran, V., Poljak, L., Vanzo, N.F., Leroy, A., Miguel, R.N., Fernandez-Recio, J., Parkinson, J., Burns, C., Carpousis, A.J. and Luisi, B.F. 2007. Recognition and Cooperation Between the ATP-dependent RNA Helicase RhlB and Ribonuclease RNase E. *Journal of Molecular Biology*. **367**(1), pp.113–132.
- Chao, Y., Li, L., Girodat, D., Förstner, K.U., Said, N., Corcoran, C., Śmiga, M., Papenfort, K., Reinhardt, R., Wieden, H.J., Luisi, B.F. and Vogel, J. 2017. In Vivo Cleavage Map Illuminates the Central Role of RNase E in Coding and Non-coding RNA Pathways. *Molecular Cell*. **65**(1), pp.39–51.
- Chen, L.H., Emory, S.A., Bricker, A.L., Bouvet, P. and Belasco, J.G. 1991. Structure and function of a bacterial mRNA stabilizer: Analysis of the 5' untranslated region of ompA mRNA. *Journal of Bacteriology*. **173**(15), pp.4578–4586.
- Cheng, Y., Grigorieff, N., Penczek, P.A. and Walz, T. 2015. *A primer to single-particle cryo-electron microscopy* [Online]. Elsevier. [Accessed 2 August 2019]. Available from: <http://www.ncbi.nlm.nih.gov/pubmed/25910204>.
- Cheng, Z.F. and Deutscher, M.P. 2002. Purification and characterization of the Escherichia coli exoribonuclease RNase R. Comparison with RNase II. *Journal of Biological Chemistry*. **277**(24), pp.21624–21629.
- Chung, D.-H.H., Min, Z., Wang, B.-C.C. and Kushner, S.R. 2010. Single amino acid changes in the predicted RNase H domain of Escherichia coli RNase G lead to complementation of RNase E deletion mutants. *RNA*. **16**(7), pp.1371–1385.

- Clarke, J.E. 2015. Direct entry by RNase E. . (September), pp.1–166.
- Clarke, J.E., Kime, L., Romero A., D. and McDowall, K.J. 2014. Direct entry by RNase E is a major pathway for the degradation and processing of RNA in *Escherichia coli*. *Nucleic Acids Research*. **42**(18), pp.11733–11751.
- Coburn, G.A. and Mackie, G.A. 1998. Reconstitution of the degradation of the mRNA for ribosomal protein S20 with purified enzymes. *Journal of Molecular Biology*. **279**(5), pp.1061–1074.
- Condon, C., Brechemier-Baey, D., Beltchev, B., Grunberg-Manago, M. and Putzer, H. 2001. Identification of the gene encoding the 5S ribosomal RNA maturase in *Bacillus subtilis*: Mature 5S rRNA is dispensable for ribosome function. *RNA*. **7**(2), pp.242–253.
- Condon, C. and Putzer, H. 2002. The phylogenetic distribution of bacterial ribonucleases. *Nucleic Acids Research*. **30**(24), pp.5339–5346.
- Cordin, O., Banroques, J., Tanner, N.K. and Linder, P. 2006. The DEAD-box protein family of RNA helicases. *Gene*. **367**, pp.17–37.
- Cormack, R.S. and Mackie, G.A. 1992. Structural requirements for the processing of *Escherichia coli* 5 S ribosomal RNA by RNase E in vitro. *Journal of Molecular Biology*. **228**(4), pp.1078–1090.
- Crooks, G.E., Hon, G., Chandonia, J.-M. and Brenner, S.E. 2004. WebLogo: a sequence logo generator. *Genome research*. **14**(6), pp.1188–90.
- Danchin, A. 2009. *A Phylogenetic View of Bacterial Ribonucleases* [Online]. Academic Press. [Accessed 16 September 2019]. Available from: <https://www.sciencedirect.com/science/article/pii/S0079660308008015>.
- Davies, B.W., Köhrer, C., Jacob, A.I., Simmons, L.A., Zhu, J., Aleman, L.M.,

- RajBhandary, U.L. and Walker, G.C. 2010. Role of escherichia coli YbeY, a highly conserved protein, in rRNA processing. *Molecular Microbiology*. **78**(2), pp.506–518.
- Deana, A. and Belasco, J.G. 2005. Lost in translation: The influence of ribosomes on bacterial mRNA decay. *Genes and Development*. **19**(21), pp.2526–2533.
- Deana, A. and Belasco, J.G. 2004. The function of RNase G in Escherichia coli is constrained by its amino and carboxyl termini. *Molecular Microbiology*. **51**(4), pp.1205–1217.
- Deana, A., Celesnik, H. and Belasco, J.G. 2008. The bacterial enzyme RppH triggers messenger RNA degradation by 5' pyrophosphate removal. *Nature*. **451**(7176), pp.355–358.
- Le Derout, J., Folichon, M., Briani, F., Dehò, G., Régnier, P. and Hajnsdorf, E. 2003. Hfq affects the length and the frequency of short oligo(A) tails at the 3' end of Escherichia coli rpsO mRNAs. *Nucleic Acids Research*. **31**(14), pp.4017–4023.
- Dessau, M.A. and Modis, Y. 2010. Protein crystallization for X-ray crystallography. *Journal of Visualized Experiments*. (47).
- Deutscher, M.P. 2009. Chapter 9 Maturation and Degradation of Ribosomal RNA in Bacteria *In:*, pp.369–391. [Accessed 16 September 2019]. Available from: <https://linkinghub.elsevier.com/retrieve/pii/S007966030800809X>.
- Deutscher, M.P. 2006. Degradation of RNA in bacteria: comparison of mRNA and stable RNA. *Nucleic Acids Research*. **34**(2), pp.659–666.
- Deutscher, M.P. 2003. Degradation of Stable RNA in Bacteria. *Journal of*

*Biological Chemistry*. **278**(46), pp.45041–45044.

- Diwa, A., Bricker, A.L., Jain, C. and Belasco, J.G. 2000. An evolutionarily conserved RNA stem-loop functions as a sensor that directs feedback regulation of RNase E gene expression. *Genes and Development*. **14**(10), pp.1249–1260.
- Diwa, A.A., Jiang, X., Schapira, M. and Belasco, J.G. 2003. Erratum: Two distinct regions on the surface of an RNA-binding domain are crucial for RNase E function (Molecular Microbiology). *Molecular Microbiology*. **47**(4), p.1183.
- Donovan, W.P. and Kushner, S.R. 1986. Polynucleotide phosphorylase and ribonuclease II are required for cell viability and mRNA turnover in *Escherichia coli* K-12. *Proceedings of the National Academy of Sciences of the United States of America*. **83**(1), pp.120–4.
- Dubochet, J., Adrian, M., Chang, J.-J., Homo, J.-C., Lepault, J., McDowell, A.W. and Schultz, P. 1988. Cryo-electron microscopy of vitrified specimens. *Quarterly Reviews of Biophysics*. **21**(2), pp.129–228.
- Durand, S., Gilet, L., Bessières, P., Nicolas, P. and Condon, C. 2012. Three Essential Ribonucleases—RNase Y, J1, and III—Control the Abundance of a Majority of *Bacillus subtilis* mRNAs S. Altuvia, ed. *PLoS Genetics*. **8**(3), p.e1002520.
- Edgar, R.C. 2004. MUSCLE: Multiple sequence alignment with high accuracy and high throughput. *Nucleic Acids Research*. **32**(5), pp.1792–1797.
- Ehretsmann, C.P., Carpousis, A.J. and Krisch, H.M. 1992. *Specificity of Escherichia coli endoribonuclease RNase E: In vivo and in vitro analysis*

*of mutants in a bacteriophage T4 mRNA processing site* [Online].  
[Accessed 13 August 2019]. Available from:  
<http://genesdev.cshlp.org/content/6/1/149.full.pdf>.

Emory, S.A. and Belasco, J.G. 1990. The ompA 5' Untranslated RNA Segment Functions in *Escherichia coli* as a Growth-Rate-Regulated mRNA Stabilizer Whose Activity Is Unrelated to Translational Efficiency.

Evans, S. and Dennis, P.P. 1985. Promoter activity and transcript mapping in the regulatory region for genes encoding ribosomal protein S15 and polynucleotide phosphorylase of *Escherichia coli*. *Gene*. **40**(1), pp.15–22.

Farnham, P.J. and Platt, T. 1981. Rho-independent termination: Dyad symmetry in DNA causes RNA polymerase to pause during transcription in vitro. *Nucleic Acids Research*. **9**(3), pp.563–577.

Franke, D., Petoukhov, M. V, Konarev, P. V, Panjkovich, A., Tuukkanen, A., Mertens, H.D.T., Kikhney, A.G., Hajizadeh, N.R., Franklin, J.M., Jeffries, C.M., Svergun, D.I. and Semenov, N.N. 2017. ATSAS 2.8: a comprehensive data analysis suite for small-angle scattering from macromolecular solutions. *J. Appl. Cryst.* **50**, pp.1212–1225.

Frazão, C., McVey, C.E., Amblar, M., Barbas, A., Vornrhein, C., Arraiano, C.M. and Carrondo, M.A. 2006. Unravelling the dynamics of RNA degradation by ribonuclease II and its RNA-bound complex. *Nature*. **443**(7107), pp.110–114.

Garner, M.M. and Revzin, A. 1981. A gel electrophoresis method for quantifying the binding of proteins to specific DNA regions: application to components of the *Escherichia coli* lactose operon regulatory system.

*Nucleic Acids Research*. **9**(13), pp.3047–3060.

- Garrey, S.M., Blech, M., Riffell, J.L., Hankins, J.S., Stickney, L.M., Diver, M., Hsu, Y.H.R., Kunanithy, V. and Mackie, G.A. 2009. Substrate binding and active site residues in RNases E and G: Role of the 5'-sensor. *Journal of Biological Chemistry*. **284**(46), pp.31843–31850.
- Garrey, S.M. and Mackie, G.A. 2011. Roles of the 5'-phosphate sensor domain in RNase E. *Molecular Microbiology*. **80**(6), pp.1613–1624.
- Ghora, B.K. and Apirion, D. 1978. Structural analysis and in vitro processing to p5 rRNA of a 9S RNA molecule isolated from an rne mutant of E. coli. *Cell*. **15**(3), pp.1055–1066.
- Ghosh, S. and Deutscher, M.P. 1999. Oligoribonuclease is an essential component of the mRNA decay pathway. *Proceedings of the National Academy of Sciences of the United States of America*. **96**(8), pp.4372–7.
- Go, H., Moore, C.J., Lee, M., Shin, E., Jeon, C.O., Cha, C.-J., Han, S.H., Kim, S.-J., Lee, S.-W., Lee, Y., Ha, N.-C., Kim, Y.-H., Cohen, S.N. and Lee, K. 2011. Upregulation of RNase E activity by mutation of a site that uncompetitively interferes with RNA binding. *RNA biology*. **8**(6), pp.1022–34.
- Goldblum, K. and Apirion, D. 1981. Inactivation of ribonucleic acid-processing enzyme ribonuclease E blocks cell division. *Journal of Bacteriology*. **146**(1), pp.128–132.
- Goodall, E.C.A., Robinson, A., Johnston, I.G., Jabbari, S., Turner, K.A., Cunningham, A.F., Lund, P.A., Cole, J.A. and Henderson, I.R. 2018. The Essential Genome of Escherichia coli K-12. *mBio*. **9**(1), pp.e02096-



17.

- Greener, J.G. and Sternberg, M.J. 2018. Structure-based prediction of protein allostery. *Current Opinion in Structural Biology*. **50**, pp.1–8.
- Guo, J. and Zhou, H.-X. 2016. Protein Allostery and Conformational Dynamics. *Chemical Reviews*. **116**(11), pp.6503–6515.
- Hadjeras, L., Poljak, L., Bouvier, M., Morin-Ogier, Q., Canal, I., Coccagn-Bousquet, M., Girbal, L. and Carpousis, A.J. 2019. Detachment of the RNA degradosome from the inner membrane of *Escherichia coli* results in a global slowdown of mRNA degradation, proteolysis of RNase E and increased turnover of ribosome-free transcripts. *Molecular Microbiology*. **111**(6), mmi.14248.
- Hajnsdorf, E., Steier, O., Coscoy, L., Teyssset, L. and Régnier, P. 1994. Roles of RNase E, RNase II and PNPase in the degradation of the rpsO transcripts of *Escherichia coli*: stabilizing function of RNase II and evidence for efficient degradation in an *ams pnp rnb* mutant. *The EMBO Journal*. **13**(14), pp.3368–3377.
- Hammarlöf, D.L., Bergman, J.M., Garmendia, E. and Hughes, D. 2015. Turnover of mRNAs is one of the essential functions of RNase E. *Molecular Microbiology*. **98**(1), pp.34–45.
- Heo, J., Seo, S., Lee, B., Yeom, J.H. and Lee, K. 2016. Implications of *Streptomyces coelicolor* RraAS1 as an activator of ribonuclease activity of *Escherichia coli* RNase E. *Korean Journal of Microbiology*. **52**(3), pp.243–248.
- Himabindu, P. and Anupama, K. 2017. Decreased expression of stable RNA can alleviate the lethality associated with RNase E deficiency in

- Escherichia coli. *Journal of Bacteriology*. **199**(8).
- Hsieh, P., Richards, J., Liu, Q. and Belasco, J.G. 2013. Specificity of RppH-dependent RNA degradation in *Bacillus subtilis*. *Proceedings of the National Academy of Sciences*. **110**(22), pp.8864–8869.
- Hulsen, T., de Vlieg, J. and Alkema, W. 2008. BioVenn – a web application for the comparison and visualization of biological lists using area-proportional Venn diagrams. *BMC Genomics*. **9**(1), p.488.
- Hurdiss, D.L., Frank, M., Snowden, J.S., Macdonald, A. and Ranson, N.A. 2018. The Structure of an Infectious Human Polyomavirus and Its Interactions with Cellular Receptors. *Structure*. **26**(6), pp.839-847.e3.
- Iadanza, M.G., Higgins, A.J., Schiffrin, B., Calabrese, A.N., Brockwell, D.J., Ashcroft, A.E., Radford, S.E. and Ranson, N.A. 2016. Lateral opening in the intact  $\beta$ -barrel assembly machinery captured by cryo-EM. *Nature Communications*. **7**(1), p.12865.
- Iost, I. and Dreyfus, M. 1995. The stability of *Escherichia coli* lacZ mRNA depends upon the simultaneity of its synthesis and translation. *The EMBO journal*. **14**(13), pp.3252–61.
- Iost, I., Guillerez, J. and Dreyfus, M. 1992. Bacteriophage T7 RNA polymerase travels far ahead of ribosomes in vivo. *Journal of bacteriology*. **174**(2), pp.619–22.
- Ito, K., Hamasaki, K., Kayamori, A., Nguyen, P.A.T., Amagai, K. and Wachi, M. 2013. A secondary structure in the 5' untranslated region of adhE mRNA required for RNase G-dependent regulation. *Bioscience, Biotechnology and Biochemistry*. **77**(12), pp.2473–2479.
- Jain, C. and Belasco, J.G. 1995. RNase E autoregulates its synthesis by

*controlling the degradation rate of its own mRNA in Escherichia coli: unusual sensitivity of the rne transcript to RNase E activity.* [Online]. Cold Spring Harbor Laboratory Press. [Accessed 2 August 2019]. Available from: <http://genesdev.cshlp.org/content/9/1/84.full.pdf>.

Januszyk, K. 2012. The eukaryotic RNA exosome. *Curr Opin Struct Biol.* **29**(6), pp.997–1003.

Jarrige, A.C., Bréchemier-Baey, D., Mathy, N., Duché, O. and Portier, C. 2002. Mutational analysis of polynucleotide phosphorylase from *Escherichia coli*. *Journal of Molecular Biology.* **321**(3), pp.397–409.

Jarrige, A.C., Mathy, N. and Portier, C. 2001. PNPase autocontrols its expression by degrading a double-stranded structure in the pnp mRNA leader. *EMBO Journal.* **20**(23), pp.6845–6855.

Jiang, X. and Belasco, J.G. 2004. Catalytic activation of multimeric RNase E and RNase G by 5'-monophosphorylated RNA. *Proceedings of the National Academy of Sciences of the United States of America.* **101**(25), pp.9211–9216.

Jiang, X., Diwa, A. and Belasco, J.G. 2000. Regions of RNase E important for 5'-end-dependent RNA cleavage and autoregulated synthesis. *Journal of Bacteriology.* **182**(9), pp.2468–2475.

Johnson, D.T., Di Stefano, L.H. and Jones, L.M. 2019. Fast photochemical oxidation of proteins(FPOP): A powerful mass spectrometry based structural proteomics tool. *Journal of Biological Chemistry.*, jbc.REV119.006218.

Jones, G.H. 2010. RNA degradation and the regulation of antibiotic synthesis in *Streptomyces*. *Future Microbiology.* **5**(3), pp.419–429.

- Jourdan, S.S. 2008. *THE RECOGNITION AND CLEAVAGE OF RNA BY MEMBERS OF THE RNase E FAMILY*. University of Leeds.
- Jourdan, S.S. and McDowall, K.J. 2007. Sensing of 5' monophosphate by Escherichia coli RNase G can significantly enhance association with RNA and stimulate the decay of functional mRNA transcripts in vivo. *Molecular Microbiology*. **67**(1), pp.102–115.
- Kaberdin, V.R. 2003. Probing the substrate specificity of Escherichia coli RNase E using a novel oligonucleotide-based assay. *Nucleic Acids Research*. **31**(16), pp.4710–4716.
- Kaberdin, V.R., Miczak, A., Jakobsen, J.S., Lin-Chao, S., McDowall, K.J. and von Gabain, A. 1998. *The endoribonucleolytic N-terminal half of Escherichia coli RNase E is evolutionarily conserved in Synechocystis sp. and other bacteria but not the C-terminal half, which is sufficient for degradosome assembly* [Online]. National Academy of Sciences. [Accessed 2 August 2019]. Available from: <http://www.ncbi.nlm.nih.gov/pubmed/9751718>.
- Kaberdin, V.R., Walsh, A.P., Jakobsen, T., McDowall, K.J. and Von Gabain, A. 2000. Enhanced cleavage of RNA mediated by an interaction between substrates and the arginine-rich domain of E. coli ribonuclease E. *Journal of Molecular Biology*. **301**(2), pp.257–264.
- Kaga, N., Umitsuki, G., Nagai, K. and Wachi, M. 2002. RNase G-Dependent Degradation of the eno mRNA Encoding a Glycolysis Enzyme Enolase in Escherichia coli. *Bioscience, Biotechnology and Biochemistry*. **66**(10), pp.2216–2220.
- Karnik, P., Taljanidisz, J., Sasvari-Szekely, M. and Sarkar, N. 1987. 3'-

- terminal polyadenylate sequences of *Escherichia coli* tryptophan synthetase  $\alpha$ -subunit messenger RNA. *Journal of Molecular Biology*. **196**(2), pp.347–354.
- Karzai, A.W. and Sauer, R.T. 2001. Protein factors associated with the SsrA\*SmpB tagging and ribosome rescue complex. *Proceedings of the National Academy of Sciences*. **98**(6), pp.3040–3044.
- Khemici, V. and Carpousis, A.J. 2003. The RNA degradosome and poly(A) polymerase of *Escherichia coli* are required in vivo for the degradation of small mRNA decay intermediates containing REP-stabilizers. *Molecular Microbiology*. **51**(3), pp.777–790.
- Khemici, V., Poljak, L., Luisi, B.F. and Carpousis, A.J. 2008. The RNase E of *Escherichia coli* is a membrane-binding protein. *Molecular Microbiology*. **70**, pp.799–813.
- Khemici, V., Poljak, L., Toesca, I. and Carpousis, A.J. 2005. Evidence in vivo that the DEAD-box RNA helicase RhlB facilitates the degradation of ribosome-free mRNA by RNase E. *Proceedings of the National Academy of Sciences*. **102**(19), pp.6913–6918.
- Kido, M., Yamanaka, K., Mitani, T., Niki, H., Ogura, T. and Hiraga, S. 1996. RNase E polypeptides lacking a carboxyl-terminal half suppress a mukB mutation in *Escherichia coli*. *Journal of Bacteriology*. **178**(13), pp.3917–3925.
- Kim, D., Song, S., Lee, M., Go, H., Shin, E., Yeom, J.-H., Ha, N.-C., Lee, K. and Kim, Y.-H. 2014. Modulation of RNase E Activity by Alternative RNA Binding Sites Y.-S. Bahn, ed. *PLoS ONE*. **9**(3), p.e90610.
- Kime, L., Clarke, J.E., Romero A., D., Grasby, J.A. and McDowall, K.J. 2014.

Adjacent single-stranded regions mediate processing of tRNA precursors by RNase E direct entry. *Nucleic Acids Research*. **42**(7), pp.4577–4589.

Kime, L., Jourdan, S.S., Stead, J. a., Hidalgo-Sastre, A. and McDowall, K.J. 2010. Rapid cleavage of RNA by RNase e in the absence of 5' monophosphate stimulation. *Molecular Microbiology*. **76**(3), pp.590–604.

Kime, L., Vincent, H.A., Gendoo, D.M.A.A., Jourdan, S.S., Fishwick, C.W.G.G., Callaghan, A.J. and McDowall, K.J. 2015. The first small-molecule inhibitors of members of the ribonuclease E family. *Scientific Reports*. **5**(1), p.8028.

Koslover, D.J., Callaghan, A.J., Marcaida, M.J., Garman, E.F., Martick, M., Scott, W.G. and Luisi, B.F. 2008. The Crystal Structure of the Escherichia coli RNase E Apoprotein and a Mechanism for RNA Degradation. *Structure*. **16**(8), pp.1238–1244.

Kostyukevich, Y., Acter, T., Zherebker, A., Ahmed, A., Kim, S. and Nikolaev, E. 2018. Hydrogen/deuterium exchange in mass spectrometry. *Mass Spectrometry Reviews*. **37**(6), pp.811–853.

Lawson, C.L., Baker, M.L., Best, C., Bi, C., Dougherty, M., Feng, P., van Ginkel, G., Devkota, B., Lagerstedt, I., Ludtke, S.J., Newman, R.H., Oldfield, T.J., Rees, I., Sahni, G., Sala, R., Velankar, S., Warren, J., Westbrook, J.D., Henrick, K., Kleywegt, G.J., Berman, H.M. and Chiu, W. 2011. EMDataBank.org: unified data resource for CryoEM. *Nucleic acids research*. **39**(Database issue), pp.D456-64.

Lee, K., Bernstein, J.A. and Cohen, S.N. 2002. RNase G complementation

of rne null mutation identifies functional interrelationships with RNase E in Escherichia coli. *Molecular Microbiology*. **43**(6), pp.1445–1456.

Lehnik-Habrink, M., Lewis, R.J., Mäder, U. and Stülke, J. 2012. RNA degradation in Bacillus subtilis: An interplay of essential endo- and exoribonucleases. *Molecular Microbiology*. **84**(6), pp.1005–1017.

Lehnik-Habrink, M., Newman, J., Rothe, F.M., Solovyova, A.S., Rodrigues, C., Herzberg, C., Commichau, F.M., Lewis, R.J. and Stulke, J. 2011. RNase Y in Bacillus subtilis: a Natively Disordered Protein That Is the Functional Equivalent of RNase E from Escherichia coli. *Journal of Bacteriology*. **193**(19), pp.5431–5441.

Leroy, A., Vanzo, N.F., Sousa, S., Dreyfus, M. and Carpousis, A.J. 2002. Function in Escherichia coli of the non-catalytic part of RNase E: role in the degradation of ribosome-free mRNA. *Molecular Microbiology*. **45**(5), pp.1231–1243.

Li, Z. and Deutscher, M.P. 2002. RNase E plays an essential role in the maturation of Escherichia coli tRNA precursors. *RNA*. **8**(1).

Li, Z., Pandit, S. and Deutscher, M.P. 1999a. Maturation of 23S ribosomal RNA requires the exoribonuclease RNase T. *RNA*. **5**(1), pp.139–146.

Li, Z., Pandit, S. and Deutscher, M.P. 1999b. RNase G (CafA protein) and RNase E are both required for the 5' maturation of 16S ribosomal RNA. *The EMBO Journal*. **18**(10), pp.2878–2885.

Lin-Chao, S., Wong, T.T., McDowall, K.J. and Cohen, S.N. 1994. Effects of nucleotide sequence on the specificity of rne-dependent and RNase E-mediated cleavages of RNA I encoded by the pBR322 plasmid. *Journal of Biological Chemistry*. **269**(14), pp.10797–10803.

- Lin, P.H. and Lin-Chao, S. 2005. RhlB helicase rather than enolase is the  $\beta$ -subunit of the Escherichia coli polynucleotide phosphorylase (PNPase)-exoribonucleolytic complex. *Proceedings of the National Academy of Sciences of the United States of America*. **102**(46), pp.16590–16595.
- Liou, G.-G., Jane, W.-N., Cohen, S.N., Lin, N.-S. and Lin-Chao, S. 2001. RNA degradosomes exist in vivo in Escherichia coli as multicomponent complexes associated with the cytoplasmic membrane via the N-terminal region of ribonuclease E. *Proceedings of the National Academy of Sciences*. **98**(1), pp.63–68.
- Liou, G.G., Chang, H.Y., Lin, C.S. and Lin-Chao, S. 2002. Dead box RhlB RNA helicase physically associates with exoribonuclease PNPase to degrade double-stranded RNA independent of the degradosome-assembling region of RNase E. *Journal of Biological Chemistry*. **277**(43), pp.41157–41162.
- Lopez, P.J., Marchand, I., Joyce, S.A. and Dreyfus, M. 1999. The C-terminal half of RNase E, which organizes the Escherichia coli degradosome, participates in mRNA degradation but not rRNA processing in vivo. *Molecular Microbiology*. **33**(1), pp.188–199.
- Luciano, D.J., Vasilyev, N., Richards, J., Serganov, A. and Belasco, J.G. 2017. A Novel RNA Phosphorylation State Enables 5' End-Dependent Degradation in Escherichia coli. *Molecular Cell*. **67**(1), pp.44-54.e6.
- Lyumkis, D. 2019. Challenges and opportunities in cryo-EM single-particle analysis. *Journal of Biological Chemistry*. **294**(13), pp.5181–5197.
- Mackie, G.A. 1998. Ribonuclease E is a 5'-end-dependent endonuclease. *Nature*. **395**(October), pp.720–723.



- Mackie, G.A. 2013. RNase E: at the interface of bacterial RNA processing and decay. *Nature Reviews Microbiology*. **11**(1), pp.45–57.
- Mahadevan, R. and Lovley, D.R. 2008. The degree of redundancy in metabolic genes is linked to mode of metabolism. *Biophysical journal*. **94**(4), pp.1216–20.
- Makeyev, A. V., Eastmond, D.L. and Liebhaber, S.A. 2002. Targeting a KH-domain protein with RNA decoys. *Rna*. **8**(9), pp.1160–1173.
- Mardle, C.E., Shakespeare, T.J., Butt, L.E., Goddard, L.R., Gowers, D.M., Atkins, H.S., Vincent, H.A. and Callaghan, A.J. 2019. A structural and biochemical comparison of Ribonuclease E homologues from pathogenic bacteria highlights species-specific properties. *Scientific reports*. **9**(1), p.7952.
- Marujo, P.E., Hajnsdorf, E., Le Derout, J., Andrade, R., Arraiano, C.M. and Régnier, P. 2000. RNase II removes the oligo(A) tails that destabilize the rpsO mRNA of Escherichia coli. *Rna*. **6**(8), pp.1185–1193.
- Marzi, S. and Romby, P. 2012. RNA mimicry, a decoy for regulatory proteins. *Molecular Microbiology*. **83**(1), pp.1–6.
- Masters, M., Colloms, M.D., Oliver, I.R., He, L., Macnaughton, E.J. and Charters, Y. 1993. The pcnB gene of Escherichia coli, which is required for ColE1 copy number maintenance, is dispensable. *Journal of Bacteriology*. **175**(14), pp.4405–4413.
- Mathy, N., Bénard, L., Pellegrini, O., Daou, R., Wen, T. and Condon, C. 2007. 5'-to-3' exoribonuclease activity in bacteria: role of RNase J1 in rRNA maturation and 5' stability of mRNA. *Cell*. **129**(4), pp.681–92.
- Matos, R.G., Barbas, A., Gómez-Puertas, P. and Arraiano, C.M. 2011.

- Swapping the domains of exoribonucleases RNase II and RNase R: Conferring upon RNase II the ability to degrade ds RNA. *Proteins: Structure, Function, and Bioinformatics*. **79**(6), pp.1853–1867.
- Matsumoto, Y., Ohta, K. and Nishio, M. 2019. Importance of tyrosine in the RNA-binding domain of human parainfluenza virus type 2 nucleoprotein for polymerase activity. *Archives of Virology*. **164**(7), pp.1851–1855.
- Mayer, M.P. 1995. A new set of useful cloning and expression vectors derived from pBlueScript. *Gene*. **163**(1), pp.41–6.
- McDowall, K.J., Hernandez, R.G., Lin-Chao, S. and Cohen, S.N. 1993. The *ams-1* and *mre-3071* temperature-sensitive mutations in the *ams* gene are in close proximity to each other and cause substitutions within a domain that resembles a product of the *Escherichia coli mre* locus. *Journal of Bacteriology*. **175**(13), pp.4245–4249.
- McDowall, K.J., Kaberdin, V.R., Wu, S.W., Cohen, S.N. and Lin-Chao, S. 1995. Site-specific RNase E cleavage of oligonucleotides and inhibition by stem-loops. *Nature*. **374**(6519), pp.287–290.
- McDowall, K.J., Lin-Chao, S. and Cohen, S.N. 1994. A + U content rather than a particular nucleotide order determines the specificity of RNase E cleavage. *Journal of Biological Chemistry*. **269**(14), pp.10790–10796.
- McLaren, R.S., Newbury, S.F., Dance, G.S.C., Causton, H.C. and Higgins, C.F. 1991. mRNA degradation by processive 3'-5' exoribonucleases in Vitro and the implications for prokaryotic mRNA decay in Vivo. *Journal of Molecular Biology*. **221**(1), pp.81–95.
- McNamara, P.J. and El-Khuffash, A. 2017. Oxygen Transport and Delivery *In: Fetal and Neonatal Physiology* [Online]. Elsevier, pp.724-737.e2.

[Accessed 19 September 2019]. Available from:

<https://www.sciencedirect.com/science/article/pii/B97803233521470007>

18.

Melefors, Ö. and von Gabain, A. 1991. Genetic studies of cleavage-initiated mRNA decay and processing of ribosomal 9S RNA show that the *Escherichia coli* *ams* and *rne* loci are the same. *Molecular Microbiology*.

**5**(4), pp.857–864.

Miller, O.L., Hamkalo, B.A. and Thomas, C.A. 1970. Visualization of bacterial genes in action. *Science (New York, N.Y.)*. **169**(3943), pp.392–5.

Milne, L., Perrin, D.M. and Sigman, D.S. 2001. Oligoribonucleotide-Based Gene-Specific Transcription Inhibitors That Target the Open Complex.

*Methods*. **23**(2), pp.160–168.

Misra, T.K. and Apirion, D. 1979. RNase E, an RNA processing enzyme from *Escherichia coli*. *Journal of Biological Chemistry*. **254**(21),

pp.11154–11159.

Mohanty, B.K. and Kushner, S.R. 2003. Genomic analysis in *Escherichia coli* demonstrates differential roles for polynucleotide phosphorylase and

RNase II in mRNA abundance and decay. *Molecular Microbiology*.

**50**(2), pp.645–658.

Morita, T., Kawamoto, H., Mizota, T., Inada, T. and Aiba, H. 2004. Enolase

in the RNA degradosome plays a crucial role in the rapid decay of glucose transporter mRNA in the response to phosphosugar stress in

*Escherichia coli*. *Molecular Microbiology*. **54**(4), pp.1063–1075.

Motlagh, H.N., Wrabl, J.O., Li, J. and Hilser, V.J. 2014. The ensemble nature of allostery. *Nature*. **508**.

- Mott, J.E., Galloway, J.L. and Platt, T. 1985. Maturation of *Escherichia coli* tryptophan operon mRNA: evidence for 3' exonucleolytic processing after rho-dependent termination. *The EMBO Journal*. **4**(7), pp.1887–1891.
- Mudd, E.A. and Higgins, C.F. 1993. *Escherichia coli* endoribonuclease RNase E: autoregulation of expression and site-specific cleavage of mRNA. *Molecular Microbiology*. **9**(3), pp.557–568.
- Mudd, E.A., Krisch, H.M. and Higgins, C.F. 1990. RNase E, an endoribonuclease, has a general role in the chemical decay of *Escherichia coli* mRNA: evidence that *rne* and *ams* are the same genetic locus. *Molecular Microbiology*. **4**(12), pp.2127–2135.
- Murashko, O.N., Kaberdin, V.R. and Lin-Chao, S. 2012. Membrane binding of *Escherichia coli* RNase E catalytic domain stabilizes protein structure and increases RNA substrate affinity. *Proceedings of the National Academy of Sciences*. **109**(18), pp.7019–7024.
- Nakazato, H., Venkatesan, S. and Edmonds, M. 1975. Polyadenylic acid sequences in *E. coli* messenger RNA. *Nature*. **256**(5513), pp.144–146.
- Newbury, S.F., Smith, N.H., Robinson, E.C., Hiles, I.D. and Higgins, C.F. 1987. Stabilization of translationally active mRNA by prokaryotic REP sequences. *Cell*. **48**(2), pp.297–310.
- Nicholson, A.W. 1999. Function, mechanism and regulation of bacterial ribonucleases. *FEMS Microbiology Reviews*. **23**(3), pp.371–390.
- Nurmohamed, S., McKay, A.R., Robinson, C. V. and Luisi, B.F. 2010. Molecular recognition between *Escherichia coli* enolase and ribonuclease E. *Acta Crystallographica Section D: Biological*

*Crystallography*. **66**(9), pp.1036–1040.

- Nurmohamed, S., Vaidialingam, B., Callaghan, A.J. and Luisi, B.F. 2009. Crystal Structure of Escherichia coli Polynucleotide Phosphorylase Core Bound to RNase E, RNA and Manganese: Implications for Catalytic Mechanism and RNA Degradosome Assembly. *Journal of Molecular Biology*. **389**(1), pp.17–33.
- Ohi, M., Li, Y., Cheng, Y. and Walz, T. 2004. Negative Staining and Image Classification - Powerful Tools in Modern Electron Microscopy. *Biological procedures online*. **6**, pp.23–34.
- Okada, Y., Wachi, M., Hirata, A., Suzuki, K., Nagai, K. and Matsushashi, M. 1994. Cytoplasmic axial filaments in Escherichia coli cells: Possible function in the mechanism of chromosome segregation and cell division. *Journal of Bacteriology*. **176**(3), pp.917–922.
- Ono, M. and Kuwano, M. 1979. A conditional lethal mutation in an Escherichia coli strain with a longer chemical lifetime of messenger RNA. *Journal of Molecular Biology*. **129**(3), pp.343–357.
- Ost, K.A. and Deutscher, M.P. 1990. RNase PH catalyzes a synthetic reaction, the addition of nucleotides to the 3' end of RNA. *Biochimie*. **72**(11), pp.813–818.
- Ow, M.C. and Kushner, S.R. 2002. Initiation of tRNA maturation by RNase E is essential for cell viability in E. coli. *Genes and Development*. **16**(9), pp.1102–1115.
- Oxford Nanopore Technologies 2018. *The value of full-length transcripts without bias* [Online]. Oxford. [Accessed 27 August 2019]. Available from: <https://nanoporetech.com/sites/default/files/s3/white-papers/ONT->

WP-RNA-Sequencing.pdf?submissionGuid=14e6fec3-4b68-497b-840c-2200a15ba595.

- Pettersen, E.F., Goddard, T.D., Huang, C.C., Couch, G.S., Greenblatt, D.M., Meng, E.C. and Ferrin, T.E. 2004. UCSF Chimera - A visualization system for exploratory research and analysis. *Journal of Computational Chemistry*.
- Pfleger, B.F., Pitera, D.J., Smolke, C.D. and Keasling, J.D. 2006. Combinatorial engineering of intergenic regions in operons tunes expression of multiple genes. . **24**(8), pp.1027–1032.
- Portier, C., Dondon, L., Grunberg-Manago, M. and Régnier, P. 1987. The first step in the functional inactivation of the Escherichia coli polynucleotide phosphorylase messenger is a ribonuclease III processing at the 5' end. *The EMBO Journal*. **6**(7), pp.2165–2170.
- Prahlad, J., Hauser, D.N., Milkovic, N.M., Cookson, M.R. and Wilson, M.A. 2014. Use of cysteine-reactive cross-linkers to probe conformational flexibility of human DJ-1 demonstrates that Glu18 mutations are dimers. *Journal of neurochemistry*. **130**(6), pp.839–53.
- Prud'homme-Généreux, A., Beran, R.K., Iost, I., Ramey, C.S., Mackie, G.A. and Simons, R.W. 2004. Physical and functional interactions among RNase E, polynucleotide phosphorylase and the cold-shock protein, CsdA: evidence for a 'cold shock degradosome'. *Molecular microbiology*. **54**(5), pp.1409–21.
- Pruitt, K.D., Tatusova, T. and Maglott, D.R. 2007. NCBI reference sequences (RefSeq): A curated non-redundant sequence database of genomes, transcripts and proteins. *Nucleic Acids Research*. **35**(SUPPL.

1).

- Py, B., Causton, H., Mudd, E.A. and Higgins, C.F. 1994. A protein complex mediating mRNA degradation in *Escherichia coli*. *Molecular Microbiology*. **14**(4), pp.717–729.
- Py, B., Higgins, C.F., Krisch, H.M. and Carpousis, A.J. 1996. A DEAD-box RNA helicase in the *Escherichia coli* RNA degradosome. *Nature*. **381**(6578), pp.169–172.
- Qu, X., Lancaster, L., Noller, H.F., Bustamante, C. and Tinoco, I. 2012. Ribosomal protein S1 unwinds double-stranded RNA in multiple steps. *Proceedings of the National Academy of Sciences*. **109**(36), pp.14458–14463.
- Rauhut, R. and Klug, G. 1999. mRNA degradation in bacteria. *FEMS Microbiology Reviews*. **23**, pp.353–370.
- Redko, Y., Tock, M.R., Adams, C.J., Kaberdin, V.R., Grasby, J.A. and McDowall, K.J. 2003. Determination of the Catalytic Parameters of the N-terminal Half of *Escherichia coli* Ribonuclease E and the Identification of Critical Functional Groups in RNA Substrates. *Journal of Biological Chemistry*. **278**(45), pp.44001–44008.
- Régnier, P. and Portier, C. 1986. Initiation, attenuation and RNase III processing of transcripts from the *Escherichia coli* operon encoding ribosomal protein S15 and polynucleotide phosphorylase. *Journal of Molecular Biology*. **187**(1), pp.23–32.
- Rhodes, D. and Lipps, H.J. 2015. G-quadruplexes and their regulatory roles in biology. *Nucleic Acids Research*. **43**(18), pp.8627–8637.
- Richards, J., Luciano, D.J. and Belasco, J.G. 2012. Influence of translation

- on RppH-dependent mRNA degradation in *Escherichia coli*. *Molecular Microbiology*. **86**(5), pp.1063–1072.
- Richards, J., Mehta, P. and Karzai, A.W. 2006. RNase R degrades non-stop mRNAs selectively in an SmpB-tmRNA-dependent manner. *Molecular Microbiology*. **62**(6), pp.1700–1712.
- Robinow, C. and Kellenberger, E. 1994. The bacterial nucleoid revisited. *Microbiological reviews*. **58**(2), pp.211–32.
- Sauer, R.T., Karzai, A.W. and Roche, E.D. 2000. The SsrA-SmpB system for protein tagging, directed degradation and ribosome rescue. *Nature Structural Biology*. **7**(6), pp.449–455.
- Scarf, C.A., Fuller, M.J.G., Thompson, R.F. and Iadanza, M.G. 2018. Variations on Negative Stain Electron Microscopy Methods: Tools for Tackling Challenging Systems. *Journal of visualized experiments: JoVE*. (132).
- Scheres, S.H.W. 2012. RELION: Implementation of a Bayesian approach to cryo-EM structure determination. *Journal of Structural Biology*.
- Schubert, M., Edge, R.E., Lario, P., Cook, M.A., Strynadka, N.C.J., Mackie, G.A. and McIntosh, L.P. 2004. Structural Characterization of the RNase E S1 Domain and Identification of its Oligonucleotide-binding and Dimerization Interfaces. *Journal of Molecular Biology*. **341**(1), pp.37–54.
- Schuck, A., Diwa, A. and Belasco, J.G. 2009. RNase E autoregulates its synthesis in *Escherichia coli* by binding directly to a stem-loop in the rne 5' untranslated region. *Molecular microbiology*. **72**(2), pp.470–478.
- Sgro, G.G. and Costa, T.R.D. 2018. Cryo-EM Grid Preparation of Membrane Protein Samples for Single Particle Analysis. *Frontiers in Molecular*



*Biosciences*. **5**, p.74.

Shahbadian, K., Jamalli, A., Zig, L. and Putzer, H. 2009. RNase Y, a novel endoribonuclease, initiates riboswitch turnover in *Bacillus subtilis*. *The EMBO journal*. **28**(22), pp.3523–33.

Shepherd, J. and Ibba, M. 2015. Bacterial transfer RNAs. *FEMS Microbiology Reviews*. **39**(3), pp.280–300.

Smolke, C.D. and Keasling, J.D. 2002. Effect of gene location, mRNA secondary structures, and RNase sites on expression of two genes in an engineered operon. *Biotechnology and Bioengineering*. **80**(7), pp.762–776.

Sorzano, C.O.S., Marabini, R., Boisset, N., Rietzel, E., Schröder, R., Herman, G.T. and Carazo, J.M. 2001. The Effect of Overabundant Projection Directions on 3D Reconstruction Algorithms. *Journal of Structural Biology*. **133**(2–3), pp.108–118.

Sousa, S., Marchand, I. and Dreyfus, M. 2008. Autoregulation allows *Escherichia coli* RNase E to adjust continuously its synthesis to that of its substrates. *Molecular Microbiology*. **42**(3), pp.867–878.

Stark, B.C., Kole, R., Bowman, E.J. and Altman, S. 1978. Ribonuclease P: An enzyme with an essential RNA component. *Proceedings of the National Academy of Sciences of the United States of America*. **75**(8), pp.3717–3721.

Stark, H. 2010. GraFix: Stabilization of Fragile Macromolecular Complexes for Single Particle Cryo-EM *In: Methods in enzymology* [Online], pp.109–126. [Accessed 24 August 2019]. Available from: <http://www.ncbi.nlm.nih.gov/pubmed/20887855>.

- Stead, M.B., Marshburn, S., Mohanty, B.K., Mitra, J., Castillo, L.P., Ray, D., Van Bakel, H., Hughes, T.R. and Kushner, S.R. 2011. Analysis of *Escherichia coli* RNase E and RNase III activity in vivo using tiling microarrays. *Nucleic Acids Research*. **39**(8), pp.3188–3203.
- Stracy, M. and Kapanidis, A.N. 2017. Single-molecule and super-resolution imaging of transcription in living bacteria. *Methods*. **120**, pp.103–114.
- Taghbalout, A. and Rothfield, L. 2008. RNaseE and RNA helicase B play central roles in the cytoskeletal organization of the RNA degradosome. *The Journal of biological chemistry*. **283**(20), pp.13850–5.
- Takata, R., Mukai, T. and Hori, K. 1987. RNA processing by RNase III is involved in the synthesis of *Escherichia coli* polynucleotide phosphorylase. *MGG Molecular & General Genetics*. **209**(1), pp.28–32.
- Takizawa, Y., Binshtein, E., Erwin, A.L., Pyburn, T.M., Mittendorf, K.F. and Ohi, M.D. 2017. While the revolution will not be crystallized, biochemistry reigns supreme. *Protein Science*. **26**(1), pp.69–81.
- Talkad, V., Achord, D. and Kennell, D. 1978. Altered mRNA metabolism in ribonuclease III-deficient strains of *Escherichia coli*. *Journal of bacteriology*. **135**(2), pp.528–41.
- Taraseviciene, L., Miczak, A. and Apirion, D. 1991. The gene specifying RNase E ( *rne* ) and a gene affecting mRNA stability ( *ams* ) are the same gene. *Molecular Microbiology*. **5**(4), pp.851–855.
- Thompson, K.J., Zong, J. and Mackie, G.A. 2015. Altering the divalent metal ion preference of RNase E. *Journal of Bacteriology*. **197**(3), pp.477–482.
- Thompson, R.F., Walker, M., Siebert, C.A. and Ranson, N.A. 2016. An

introduction to sample preparation and imaging by cryo-electron microscopy for structural biology. *Methods*. **100**, pp.3–15.

Tiede, C., Tang, A.A.S., Deacon, S.E., Mandal, U., Nettleship, J.E., Owen, R.L., George, S.E., Harrison, D.J., Owens, R.J., Tomlinson, D.C. and McPherson, M.J. 2014. Adhiron: a stable and versatile peptide display scaffold for molecular recognition applications. *Protein Engineering, Design and Selection*. **27**(5), pp.145–155.

Tourrière, H., Chebli, K. and Tazi, J. 2002. mRNA degradation machines in eukaryotic cells. *Biochimie*. **84**(8), pp.821–837.

Tsai, Y.-C., Du, D., Domínguez-Malfavón, L., Dimastrogiovanni, D., Cross, J., Callaghan, A.J., García-Mena, J. and Luisi, B.F. 2012. Recognition of the 70S ribosome and polysome by the RNA degradosome in *Escherichia coli*. *Nucleic Acids Research*. **40**(20), pp.10417–10431.

Tseng, Y.-T., Chiou, N.-T., Gogiraju, R. and Lin-Chao, S. 2015. The Protein Interaction of RNA Helicase B (RhIB) and Polynucleotide Phosphorylase (PNPase) Contributes to the Homeostatic Control of Cysteine in *Escherichia coli*. *The Journal of biological chemistry*. **290**(50), pp.29953–63.

Umitsuki, G., Wachi, M., Takada, A., Hikichi, T. and Nagai, K. 2001. Involvement of RNase G in in vivo mRNA metabolism in *Escherichia coli*. *Genes to Cells*. **6**(5), pp.403–410.

Updegrave, T.B., Kouse, A.B., Bandyra, K.J. and Storz, G. 2019. Stem-loops direct precise processing of 3' UTR-derived small RNA MicL. *Nucleic Acids Research*. **47**(3), pp.1482–1492.

Urlaub, H., Kühn-Hölsken, E. and Lührmann, R. 2008. Analyzing RNA-

Protein Crosslinking Sites in Unlabeled Ribonucleoprotein Complexes by Mass Spectrometry *In: Methods in molecular biology (Clifton, N.J.)* [Online]., pp.221–245. [Accessed 20 September 2019]. Available from: <http://www.ncbi.nlm.nih.gov/pubmed/18982295>.

Vanzo, N.F., Li, Y.S., Py, B., Blum, E., Higgins, C.F., Raynal, L.C., Krisch, H.M. and Carpousis, A.J. 1998. *Ribonuclease E organizes the protein interactions in the Escherichia coli RNA degradosome* [Online]. Cold Spring Harbor Laboratory Press. [Accessed 15 August 2019]. Available from: [www.genesdev.org](http://www.genesdev.org).

Vincent, H.A. and Deutscher, M.P. 2006. Substrate recognition and catalysis by the exoribonuclease RNase R. *Journal of Biological Chemistry*. **281**(40), pp.29769–29775.

Wachi, M., Umitsuki, G. and Nagai, K. 1997. Functional relationship between Escherichia coli RNase E and the CafA protein. *Molecular and General Genetics*. **253**(4), pp.515–519.

Wachi, M., Umitsuki, G., Shimizu, M., Takada, A. and Nagai, K. 1999. Escherichia coli cafA Gene Encodes a Novel RNase, Designated as RNase G, Involved in Processing of the 5' End of 16S rRNA. *Biochemical and Biophysical Research Communications*. **259**(2), pp.483–488.

Walsh, A.P., Tock, M.R., Mallen, M.H., Kaberdin, V.R., von Gabain, A. and McDowall, K.J. 2001. Cleavage of poly(A) tails on the 3'-end of RNA by ribonuclease E of Escherichia coli. *Nucleic acids research*. **29**(9), pp.1864–71.

Waters, S.A., McAteer, S.P., Kudla, G., Pang, I., Deshpande, N.P., Amos,

- T.G., Leong, K.W., Wilkins, M.R., Strugnell, R., Gally, D.L., Tollervey, D. and Tree, J.J. 2017. Small RNA interactome of pathogenic *E. coli* revealed through crosslinking of RNase E. *The EMBO Journal*. **36**(3), pp.374–387.
- Webster, M.W., Stowell, J.A. and Passmore, L.A. 2019. RNA-binding proteins distinguish between similar sequence motifs to promote targeted deadenylation by Ccr4-Not. *eLife*. **8**.
- Worrall, J.A.R., Howe, F.S., McKay, A.R., Robinson, C. V. and Luisi, B.F. 2008. Allosteric Activation of the ATPase Activity of the *Escherichia coli* RhlB RNA Helicase. *Journal of Biological Chemistry*. **283**(9), pp.5567–5576.
- Wu, X. and Brewer, G. 2012. The Regulation of mRNA Stability in Mammalian Cells: 2.0. *Gene*. **500**(1), p.10.
- Xu, F., Sue, L.C. and Cohen, S.N. 1993. The *Escherichia coli* *pcnB* gene promotes adenylation of antisense RNAI of ColE1-type plasmids in vivo and degradation of RNAI decay intermediates. *Proceedings of the National Academy of Sciences of the United States of America*. **90**(14), pp.6756–6760.
- Yao, S. and Bechhofer, D.H. 2010. Initiation of decay of *Bacillus subtilis* *rpsO* mRNA by endoribonuclease RNase Y. *Journal of bacteriology*. **192**(13), pp.3279–86.
- Yehudai-Resheff, S., Hirsh, M. and Schuster, G. 2001. Polynucleotide phosphorylase functions as both an exonuclease and a poly(A) polymerase in spinach chloroplasts. *Molecular and cellular biology*. **21**(16), pp.5408–16.

- Young, R.A. and Steitz, J.A. 1978. Complementary sequences 1700 nucleotides apart from a ribonuclease III cleavage site in *Escherichia coli* ribosomal precursor RNA. *Proceedings of the National Academy of Sciences of the United States of America*. **75**(8), pp.3593–3597.
- Zangrossi, S., Briani, F., Ghisotti, D., Regonesi, M.E., Tortora, P. and Dehò, G. 2002. Transcriptional and post-transcriptional control of polynucleotide phosphorylase during cold acclimation in *Escherichia coli*. *Molecular Microbiology*. **36**(6), pp.1470–1480.
- Zhang, X., Zhang, D., Zhao, C., Tian, K., Shi, R., Du, X., Burcke, A.J., Wang, J., Chen, S.-J. and Gu, L.-Q. 2017. Nanopore electric snapshots of an RNA tertiary folding pathway. *Nature Communications*. **8**(1), p.1458.
- Zilhão, R., Cairrão, F., Régnier, P. and Arraiano, C.M. 1996. PNPase modulates RNase II expression in *Escherichia coli*: implications for mRNA decay and cell metabolism. *Molecular Microbiology*. **20**(5), pp.1033–1042.
- Zuker, M. 2003. Mfold web server for nucleic acid folding and hybridization prediction. *Nucleic Acids Research*. **31**(13), pp.3406–3415.
- Zuo, Y. and Deutscher, M.P. 2001. Exoribonuclease superfamilies: structural analysis and phylogenetic distribution. *Nucleic Acids Research*. **29**(5), pp.1017–1026.